NASA Contractor Report 166214

Analysis of Mach Number 0.8 Turboprop Slipstream Wing/Nacelle Interactions

H. Robert Welge
Dan H. Neuhart
John A. Dahlin

McDonnell Douglas Corporation
Douglas Aircraft Company
Long Beach, California 90846

Contract NAS2-10881
August 6, 1981

National Aeronautics and Space Administration

Ames Research Center
Moffett Field, California 94035

NASA Contractor Report 166214

Analysis of Mach Number 0.8 Turboprop Slipstream Wing/Nacelle Interactions

H. Robert Welge
Dan H. Neuhart
John A. Dahlin

McDonnell Douglas Corporation
Douglas Aircraft Company
Long Beach, California 90846

Contract NAS2-10881
August 6, 1981

National Aeronautics and
Space Administration

Ames Research Center
Moffett Field, California 94035

TABLE OF CONTENTS

I. SUMMARY

An experimental test program of a powered propeller and nacelle mounted on a supercritical wing was conducted by the NASA Ames Research Center in the 14-Foot Tunnel. Analysis of this data by the Douglas Aircraft Company, under contract to NASA with Al Lavin as the program manager, is contained in this report. The design condition for this study was $M_0 = 0.8$.

Analysis of the data indicated that the installation of the nacelle significantly affected the wing flow and that the flow on the upper surface of the wing is separated near the leading edge under powered conditions. Comparisons of various theories with the data indicated that the Neumann surface panel solution and the Jameson transonic solution gave results adequate for design purposes. A modified wing design was developed (Mod 3) which reduces the wing upper surface pressure coefficients and section lift coefficients at powered conditions to levels below those of the original wing without nacelle or power. A contoured over-the-wing nacelle is described that can be installed on the original wing without any appreciable interference to the wing upper surface pressures.

Page Intentionally Left Blank

II. INTRODUCTION

The recent increases in fuel prices for aircraft has resulted in the consideration of alternate propulsion system concepts that would reduce fuel consumption. One of the primary candidates is a propeller-turboshaft (turboprop) powerplant. Several system studies have been conducted that indicate fuel savings from 15 to 30% in fuel burned for a given mission when compared to turbofan engines (References 1 through 6). Flight speeds of $M_o = 0.8$ are considered necessary for compatibility with existing airline operation and advanced propeller designs called Prop-Fans have been developed that give efficient performance at these speeds. A wing of the supercritical type is recommended to maximize performance.

One of the aerodynamic concerns about the turboprop installation is the interference drag that will result from the placement of the gas generator/nacelle and propeller on a supercritical type wing. Several years ago, a test was run by Douglas Aircraft under contract to NASA Ames (Reference 7) to experimentally evaluate these interferences. A flow-through ejector powered nacelle located ahead of the wing was used to simulate the onset flow of the propeller. This experimental approach permitted independently varying the various propeller parameters to obtain a basic understanding of the power-wing interactions. Many useful results and observations resulted from this early exploratory program but a more accurate representation of the flow is obtained by using an actual rotating propeller.

The test results discussed in this report used the same wing design as the previous simulator test. A semispan test installation was used mounted to the floor of the Ames 14-foot tunnel. Test conditions covered the Mach range from 0.6 to 0.85. The Reynolds numbers based on the mean aerodynamic chord varied from 7.8×10^6 at $M_o = 0.6$ to 9.1×10^6 at $M_o = 0.85$. An air-driven motor powered an 8 bladed propfan propeller designated SR-2C (Reference 8). The installation, development of the motor, fabrication and testing were all done by NASA Ames. This report covers the analysis of the data, comparison with theory and configuration modifications performed by the Douglas Aircraft Company (a division of the McDonnell Douglas Corporation) located in Long Beach, California.

III. NOMENCLATURE

AR	Wing aspect ratio
b	Wing span
c	Local chord
C_D	Configuration drag coefficient
c_ℓ	Section lift coefficient
$C_{L_{W_B}}$	Wing-body lift coefficient based on wing trapezoidal area
C_{L_W}	Wing lift coefficient based on exposed wing trapezoidal area
C_p	Pressure coefficient
ΔC_{D_i}	Incremental induced drag coefficient
C_{mac}	Mean aerodynamic chord
M_o	Free stream Mach number
M_L	Local Mach number
$P_{T/P_{T_0}}$	Propeller total pressure to freestream total pressure ratio
R_{e_c}	Reynolds number based on chord
RPM	Revolutions per minute
r/R	Propeller blade local radius divided by maximum radius
$S_{TRAP_{EXP}}$	Exposed trapezodial reference area
t/c	Wing thickness to chord ratio
x,y,z	Coordinate system x streamwise, y spanwise, z vertical
x/c	Fraction of local chord
α	Configuration angle of attack measured relative to fuselage reference plane
α_s	Swirl angle, degrees
β	propeller blade angle setting, degrees
η	Percent semispan of wing

λ	Taper ratio
$\Lambda c/4$	Wing quarter chord sweep

IV. DESCRIPTION OF THE MODEL

A photograph of the model is shown in Figure 1. The wing coordinates were obtained from Douglas Aircraft. The wing had been tested previously as part of the Douglas Aircraft supercritical wing development program and had demonstrated good drag rise characteristics near M_o = 0.8. The design also had been used previously as part of an earlier NASA sponsored test where the propeller onset flow had been simulated by using an ejector powered flow through nacelle mounted ahead of the wing (Reference 7 and Figure 2). The planform of the NASA model with the nacelle installed is shown in Figure 3 including the location of pressure rows to be discussed later. Coordinates for the wing are given in Table 1 and Figure 4 shows a side view of the nacelle.

The propeller was an SR-2C design (Reference 8) and was powered by an air driven turbine. Air to power the turbine was supplied through the floor and wing and exhausted under the wing through a nozzle at about 50% chord.

Page Intentionally Left Blank

V. ANALYSIS OF THE DATA

Force Data

Analysis by NASA and Douglas determined that the force data for this test was not reliable. Subsequent analysis by NASA did result in some usable force data, but for the purposes of the work described in this report the force data will not be referred to.

Pressure Data

The pressure data on the wing were integrated to obtain the wing lift coefficient (C_{L_W}), and these results are shown on Figure 5. The analysis will focus on an angle of attack of 2 degrees or a C_{L_W} near 0.5.

The pressure distributions on the wing are shown in Figures 6 through 12 for a fixed propeller blade angle of 57°. Figures 6 through 10 show the flow development for a fixed angle of attack of 2° and Figures 11 and 12 show the variation with angle of attack at $M_0 = 0.8$. The data indicates that there is a significant effect of the nacelle on the pressures inboard of the nacelle at 36.5 and 41.5 percent semispan, but that there is a negligible effect outboard of the nacelle. The pressure distributions indicate that small separations may occur inboard due to the nacelle installation, and at $M_0 = 0.8$, a normal shock is indicated. Available oil flow photographs shown in Figures 13 and 14 indicate that the flow has been significantly disturbed by the nacelle but large regions of flow separation are not apparent. The presence of the normal shock inboard of the nacelle can be seen in Figure 14.

When full propeller power is added, the flow velocities are increased in the propeller wash region (included on the figures) and there is also a change in the local angle of attack. The isolated propeller flow one blade chord downstream of the propeller is shown in Figure 15. (These data were not part of the current test but were measured separately as part of NASA's propeller development program.) The propeller rotation for this test created increased wing section angle of attack inboard of the nacelle (upwash) and decreased angle of attack outboard (downwash). The pressure distributions on the wing due to power show increased upper surface pressure peaks and as the Mach number is increased, the presence of a flow spearation becomes more apparent. Available oil flow photographs with power-on, shown in Figures 16 and 17, illustrate clearly that there is a significant flow separation and extreme inboard flow from the outboard region of the nacelle.

The section lift data obtained by integrating the above pressure distributions (and removing obviously bad points) are shown in Figures 18 and 19. The installation of the nacelle reduces the c_ℓ at the inboard stations with little effect outboard. The windmilling propeller reduces the c_ℓ further probably due to a loss in dynamic pressure. The application of power significantly increases the c_ℓ values inboard due to propeller upwash and increases the velocity to levels which caused the flow separations. Outboard the c_ℓ is reduced because of the propeller downwash.

At M_o = 0.7, the c_ℓ data (solid symbols Figure 20) was used to calculate the induced drag increment due to the nacelle installation by a Trefftz plane method. The increment was found to be 12 counts (ΔC_{D_i} = 0.0012).

To summarize these results for later reference during the wing redesign discussion (Section VII), the region outboard of the nacelle is not seriously affected by the installation of the nacelle or power and wing modifications are not required in this region. However, inboard the nacelle significantly increases the upper surface pressure peaks but not to levels that cause large flow separations. However, a significant 12 count induced drag penalty was calculated. At M_o = 0.8, a small normal shock is present near the nacelle on the wing, further contributing to the drag. The increased flow velocity and upwash due to power are sufficient to increase upper surface pressure levels and c_ℓ's to conditions where attached flow can not be maintained by the original wing design.

Comparison With Simulator Data (Reference 7).

It was found that the flow from the ejector powered simulator most nearly matched the 59^o blade angle data (Figure 21), therefore the comparisons are made for this blade angle. Since the simulator test did not have a nacelle mounted on the wing, only incremental effects due to power from each test are compared.

Figures 22 through 27 compare the pressure distributions and span loads between the two tests at M_o = 0.7 and 0.8. Qualitatively the pressure distributions agree fairly well, with the peak pressure levels and the general shape of the plots being very similar. It is interesting to note that the pressure increase near 60% chord at 50% semispan on the upper surface due to power is indicated in both sets of data (Figure 25).

The incremental c_ℓ values are not as large for the simulator test as for the propeller test as shown on Figures 26 and 27. However, the c_ℓ levels with power are comparable.

Page Intentionally Left Blank

VI. COMPARISON WITH THEORY

Lifting Line Program

The lifting line program is a method which uses a vortex filament at the quarter chord point at several spanwise locations on the wing and a control point at the three-quarter chord location. The wing zero-lift-line and the propeller onset flow are input. The nacelle geometry cannot be input. The strength of the vortex is then determined to satisfy the condition of tangential flow at the control point. Forces are calculated by repeated application of the Kutta-Joukowski law. This theory is compared to the simulator data in Figures 28 and 29. Agreement with the clean wing is good but the increments due to power are overpredicted. Both positive (up-inboard) and negative (up-outboard) swirl cases are shown.

Comparisons with the propeller data are shown in Figures 30 and 31. Increments due to the nacelle taken from the previous Figures (18 and 19) are indicated. At M_0 = 0.7, the clean wing data is below predictions inboard in contradiction to the data measured for the simulator case, suggesting a difference in wing geometry. This may have been caused by a difference in wing twist under load caused by the difference in wing fabrication methods or scale. The powered data are well predicted except in the region immediately outboard of the nacelle. At M_0 = 0.8 the same conclusions apply except the clean wing data is underpredicted outboard, again suggesting a difference in wing twist.

In summary, the powered data for the simulator is underpredicted by the theory perhaps because of the presence of the ejector nacelle or nacelle

boundary layer flowing over the wing. Powered predictions for the propeller are generally good except just outboard of the nacelle. Nacelle interferences, not included in the theory, may cause this discrepancy.

Neumann Theory

The Neumann program is an incompressible surface panel solution using unknown source and dipole singularities to satisfy the zero normal flow condition at control points located in a number of panels describing the body surface (Reference 9). In regions washed by the propeller, the propeller onset flow is input at each affected control point to be included with the free stream flow when the singularity strengths are found. The program can calculate flows about completely arbitrary configurations.

The program contains the option of using the Goethert correction for compressibility. However, when this option is applied, the zero normal flow boundary condition is not exactly satisfied. Because of the complex geometries dealt with and the small included angles between some body surface panels, the compressibility option was not employed in order to avoid potential numerical errors in some cases.

A description of the paneling used for the simulator case is shown in Figure 32. The results are shown in Figures 33 and 34. (The Neumann program is compared to the data at the same configuration C_{L_W}. Since the Neumann program did not include viscous effects, the same C_{L_W} is achieved at an angle of attack 1^0 less than the data, Figure 5.) The pressure distributions generally agree well but the upper surface peaks near the leading edge are underpredicted. Agreement is good if incremental effects are compared. The section lift agreement is good with the exception of the power and swirl case at 35% semispan.

The paneling for the propeller case is shown in Figure 35. The circular body extending aft of the wing trailing edge is the representation of the exhaust flow. The pressure distributions inboard and outboard of the nacelle for the clean wing, wing plus nacelle and wing plus nacelle plus power are shown in Figures 36 through 41. (Again, note the 1^{o} angle difference. The powered data are for $\beta = 57^{o}$, run 69). The agreement of the theory with the data is good. The experimental separation inboard of the nacelle with power can be easily identified in Figure 38.

The section lift distribution data (Figure 42) does not agree as well. Neither the level nor the increments are reasonably predicted inboard of the nacelle but outboard the agreement is better. The disagreement inboard may be caused by local separations and transonic flows not correctly included in the theory.

The Neumann pressure distributions are compared to the data at the same angle of attack as the data (2^{o}) in Figures 43 through 48.

Jameson Theory

The Jameson Theory is a fully transonic solution restricted to wings only. The wing is mapped into a computational plane and the full compressible potential flow equations are solved (Reference 10).

The Jameson theory agreement with the data for the clean wing is excellent as shown on Figures 49 and 50. To approximately account for propeller onset flow effects, the wing was twisted in accordance with the propeller swirl and an incremental free stream Mach number was applied to account for slipstream velocity increases. The nacelle effect is not

accounted for. These results are shown in Figures 51 through 56. As noted, if the incremental Mach effect is not included, the agreement between the theory and data is adequate to be used for design purposes.

The Jameson theory, applied in the manner discussed above, was the primary method used to design the modified wings described in the next section. This computer code was used because it is a transonic method and would give an adequate representation of the transonic flow development. However, nacelle effects are not properly accounted for and the Neumann computer code was used to include these effects. Uncertainty exists by using either program because of a limitation in the geometry capability (lack of a nacelle in Jameson) or transonic flow computational capability (Neumann). These factors will be discussed further during the discussion of the wing design in the next section.

VII. DESIGN PHILOSOPHY

Design Criteria

To reduce upper surface separations (Figures 16 and 17) and subsequent degredations in wing performance, it was necessary to reduce the magnitude of the high negative pressures on the wing upper surface inboard of the nacelle (Figures 7 and 9) and reduce the wing c_ℓ values (Figures 18 and 19) to acceptable design limits. Since the clean original wing performed well and did not have any flow separations, the clean wing data was used to establish the design criteria. These criteria were minimum upper surface pressure levels, chordwise pressure gradients and spanwise upper surface isobar patterns. The c_ℓ levels at any span station and the distribution of c_ℓ as it affects induced drag were also used. The objective of the redesign work was to achieve levels on the new wing which were equal to or less than the above criteria.

Wing Redesign

The airfoil section shape inboard of the nacelle was modified to conform to the above described criteria within the constraints of the existing hardware. No problems were identified outboard of the nacelle so no modifications were made there. The hardware constraints were that the airfoil remain unchanged except for the forward or aft 20 to 25% of the chord.

Modified airfoils that fit within the existing planform could not be found which conformed to the design criteria. Therefore, a leading or trailing edge extension was required. A trailing edge extension was ruled out because of diffuculities with the aft pressure gradients and unsweeping

of the isobars. Therefore, a 15% leading edge extension was selected as shown on Figure 57. The closer proximity of the propeller to the leading edge is a concern and may shorten useable propeller test time.

The airfoil section for the modified planform was developed to reduce upper surface peaks and gradients at transonic conditions (M_0 = 0.8, C_{L_w} = 0.5) and fair smoothly into the existing airfoil shape at about 25% chord. The airfoil shapes were developed using a 2-D transonic analysis method prior to 3-D analysis to insure a pressure distribution over the entire airfoil that conformed to accepted design practice. The 3-D Jameson computer code was used to evaluate the various designs in three dimensions.

Two of the best designs developed are shown in Figures 58 through 62, and are identified as Mod 2 and Mod 3. The η= 0.12 section shape is the same for either Mod. The Jameson results with and without power, compared to the original wing, are shown in Figures 63 and 64. Mod 3 has pressure peaks near the leading edge about half of the original wing and the transonic flow over the entire upper surface is free of shock waves even with power. The C_p levels with power are less than the clean original wing, the gradients are less and constant C_p levels occur at similar x/c values indicating swept isobar patterns. Mod 2 has higher nose peaks than Mod 3 but, as will be discussed, Mod 2 may be less sensitive to nacelle interferences. The spanwise distribution of lift is shown on Figure 65 and the c_ℓ values are less everywhere than for the clean original wing. The desired spanwise distribution of lift to reduce induced drag could not be achieved.

Incompressible Jameson solutions at M_0 = 0.1 were calculated for reference to subsequent discussions of the incompressible Neumann solutions to follow which calculated results for the wing/fuselage and the nacelle.

The Jameson results are shown in Figures 66 and 67. Note that the Mod 3 design has higher nose peaks than Mod 2. However, the transonic development of Mod 3 was much better than Mod 2 indicating that at the design condition of M_0 = 0.8, Mod 3 will be the better design.

The incompressible Neumann solutions for the 3 wings (original wing, Mod 2, and Mod 3) with and without the nacelle and power at the 37% semispan station are shown in Figures 68, 69 and 70. In all cases, Mod 3 has lower pressure coefficients and gradient levels near the leading edge on the upper surface than the clean original wing, and it is also better than Mod 2.

The same data presentation is shown at the 41% semispan station in Figures 71, 72 and 73. At this station, the Mod 3 design significantly reduces the negative C_p peaks compared to the original wing, especially with power as shown in Figure 73. However, the negative C_p peaks are higher than the original wing without nacelle and power and are higher than Mod 2 with nacelle and power. The uncertainty here is whether the results shown at the 41% semispan would also occur at transonic conditions. The Mod 3 results were worse in the Jameson code at freestream conditions similar to the Neumann solution (M_0 = 0) but the pressure distribution development into the transonic region (M_0 = 0.8) was better. Since a transonic code including the nacelle body was not available for this study, the transonic development in the presence of the nacelle could not be evaluated. Since the Mod 3 design is better at 37% semispan using the Neumann and is better everywhere at transonic conditions as evaluated in the Jameson, it has been selected as the preferred design and is recommended for test. If the adverse effects nearer the nacelle (41%) occur during test, these effects can be treated locally with a small fillet.

To evaluate whether or not the pressure peak calculated for Mod 3 at 41% semispan will cause a flow separation, the results shown on Figure 72 are compared to the power-off flow visualization photos on Figures 13 and 14. The flow photos did not indicate a large region of flow separation although a limited normal shock was indicated at $M_o = 0.8$. The pressure peak calculated by the Neumann at these conditions was -1.4 as shown on Figure 72. Therefore, a -1.4 C_p should be marginally acceptable to avoid significant flow separation.

The peak C_p for Mod 3 with nacelle and power calculated by the Neumann is -1.4 as shown on Figure 73. This level indicates that flow conditions similar to the power-off case on the original wing would occur (like Figure 13 and 14) and the powered performance of Mod 3 should be acceptable.

Figure 74 shows results for all the configurations and conditions at 56% semispan. In all cases, the pressure distributions are more favorable than the original wing.

The spanwise distribution of lift for all cases is shown in Figure 75. The desired c_ℓ values (less than the original wing) are achieved inboard of the nacelle for either Mod 2 or 3.

To amplify the conclusions drawn and to indicate sensitivity to angle of attack, the Neumann results are shown at 1^o higher angle of attack in Figures 76 through 81. All the conclusions drawn previously apply to these data. Note that in Figure 79, Mod 3 has a higher negative C_p at the nose without nacelle and power than Mod 2, just like the Jameson results.

Nacelle Contouring

The streamlines about the isolated wing computed using the Neumann program are shown in Figures 82 and 83.

Underwing Nacelle - The nacelle geometry for this case was constrained to adding fairings to the existing nacelle or contouring aft of the motor so that installation of the air drive motor would be assured.

The aft part of the nacelle and nozzle centerline were contoured to the lower surface streamline as indicated in Figure 84. This contouring did not produce adequate favorable effects to warrant further consideration as shown in Figure 85.

Limited contouring of the nacelle was developed using the upper surface streamlines. As indicated in Figure 83, no contouring is possible inboard of the nacelle because of the relationship of the wing leading edge and rotating hub and propeller. A local fillet can be used outboard to fair between the nacelle and the wing leading edge. In the profile view (Figure 82) a local "bump" on the nacelle upper surface in the region of the wing leading edge will make the nacelle conform more closely with the streamline. The two fairings are shown by photographs of a subscale mock-up in Figure 86.

These limited fairings probably won't have a significant impact on the performance. The geometric limitations precluded contouring to the extent necessary. These fairings can be tested in the tunnel depending on test results of the modified wing and basic nacelle.

Overwing Nacelle - An overwing nacelle was also considered and is shown in Figure 87. For this case, the approach was to aerodynamically contour the nacelle and then determine if the air drive motor can be installed. Since this work was done in parallel with the development of Mod 3, the original

wing was used. Also, because the objective of this work was to evaluate what can be achieved by nacelle contouring with the power effects being treated using wing modifications, the power effects were not included.

The contouring was accomplished by maintaining the longitudinal cross-sectional area distribution of the nacelle to give the best chance of the motor fitting inside. The centers of these areas were shaped to conform to the flow streamlines. The resulting nacelle shape is shown in Figures 88 and 89. The contouring achieved excellent results as shown in Figures 90 through 92. At the 43% semispan location, the upper surface pressure peak and gradient with the nacelle installed is significantly less than for the non-contoured nacelle case and is almost identical to the original wing without the nacelle. Significantly better span loading is also achieved as shown in Figure 93, which should provide significantly less induced drag. It is recommended that this contoured nacelle and the non-contoured nacelle be tested to confirm these results.

VIII. DESIGN MODIFICATIONS

The wing coordinates for Mod 3 are given at 10 spanwise locations in Table 2. These coordinates conform to the existing wing at approximately 25% of the original wing chord. The geometry of the overwing contoured nacelle has been given to NASA Ames in the form of a computer tape containing a parametric cubic definition of the nacelle. The plan and profile view were shown in Figures 88 and 89.

Page Intentionally Left Blank

IX. CONCLUSIONS AND RECOMMENDATIONS

The following conclusions are drawn from this study:

1) The force data could not be used during this study because of uncertainties in accuracy.

2) Both the nacelle and power had significant effects on the wing flow. With power, the upper surface of the wing was separated at a wing C_{L_W} near 0.5.

3) The increments in the pressure data due to power agreed fairly well between the earlier simulator test and the propeller test. The absence of a nacelle in the simulator test makes a direct comparison impossible.

4) The Lifting Line computer code agreed better with the propeller power-on data than with the previous simulator data. This program could be used for preliminary design purposes.

5) The Neumann Surface Panel computer code predicted the wing surface pressure distributions with sufficient accuracy for design purposes. The agreement with the propeller model Cp distributions was excellent. The c_ℓ values were not predicted as well.

6) The Jameson Transonic Program gives results adequate for design purposes if the power effects are accounted for by wing twist.

7) A new wing planform and new airfoil sections were developed (Mod 3). At $M_o = 0.8$, the upper surface peak C_p values with power for this configuration are approximately half of the original wing with power. The pressure distribution is shock free and should result in performance with power approaching that of the original clean wing without power. Some uncertainty is present regarding the effects of the nacelle on this wing at transonic speeds. It is recommended that test data on Mod 3 be obtained to evaluate its performance.

8) A contoured upper surface nacelle was developed for the original wing which can be installed on the wing without producing any appreciable interference to the wing pressures. It is recommended that this nacelle be built and tested to evaluate performance.

X. REFERENCES

1. J. P. Hopkins, and H. E. Wharton, "Study of the Cost/Benefit Tradeoffs for Reducing the Energy Consumption of the Commercial Air Transportation System." (LR-27769-1, Lockheed-California Co.; NASA Contract NAS2-8612.) NASA CR-137927, 1976.

2. J. P. Hopkins, "Study of the Cost/Benefit Tradeoffs for Reducing the Energy Consumption of the Commercial Air Transportation System." (LR-27769-2, Lockheed-California Co.; NASA Contract NAS2-8612.) NASA CR-137926, 1976.

3. E. F. Kraus, and J. C. Van Abkoude, "Cost/Benefit Tradeoffs for Reducing the Energy Consumption of the Commercial Air Transportation System. Vol. I: Technical Analysis." (MDC-J7340-Vol.-1, Douglas Aircraft Co., Inc.; NASA Contract NAS2-8618.) NASA CR-137923, 1976.

4. Energy Consumption Characteristics of Transports Using the Prop-Fan Concept: Summary." (D6-75780, Boeing Commercial Airplane Co.; NASA Contract NAS2-9104.) NASA CR-137938, 1976.

5. "Energy Consumption Characteristics of Transports Using the Prop-Fan Concept: Final Report." (D6-75780, Boeing Commercial Airplane Co.; NASA Contract NAS2-9104.) NASA CR-137938, 1976.

6. I. M. Goldsmith, "A Study to Define the Research and Technology Requirements for Advanced Turbo/Propfan Transport Aircraft." (Douglas Aircraft Company; NASA Contract NAS2-10178) NASA CR 166138, February 1981.

7. H. R. Welge, and J. P. Crowder, "Simulated Propeller Slipstream Effects on a Supercritical Wing." (Douglas Aircraft Company; NASA Contract NAS2-9472.) NASA CR-152138, June 1978.

8. R. J. Jeracki, D. C. Mikkelson, and B. J. Blaha, "Wind Tunnel Performance of Four Energy Efficient Propellers Designed for Mach 0.8 Cruise." NASA TM-79124, April 1979.

9. Hess, J. L.: The Problem of Three-Dimensional Lifting Potential Flow and Its Solution by Means of Surface Singularity Distribution, Computer Methods in Applied Mechanics and Engineering, Vol. 4, 1974, pp. 283-319.

10. Henne, P. A.: Transonic Wing Analysis Using Advanced Computational Methods, AIAA Paper 78-105, 1978.

TABLE 1
ORIGINAL AIRFOIL COORDINATES

X IS IN WRP / Z CHORD	UPPER SURFACE							
	12 Z X = 10.5904		35 Z X = 30.8888		70 Z X = 61.7775		100 Z X = 88.2537	
	Y	Z	Y	Z	Y	Z	Y	Z
100 Z	30.2101	-6.1735	50.9467	-2.0879	63.1242	-1.1630	73.5625	-.4263
97.5	49.1409	-5.9629	50.2149	-1.8628	62.6302	-1.0284	73.2718	-.3584
95.	48.0713	-5.7071	49.4831	-1.6549	62.1359	-.8976	72.9810	-.2963
92.5	47.0017	-5.4580	48.7513	-1.4684	61.6415	-.7803	72.6899	-.2378
90.	45.9325	-5.1671	48.0199	-1.3004	61.1472	-.6756	72.3992	-.1856
85	43.7933	-4.6320	46.5562	-1.0053	60.1584	-.4940	71.8177	-.0981
80.	41.6545	-4.1119	45.0926	-.7517	59.1701	-.3407	71.2362	-.0272
75	39.5157	-3.6142	43.6290	-.5358	58.1813	-.2128	70.6447	.0290
70	37.3769	-3.1441	42.1654	-.3529	57.1926	-.1077	70.0733	.0720
65	35.2377	-2.7030	40.7022	-.2055	56.2042	-.0243	69.4918	.1029
58.5	32.4571	-2.1741	38.7993	-.0595	54.9189	.0518	68.7357	.1263
55	30.9601	-1.9062	37.7749	.0022	54.2268	.0823	68.3285	.1316
50	28.8209	-1.5504	36.3113	.0639	53.1061	.1088	67.7470	.1312
45	26.6821	-1.2214	34.8477	.1011	52.2497	.1195	67.1655	.1228
40	24.5433	-.9193	33.3845	.1150	51.2610	.1150	66.5841	.1059
36	22.4041	-.6421	31.9209	.1037	50.2726	.0948	66.0022	.0809
30	20.2653	-.3900	30.4572	.0687	49.2839	.0573	65.4207	.0489
25	18.1264	-.1658	28.9936	.0004	48.2952	.0004	64.8393	0
20	15.9876	.0243	27.5300	-.0967	47.3064	-.0783	64.2578	-.0573
15	13.8484	.1338	26.0668	-.2319	46.3346	-.1805	63.6763	-.1283
10	11.7096	.0386	24.6032	-.4220	45.3293	-.3187	63.0948	-.2188
7.5	10.6400	-.1251	23.8714	-.5517	44.8350	-.4142	62.8041	-.2768
5.	9.5708	-.3889	23.1396	-.7164	44.3406	-.5252	62.5130	-.3462
2.5	8.5012	-.8483	22.4077	-.9560	43.8466	-.6884	62.2223	-.4485
1.25	7.9664	-1.2578	22.0420	-1.1490	43.6992	-.8182	62.0771	-.5168
.5	7.6456	-1.6716	21.8222	-1.3324	43.4511	-.9391	61.9900	-.5866
.25	7.5386	-1.8911	21.7491	-1.4353	43.4015	-1.0067	61.9606	-.6237
.05	7.4633	-2.1671	21.6906	-1.5798	43.3622	-1.1019	61.9374	-.6767
0.00	7.4316	-2.3917	21.6759	-1.6625	43.3522	-1.1791	61.9315	-.7189
				LOWER SURFACE				
0.00	7.4316	-2.3917	21.6759	-1.6625	43.3522	-1.1791	61.9315	-.7189
.05	7.4533	-2.6185	21.6906	-1.8099	43.3622	-1.2656	61.9374	-.7605
.25	7.5386	-2.9817	21.7491	-1.9605	43.4015	-1.3837	61.7606	-.8141
.5	7.6456	-3.1456	21.8222	-2.0727	43.4511	-1.4269	61.9900	-.8542
1.25	7.9664	-3.6215	22.0420	-2.2622	43.5992	-1.5629	62.0771	-.9284
2.5	8.5012	-4.1920	22.4077	-2.5174	43.8466	-1.7143	62.2223	-1.0089
5.	9.5708	-4.9467	23.1396	-2.8162	44.3406	-1.9050	62.5130	-1.1089
7.5	10.6400	-5.4873	23.8714	-3.0140	44.8350	-2.0285	62.8041	-1.1707
10.	11.7096	-5.8464	24.6032	-3.1621	45.3293	-2.1157	63.0948	-1.2151
15.	13.8484	-6.3087	26.0668	-3.3664	46.3346	-2.2414	63.6763	-1.2688
20.	15.9876	-6.5932	27.5300	-3.5013	47.3064	-2.3163	64.2578	-1.2967
25.	18.1264	-6.7653	28.9936	-3.5936	48.2952	-2.3649	64.8393	-1.3096
30.	20.2653	-6.8535	30.4572	-3.6565	49.2839	-2.3913	65.4207	-1.3100
35.	22.4041	-6.8843	31.9209	-3.6759	50.2726	-2.3979	66.0022	-1.2997
40.	24.5433	-6.8744	33.3845	-3.6873	51.2610	-2.3847	66.5841	-1.2784
45	26.6821	-6.8166	34.8477	-3.6517	52.2497	-2.3476	67.1656	-1.2445
50.	28.8209	-6.7770	36.3113	-3.5782	53.1061	-2.2855	67.7470	-1.1949
55.	30.9601	-6.7006	37.7749	-3.4428	54.2268	-2.1866	68.3285	-1.1266
58.5	32.4571	-6.6407	38.7993	-3.3213	54.9189	-2.0980	67.7357	-1.0648
65.	35.2377	-6.5234	40.7022	-3.0445	56.2042	-1.8914	69.4918	-.9321
70.	37.3769	-6.4326	42.1654	-2.7864	57.1926	-1.7069	70.0733	-.8134
75.	39.5157	-6.3422	43.6290	-2.5145	58.1813	-1.5129	70.6447	-.6899
80.	41.6545	-6.2869	45.0926	-2.2560	59.1701	-1.3276	71.2362	-.5783
85.	43.7933	-6.1841	46.5562	-2.0352	60.1584	-1.1692	71.8177	-.4705
90.	45.9325	-6.1307	48.0199	-1.8311	61.1472	-1.0619	72.3992	-.3977
92.5	47.0017	-6.1272	48.7513	-1.8727	61.6415	-1.0446	72.6899	-.3834
95.	48.0713	-6.1320	49.4831	-1.9036	62.1359	-1.0600	72.9810	-.3911
97.5	49.1409	-6.1566	50.2149	-1.9940	62.6302	-1.1170	73.2718	-.4846
100.	50.2072	-6.2327	50.9463	-2.1462	63.1246	-1.2218	73.5632	-.4837

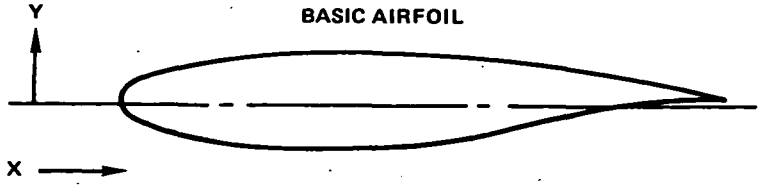

BASIC AIRFOIL

81-GEN-24220

Page Intentionally Left Blank

TABLE 2

MOD 3 WING COORDINATES

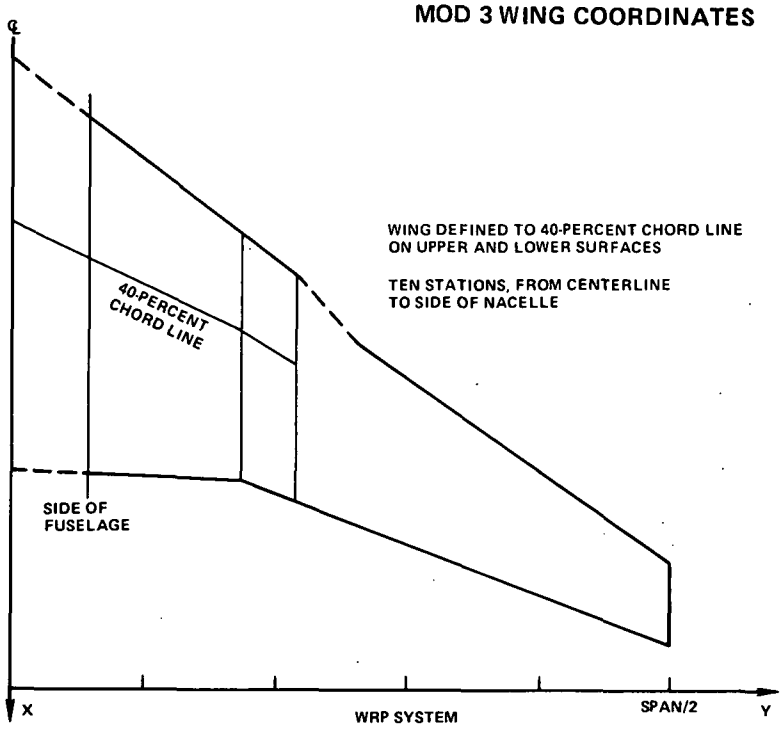

Y= 0.0

X	Y	Z
15.812060	0.0	-0.740680
14.054580	0.0	-0.460690
12.325220	0.0	-0.207010
10.630840	0.0	0.010970
8.978100	0.0	0.183100
7.373530	0.0	0.316320
5.823460	0.0	0.414910
4.333990	0.0	0.478790
2.911010	0.0	0.508770
1.560150	0.0	0.506260
0.286730	0.0	0.472290
-0.904210	0.0	0.407260
-2.007980	0.0	0.312010
-3.020230	0.0	0.187120
-3.936950	0.0	0.033570
-4.754530	0.0	-0.146090
-5.469750	0.0	-0.350210
-6.079780	0.0	-0.577320
-6.582210	0.0	-0.826880
-6.975060	0.0	-1.098890
-7.256770	0.0	-1.392240
-7.426250	0.0	-1.705150
-7.482820	0.0	-2.041560
-7.426250	0.0	-2.379360
-7.256770	0.0	-2.739880
-6.975060	0.0	-3.103160
-6.582210	0.0	-3.472570
-6.079780	0.0	-3.847270
-5.469750	0.0	-4.226230
-4.754530	0.0	-4.606940
-3.936950	0.0	-4.987230
-3.020230	0.0	-5.364220
-2.007980	0.0	-5.734170
-0.904210	0.0	-6.095380
0.286730	0.0	-6.445230
1.560150	0.0	-6.780510
2.911010	0.0	-7.098600
4.333990	0.0	-7.395130
5.823460	0.0	-7.666320
7.373530	0.0	-7.909590
8.978100	0.0	-8.120780
10.630840	0.0	-8.299130
12.325220	0.0	-8.412710
14.054580	0.0	-8.496420
15.812060	0.0	-8.542960

81-GEN-24215

TABLE 2 (CONT)

MOD 3 WING COORDINATES

Y=10.5904

X	Y	Z
21.010529	10.590440	-0.474080
19.501648	10.590440	-0.303140
18.016922	10.590440	-0.152090
16.562256	10.590440	-0.028640
15.143310	10.590440	0.063920
13.765720	10.590440	0.128370
12.434910	10.590440	0.167240
11.156130	10.590440	0.180550
9.934440	10.590440	0.168860
8.774670	10.590440	0.133300
7.681380	10.590440	0.075040
6.658910	10.590440	-0.005340
5.711270	10.590440	-0.106710
4.842210	10.590440	-0.228500
4.055160	10.590440	-0.370010
3.353230	10.590440	-0.529380
2.739190	10.590440	-0.705650
2.215450	10.590440	-0.897760
1.784100	10.590440	-1.104400
1.446820	10.590440	-1.325060
1.204950	10.590440	-1.558400
1.059440	10.590440	-1.801500
1.010880	10.590440	-2.057810
1.059440	10.590440	-2.314670
1.204950	10.590440	-2.585460
1.446820	10.590440	-2.859330
1.784100	10.590440	-3.137140
2.215450	10.590440	-3.417410
2.739190	10.590440	-3.698900
3.353230	10.590440	-3.979450
4.055160	10.590440	-4.257800
4.842210	10.590440	-4.532260
5.711270	10.590440	-4.800430
6.658910	10.590440	-5.061160
7.681390	10.590440	-5.312740
8.774670	10.590440	-5.553420
9.934440	10.590440	-5.781800
11.156130	10.590440	-5.995530
12.434910	10.590440	-6.192460
13.765720	10.590440	-6.371090
15.143320	10.590440	-6.529240
16.562241	10.590440	-6.661230
18.016922	10.590440	-6.762860
19.501648	10.590440	-6.834500
21.010529	10.590440	-6.877040

81 GEN-24221

TABLE 2 (CONT)
MOD 3 WING COORDINATES

	Y=13.9735	
X	Y	Z
22.670883	13.973500	-0.380840
21.241409	13.973500	-0.244560
19.834808	13.973500	-0.127530
18.456696	13.973500	-0.033600
17.112411	13.973500	0.033020
15.807320	13.973500	0.076130
14.546550	13.973500	0.094580
13.335060	13.973500	0.091360
12.177660	13.973500	0.065990
11.078910	13.973500	0.019470
10.043160	13.973500	-0.046970
9.074490	13.973500	-0.132730
8.176720	13.973500	-0.236570
7.353390	13.973500	-0.357910
6.607760	13.973500	-0.496880
5.942770	13.973500	-0.649450
5.361040	13.973500	-0.817250
4.864860	13.973500	-0.998650
4.456210	13.973500	-1.192140
4.136670	13.973500	-1.397610
3.907530	13.973500	-1.611980
3.769680	13.973500	-1.833570
3.723680	13.973500	-2.064290
3.769680	13.973500	-2.295470
3.907530	13.973500	-2.538880
4.136670	13.973500	-2.783540
4.456210	13.973500	-3.032290
4.864860	13.973500	-3.286660
5.361040	13.973500	-3.533300
5.942770	13.973500	-3.782090
6.607760	13.973500	-4.028850
7.353390	13.973500	-4.269810
8.176720	13.973500	-4.505470
9.074490	13.973500	-4.734050
10.043160	13.973500	-4.954100
11.078910	13.973500	-5.164330
12.177660	13.973500	-5.363710
13.335060	13.973500	-5.550510
14.546540	13.973500	-5.723140
15.807320	13.973500	-5.880490
17.112411	13.973500	-6.020890
18.456688	13.973500	-6.138830
19.834808	13.973500	-6.234190
21.241409	13.973500	-6.301640
22.670883	13.973500	-6.342700

	Y=17.3565	
X	Y	Z
24.331223	17.356491	-0.287610
22.981155	17.356491	-0.185980
21.652679	17.356491	-0.102070
20.351105	17.356491	-0.038560
19.081497	17.356491	0.002130
17.848892	17.356491	0.021900
16.658142	17.356491	0.021910
15.513960	17.356491	0.002170
14.420840	17.356491	-0.036870
13.383130	17.356491	-0.094350
12.404910	17.356491	-0.168980
11.490040	17.356491	-0.260130
10.642130	17.356491	-0.366440
9.864540	17.356491	-0.487330
9.160330	17.356491	-0.622160
8.532270	17.356491	-0.769520
7.982850	17.356491	-0.928850
7.514230	17.356491	-1.099550
7.128280	17.356491	-1.279870
6.826500	17.356491	-1.468970
6.610080	17.356491	-1.665400
6.479890	17.356491	-1.865650
6.436440	17.356491	-2.070780
6.479890	17.356491	-2.276280
6.610080	17.356491	-2.490700
6.826500	17.356491	-2.707750
7.128280	17.356491	-2.927450
7.514230	17.356491	-3.147920
7.982850	17.356491	-3.367700
8.532270	17.356491	-3.584740
9.160330	17.356491	-3.798300
9.864540	17.356491	-4.007360
10.642130	17.356491	-4.210510
11.490040	17.356491	-4.406950
12.404910	17.356491	-4.595460
13.383130	17.356491	-4.775250
14.420850	17.356491	-4.946620
15.513950	17.356491	-5.105490
16.658142	17.356491	-5.253830
17.848892	17.356491	-5.389890
19.081497	17.356491	-5.512540
20.351089	17.356491	-5.618440
21.652679	17.356491	-5.706510
22.981155	17.356491	-5.768890
24.331223	17.356491	-5.808360

81-GEN-24216

TABLE 2 (CONT)
MOD 3 WING COORDINATES

	Y=20.7396	
X	Y	Z
25.991608	20.739578	-0.194370
24.720947	20.739578	-0.127410
23.470596	20.739578	-0.076690
22.245560	20.739578	-0.043520
21.050620	20.739578	-0.028770
19.890518	20.739578	-0.031330
18.769791	20.739578	-0.050750
17.692982	20.739578	-0.087030
16.664078	20.739578	-0.139740
15.687400	20.739578	-0.208180
14.766710	20.739578	-0.291000
13.905650	20.739578	-0.387530
13.107610	20.739578	-0.496310
12.375750	20.739578	-0.616740
11.712960	20.739578	-0.748230
11.121840	20.739578	-0.889590
10.604740	20.739578	-1.040450
10.163680	20.739578	-1.200450
9.800420	20.739578	-1.367610
9.516390	20.739578	-1.540920
9.312700	20.739578	-1.718890
9.190160	20.739578	-1.897730
9.149270	20.739578	-2.077260
9.190160	20.739578	-2.257080
9.312700	20.739578	-2.443320
9.516390	20.739578	-2.631960
9.800420	20.739578	-2.822600
10.163680	20.739578	-3.013170
10.604730	20.739578	-3.202100
11.121840	20.739578	-3.387370
11.712960	20.739578	-3.568550
12.375750	20.739578	-3.744910
13.107610	20.739578	-3.915540
13.905650	20.739578	-4.079840
14.766710	20.739578	-4.236810
15.687400	20.739578	-4.386170
16.664078	20.739578	-4.527520
17.692982	20.739578	-4.660460
18.769791	20.739578	-4.784500
19.890518	20.739578	-4.899200
21.050620	20.739578	-5.004180
22.245560	20.739578	-5.097040
23.470596	20.739578	-5.176830
24.720947	20.739578	-5.239540
25.991608	20.739578	-5.274000

	Y=24.1227	
X	Y	Z
27.651993	24.122681	-0.101130
26.460739	24.122681	-0.068830
25.288528	24.122681	-0.051140
24.140930	24.122681	-0.048480
23.019780	24.122681	-0.059660
21.932144	24.122681	-0.084560
20.881454	24.122681	-0.123410
19.871057	24.122681	-0.176220
18.907318	24.122681	-0.242610
17.991669	24.122681	-0.322010
17.128525	24.122681	-0.413010
16.321259	24.122681	-0.514930
15.573100	24.122681	-0.626170
14.886970	24.122681	-0.746150
14.265590	24.122681	-0.874310
13.711420	24.122681	-1.009660
13.226630	24.122681	-1.152050
12.813130	24.122681	-1.301340
12.472570	24.122681	-1.455340
12.206290	24.122681	-1.612880
12.015320	24.122681	-1.772390
11.900450	24.122681	-1.929800
11.862110	24.122681	-2.083750
11.900450	24.122681	-2.237890
12.015320	24.122681	-2.395940
12.206290	24.122681	-2.556170
12.472570	24.122681	-2.717750
12.813130	24.122681	-2.878420
13.226630	24.122681	-3.036490
13.711420	24.122681	-3.190010
14.265590	24.122681	-3.338790
14.886970	24.122681	-3.482460
15.573100	24.122681	-3.620570
16.321259	24.122681	-3.752730
17.128525	24.122681	-3.878170
17.991669	24.122681	-3.997080
18.907318	24.122681	-4.109430
19.871057	24.122681	-4.215430
20.881454	24.122681	-4.315180
21.932144	24.122681	-4.408580
23.019780	24.122681	-4.495820
24.140930	24.122681	-4.575640
25.288528	24.122681	-4.648140
26.460739	24.122681	-4.703080
27.651993	24.122681	-4.739650

81-GEN-24217

TABLE 2 (CONT)
MOD 3 WING COORDINATES

Y=27.5057

X	Y	Z
29.312332	27.505692	-0.007890
28.200485	27.505692	-0.010250
27.106400	27.505692	-0.025680
26.034454	27.505692	-0.053440
24.988846	27.505692	-0.090660
23.973724	27.505692	-0.137790
22.993057	27.505692	-0.196070
22.050751	27.505692	-0.265410
21.150513	27.505692	-0.345480
20.295883	27.505692	-0.435830
19.490265	27.505692	-0.535020
18.736801	27.505692	-0.642320
18.038513	27.505692	-0.756040
17.398117	27.505692	-0.875560
16.818146	27.505692	-1.000390
16.300919	27.505692	-1.129730
15.848440	27.505692	-1.263650
15.462500	27.505692	-1.402240
15.144650	27.505692	-1.543080
14.896110	27.505692	-1.684830
14.717870	27.505692	-1.825890
14.610650	27.505692	-1.961880
14.574870	27.505692	-2.090240
14.610650	27.505692	-2.210590
14.717870	27.505692	-2.348570
14.896110	27.505692	-2.480380
15.144650	27.505692	-2.612910
15.462500	27.505692	-2.743680
15.848440	27.505692	-2.870900
16.300919	27.505692	-2.992650
16.818146	27.505692	-3.109040
17.398117	27.505692	-3.220010
18.038513	27.505692	-3.325610
18.736801	27.505692	-3.425630
19.490265	27.505692	-3.519530
20.295883	27.505692	-3.608800
21.150513	27.505692	-3.691340
22.050751	27.505692	-3.770410
22.993057	27.505692	-3.845870
23.973724	27.505692	-3.918090
24.988846	27.505692	-3.987470
26.034454	27.505692	-4.054250
27.106400	27.505692	-4.119470
28.200485	27.505692	-4.170240
29.312332	27.505692	-4.205310

Y=30.8888

X	Y	Z
30.972717	30.888779	0.085340
29.940262	30.888779	0.048330
28.924316	30.888779	-0.000220
27.928909	30.888779	-0.058400
26.957977	30.888779	-0.121450
26.015335	30.888779	-0.191020
25.104706	30.888779	-0.268730
24.229691	30.888779	-0.354600
23.393738	30.888779	-0.448350
22.600143	30.888779	-0.549650
21.852061	30.888779	-0.657840
21.152405	30.888779	-0.769720
20.503967	30.888779	-0.885910
19.909382	30.888779	-1.004880
19.370758	30.888779	-1.126460
18.890457	30.888779	-1.249810
18.470291	30.888779	-1.375260
18.111988	30.888779	-1.503140
17.816757	30.888779	-1.630810
17.585968	30.888779	-1.756790
17.420456	30.888779	-1.879390
17.320892	30.888779	-1.993960
17.287674	30.888779	-2.096730
17.320892	30.888779	-2.195500
17.420456	30.888779	-2.301190
17.585968	30.888779	-2.404590
17.816757	30.888779	-2.508060
18.111988	30.888779	-2.608930
18.470291	30.888779	-2.705300
18.890457	30.888779	-2.795290
19.370758	30.888779	-2.879290
19.909382	30.888779	-2.957560
20.503967	30.888779	-3.030640
21.152405	30.888779	-3.098530
21.852061	30.888779	-3.160890
22.600143	30.888779	-3.218920
23.393738	30.888779	-3.273250
24.229691	30.888779	-3.325390
25.104706	30.888779	-3.376550
26.015335	30.888779	-3.427500
26.957977	30.888779	-3.479120
27.928909	30.888779	-3.532850
28.924316	30.888779	-3.590800
29.940262	30.888779	-3.637390
30.972717	30.888779	-3.670970

81-GEN-24218

TABLE 2 (CONT)
MOD 3 WING COORDINATES

Y=34.4630

X	Y	Z
33.245972	34.462982	0.088360
32.258194	34.462982	0.051400
31.286209	34.462982	0.005540
30.333862	34.462982	-0.049490
29.404938	34.462982	-0.109650
28.503098	34.462982	-0.176630
27.631866	34.462982	-0.252210
26.794708	34.462982	-0.335920
25.994919	34.462982	-0.427360
25.235672	34.462982	-0.525990
24.519943	34.462982	-0.630460
23.850571	34.462982	-0.740110
23.230194	34.462982	-0.853460
22.661255	34.462982	-0.970360
22.146011	34.462982	-1.090500
21.686493	34.462982	-1.212340
21.284500	34.462982	-1.335360
20.941635	34.462982	-1.459190
20.659241	34.462982	-1.588840
20.438446	34.462982	-1.699460
20.280090	34.462982	-1.814020
20.184845	34.462982	-1.922480
20.153076	34.462982	-2.021910
20.184845	34.462982	-2.121340
20.280090	34.462982	-2.218250
20.438446	34.462982	-2.315170
20.659241	34.462982	-2.412840
20.941635	34.462982	-2.508740
21.284500	34.462982	-2.601290
21.686493	34.462982	-2.688630
22.146011	34.462982	-2.770520
22.661255	34.462982	-2.846540
23.230194	34.462982	-2.917570
23.850571	34.462982	-2.983670
24.519943	34.462982	-3.044670
25.235672	34.462982	-3.101580
25.994919	34.462982	-3.154980
26.794708	34.462982	-3.206790
27.631866	34.462982	-3.256060
28.503098	34.462982	-3.303280
29.404938	34.462982	-3.351330
30.333862	34.462982	-3.400260
31.286209	34.462982	-3.451680
32.258194	34.462982	-3.493250
33.245972	34.462982	-3.522940

Y=38.0373

X	Y	Z
35.519333	38.037338	0.087380
34.576218	38.037338	0.054470
33.648193	38.037338	0.011200
32.738922	38.037338	-0.040580
31.852005	38.037338	-0.097840
30.990952	38.037338	-0.162240
30.159134	38.037338	-0.235680
29.359833	38.037338	-0.317230
28.596207	38.037338	-0.406380
27.871292	38.037338	-0.502320
27.187943	38.037338	-0.603880
26.548943	38.037338	-0.710500
25.956528	38.037338	-0.821020
25.413315	38.037338	-0.935750
24.921371	38.037338	-1.054550
24.482635	38.037338	-1.174870
24.098831	38.037338	-1.295460
23.771469	38.037338	-1.415240
23.501846	38.037338	-1.530870
23.291031	38.037338	-1.642130
23.139847	38.037338	-1.748660
23.048904	38.037338	-1.851010
23.018585	38.037338	-1.947090
23.048904	38.037338	-2.043170
23.139847	38.037338	-2.135310
23.291031	38.037338	-2.225760
23.501846	38.037338	-2.317620
23.771469	38.037338	-2.408560
24.098831	38.037338	-2.497290
24.482635	38.037338	-2.581960
24.921371	38.037338	-2.661750
25.413315	38.037338	-2.735510
25.956528	38.037338	-2.804490
26.548943	38.037338	-2.868810
27.187943	38.037338	-2.928460
27.871292	38.037338	-2.984240
28.596207	38.037338	-3.036550
29.359833	38.037338	-3.086180
30.159134	38.037338	-3.133570
30.990952	38.037338	-3.179060
31.852005	38.037338	-3.223530
32.738922	38.037338	-3.267650
33.648193	38.037338	-3.312560
34.576218	38.037338	-3.349110
35.519333	38.037338	-3.374900

81-GEN-24219

81-GEN-23245

FIGURE 1. NASA MODEL INSTALLED IN AMES 14-FOOT TUNNEL

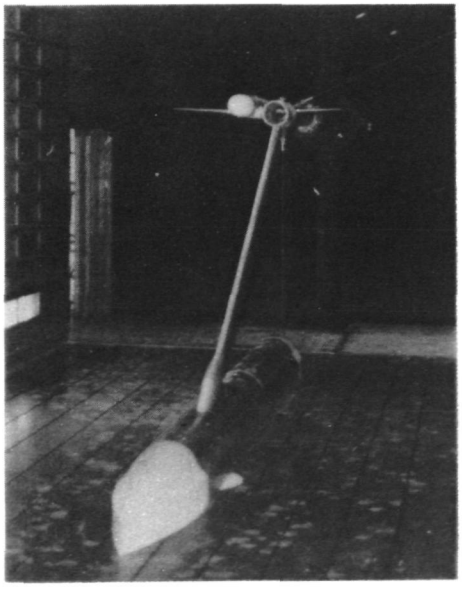

FROM UPSTREAM OF THE MODEL

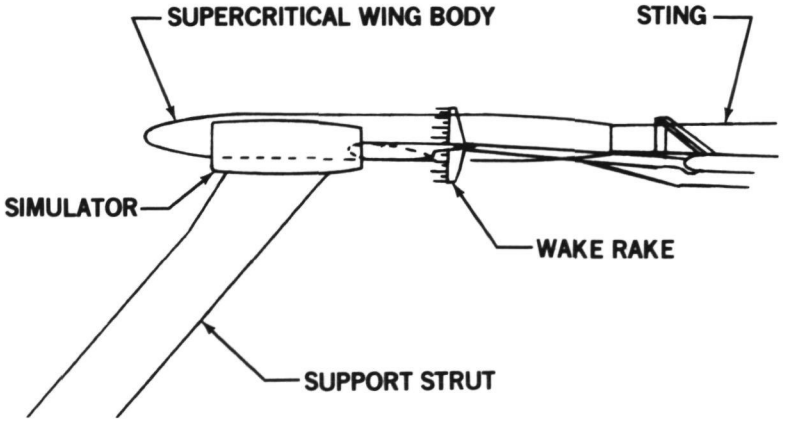

81-GEN-23244

FIGURE 2. SIMULATOR TEST INSTALLATION

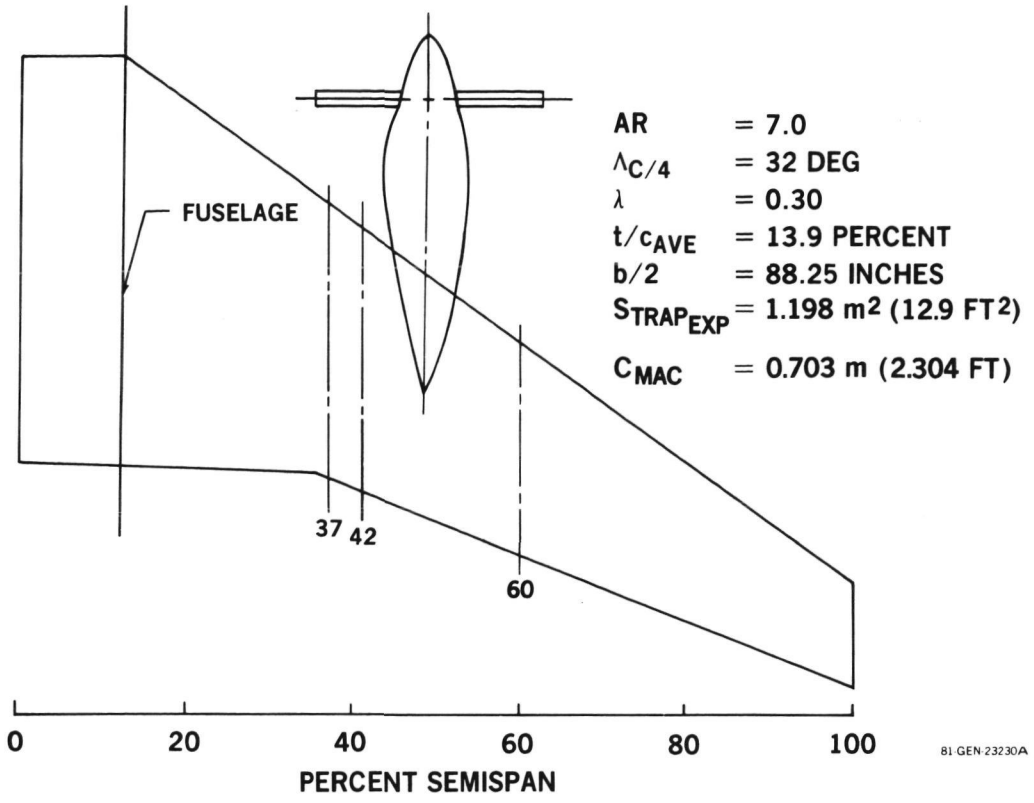

FIGURE 3. NASA MODEL PLANFORM

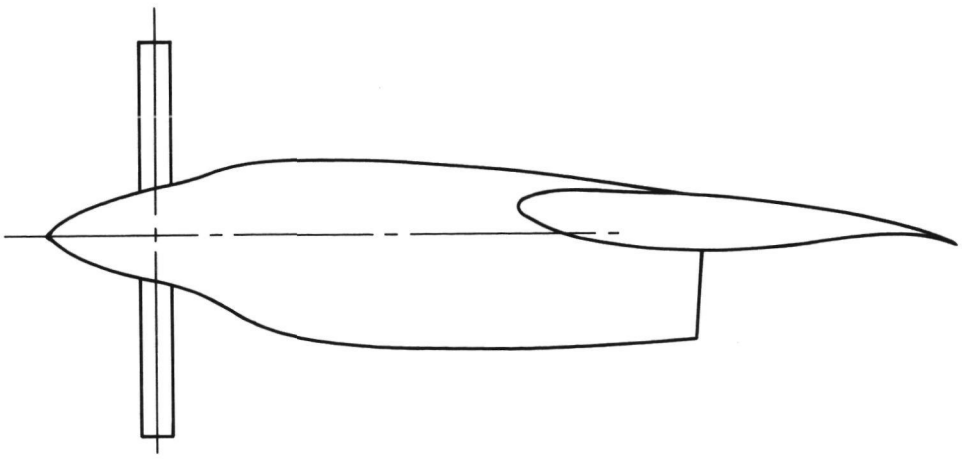

81 GEN 23204

FIGURE 4. SIDE VIEW OF UNDERWING NACELLE

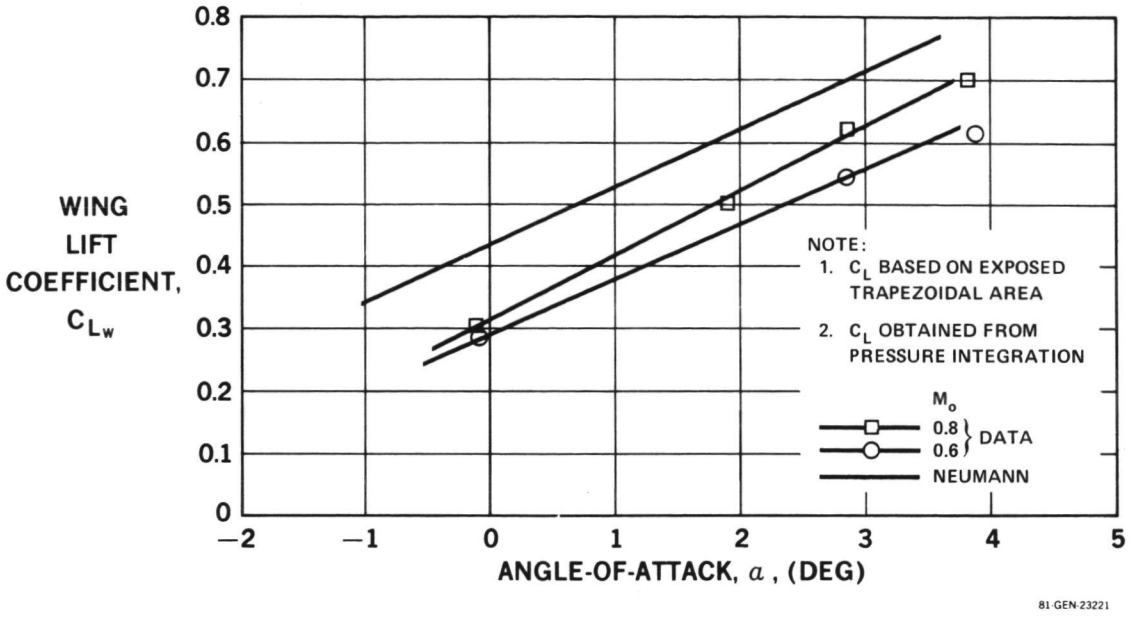

FIGURE 5. WING LIFT CURVES

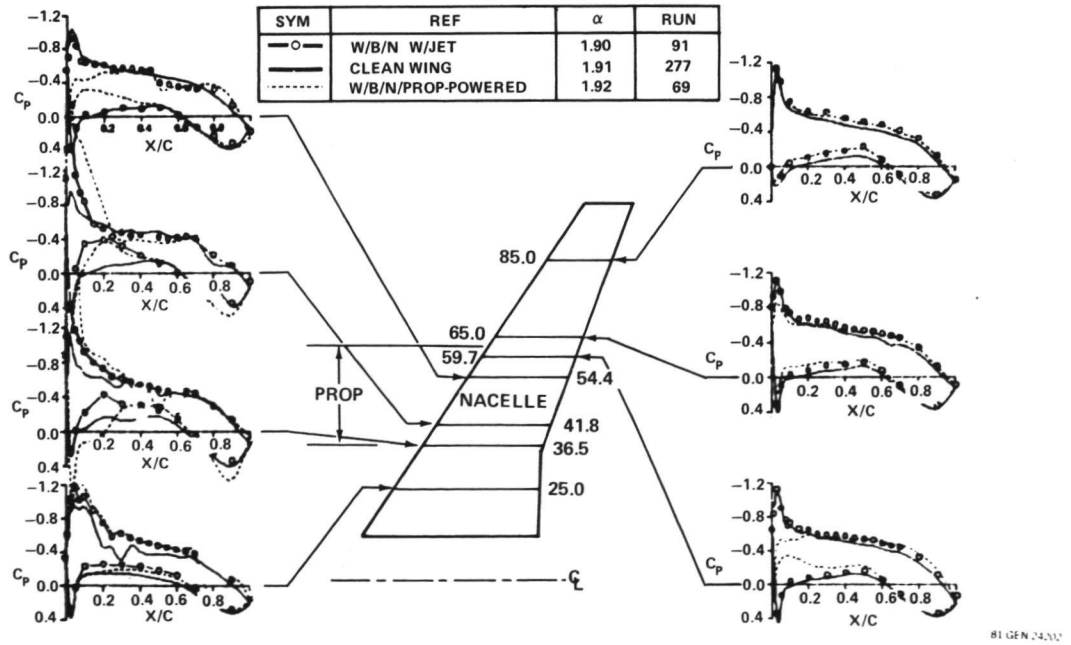

FIGURE 6. CHORDWISE PRESSURE DISTRIBUTION FOR ORIGINAL TURBOPROP CONFIGURATION AT M_o = 0.6

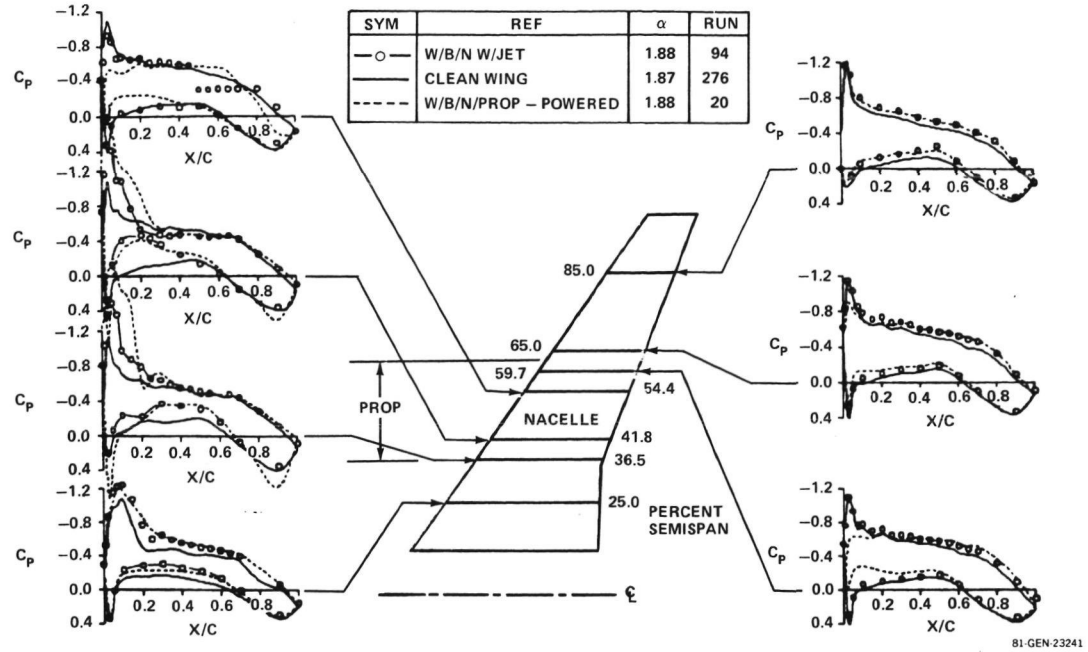

FIGURE 7. CHORDWISE PRESSURE DISTRIBUTIONS FOR ORIGINAL TURBOPROP CONFIGURATIONS AT M_o = 0.7

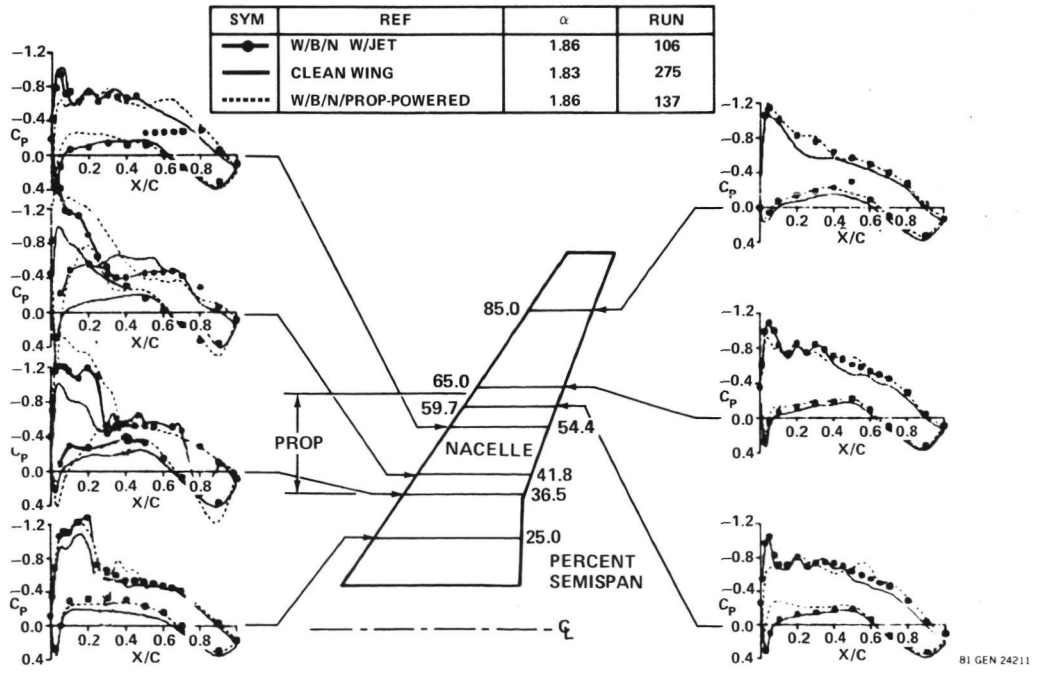

FIGURE 8. CHORDWISE PRESSURE DISTRIBUTION FOR ORIGINAL TURBOPROP CONFIGURATION AT M_o = 0.78

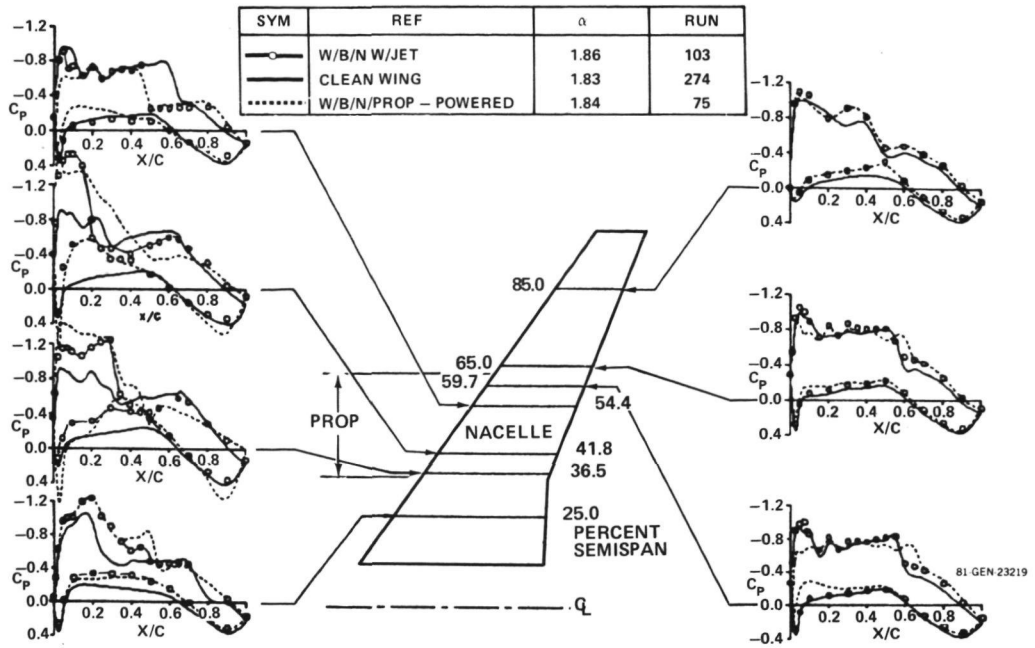

FIGURE 9. CHORDWISE PRESSURE DISTRIBUTIONS FOR ORIGINAL TURBOPROP CONFIGURATION AT M_o = 0.8

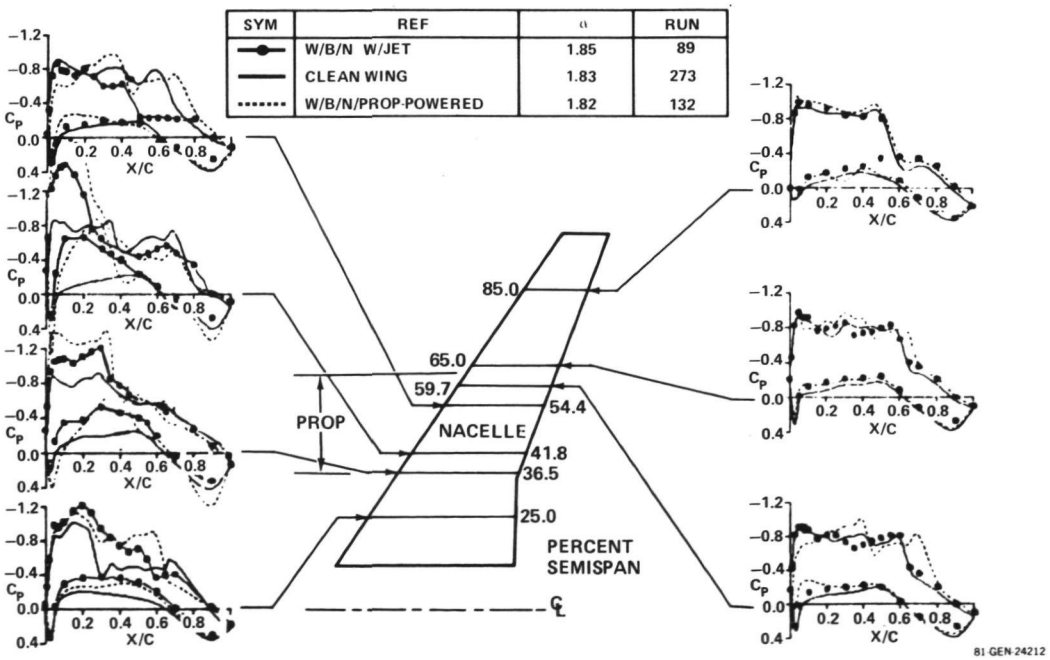

FIGURE 10. CHORDWISE PRESSURE DISTRIBUTION OR ORIGINAL TURBOPROP CONFIGURATION AT M_o = 0.82

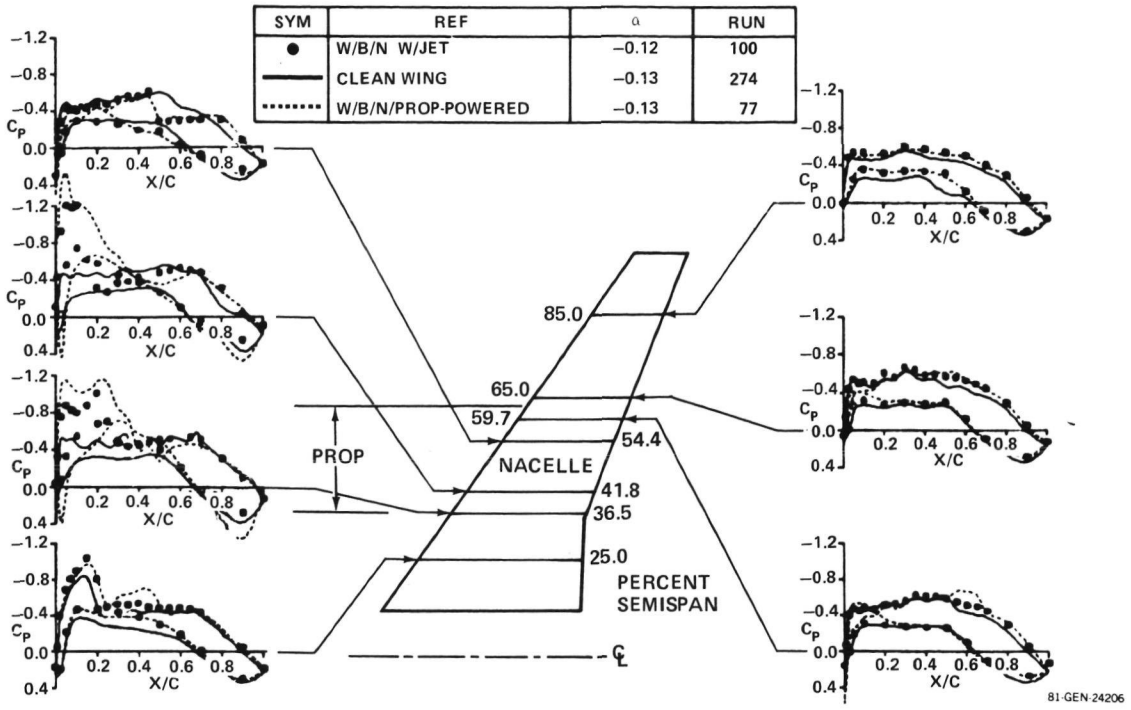

FIGURE 11. PRESSURE DISTRIBUTION AT REDUCED ANGLE OF ATTACK FOR M_o = 0.8 AND ORIGINAL CONFIGURATION

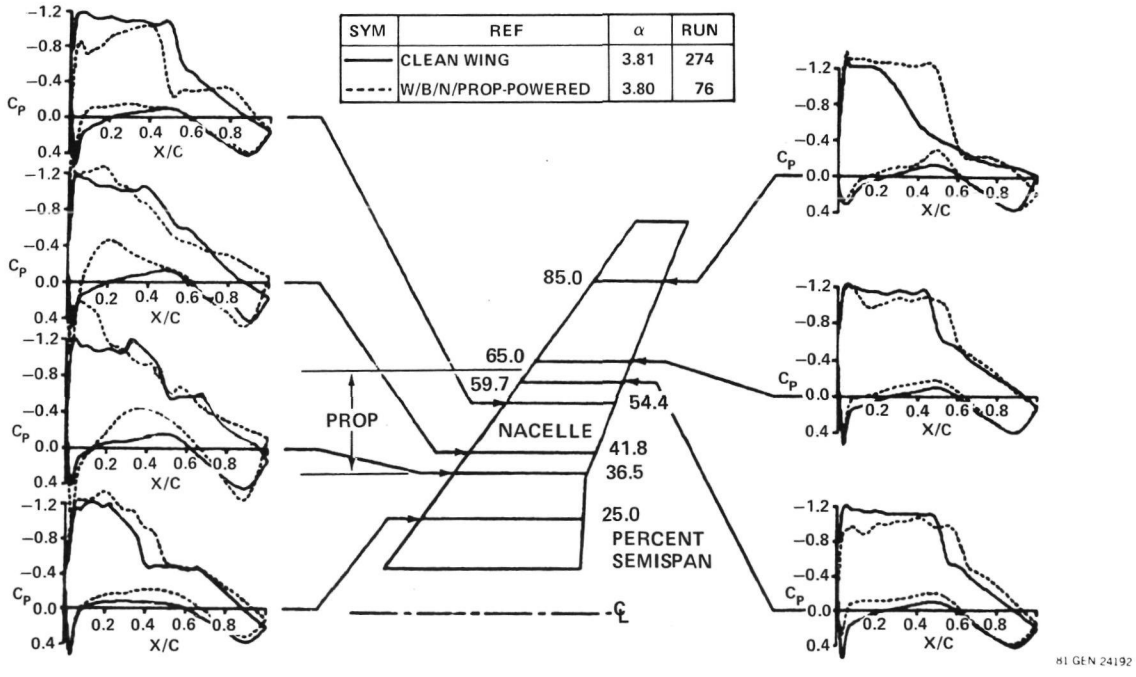

FIGURE 12. PRESSURE DISTRIBUTION AT INCREASED ANGLE OF ATTACK FOR M_o = 0.8 AND ORIGINAL CONFIGURATION

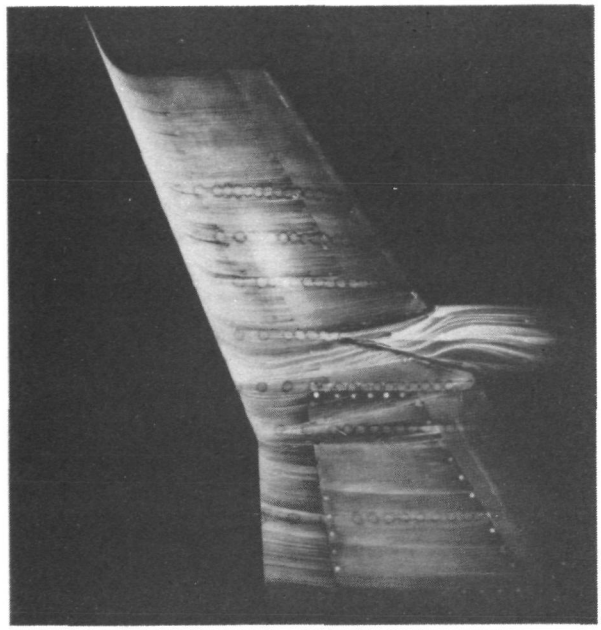

$M_0 = 0.75$
$\alpha = 2$ DEG
WINDMILL
UPPER SURFACE

81 GEN 23184A

FIGURE 13. OIL FLOW PHOTOGRAPH AT M_o = 0.75 – WINDMILL CONDITIONS

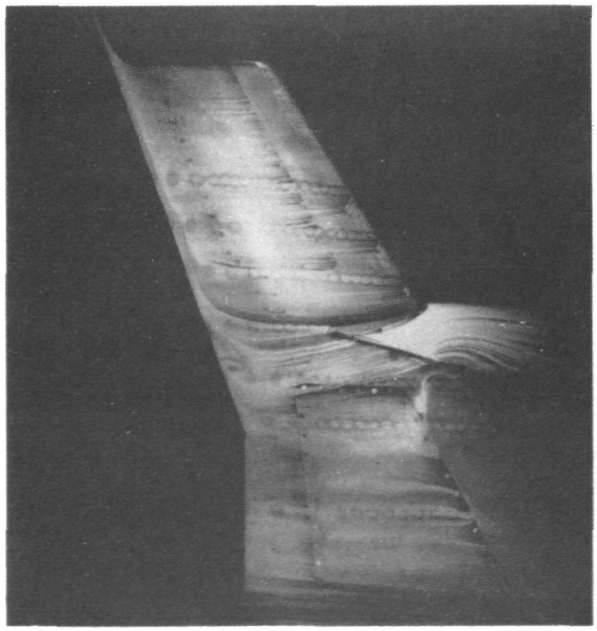

$M_0 = 0.8$
$\alpha = 2$ DEG
WINDMILL
UPPER SURFACE

81 GEN 23181A

FIGURE 14. OIL FLOW PHOTOGRAPH AT M_o = 0.8 – WINDMILL CONDITIONS

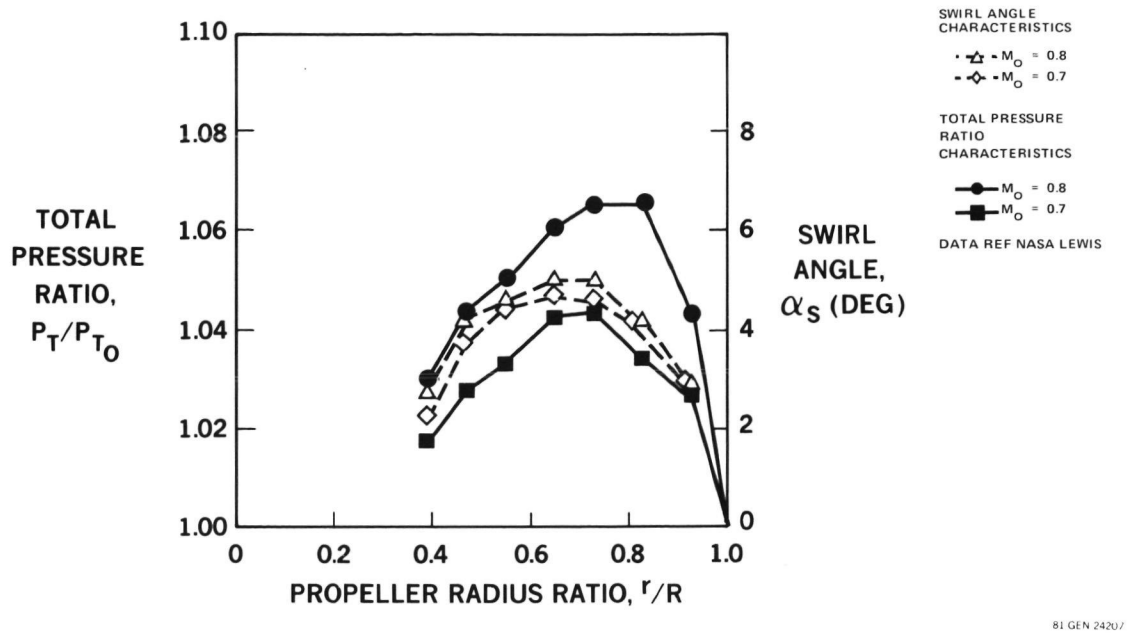

FIGURE 15. PROPELLER SWIRL AND TOTAL PRESSURE RATIO CHARACTERISTICS – ONE BLADE CHORD DOWNSTREAM – BLADE ANGLE, β = 57 DEGREES

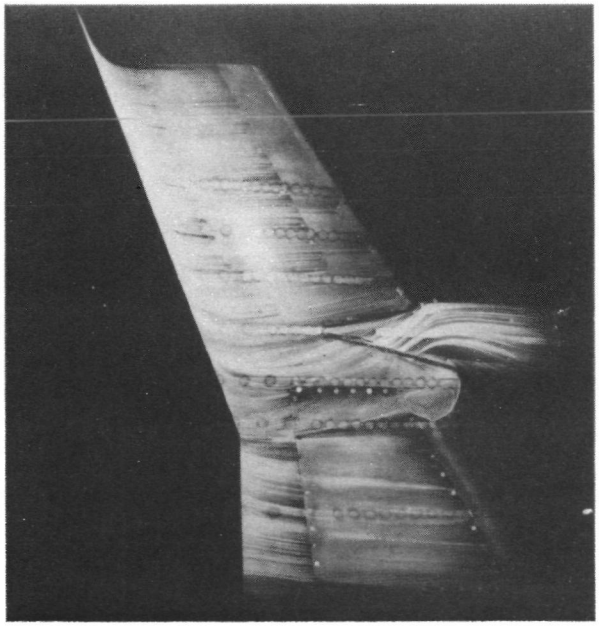

FIGURE 16. OIL FLOW PHOTOGRAPH AT M_o = 0.75 – MAXIMUM POWER

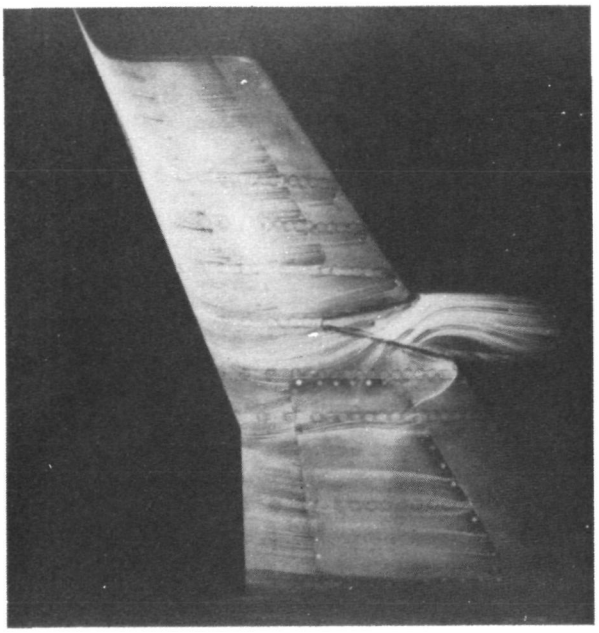

FIGURE 17. OIL FLOW PHOTOGRAPH AT M_o = 0.8 – MAXIMUM POWER

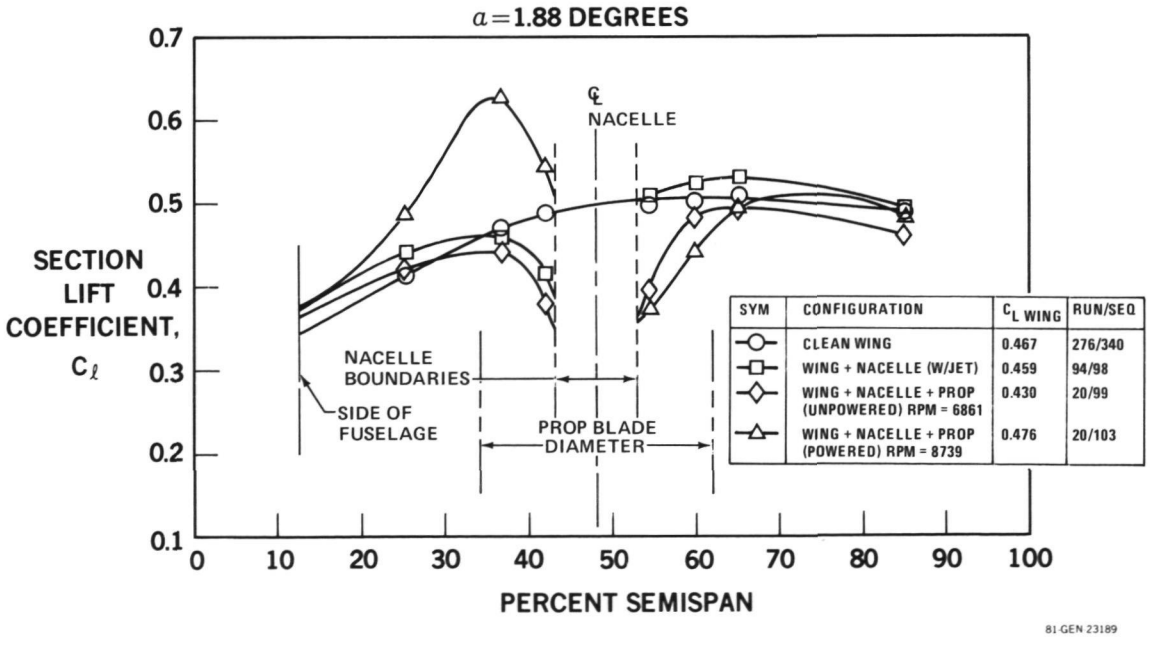

FIGURE 18. COMPARISON OF WING SECTION LIFT DISTRIBUTIONS AT M_o = 0.7

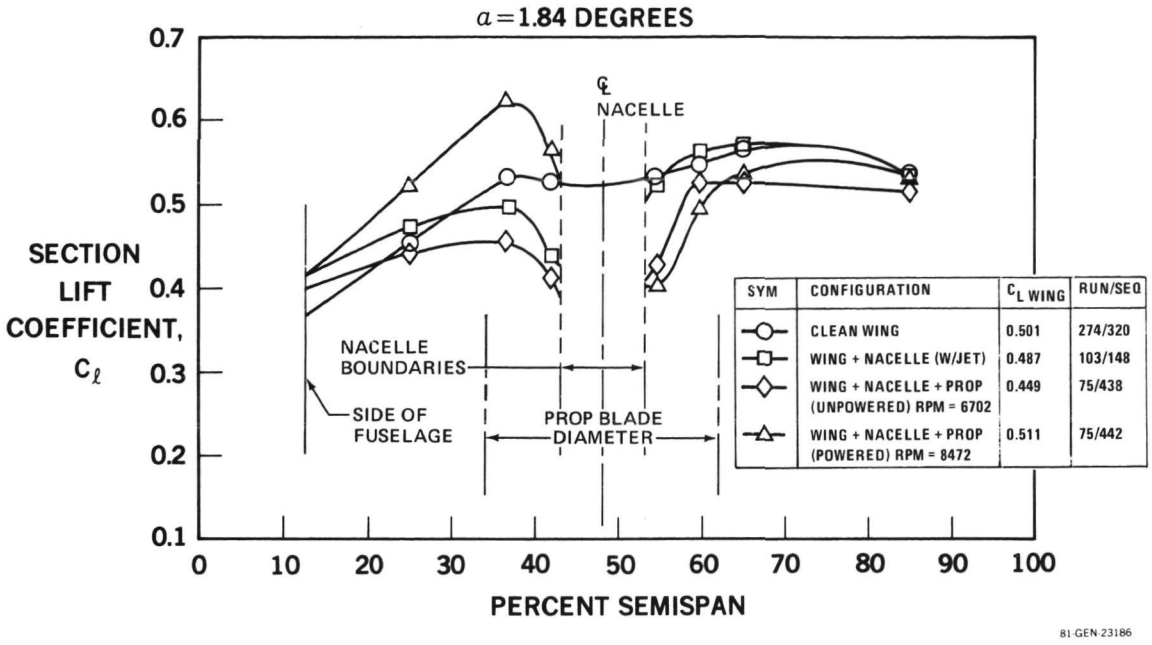

FIGURE 19. COMPARISON OF WING SECTION LIFT DISTRIBUTIONS AT M_O = 0.8

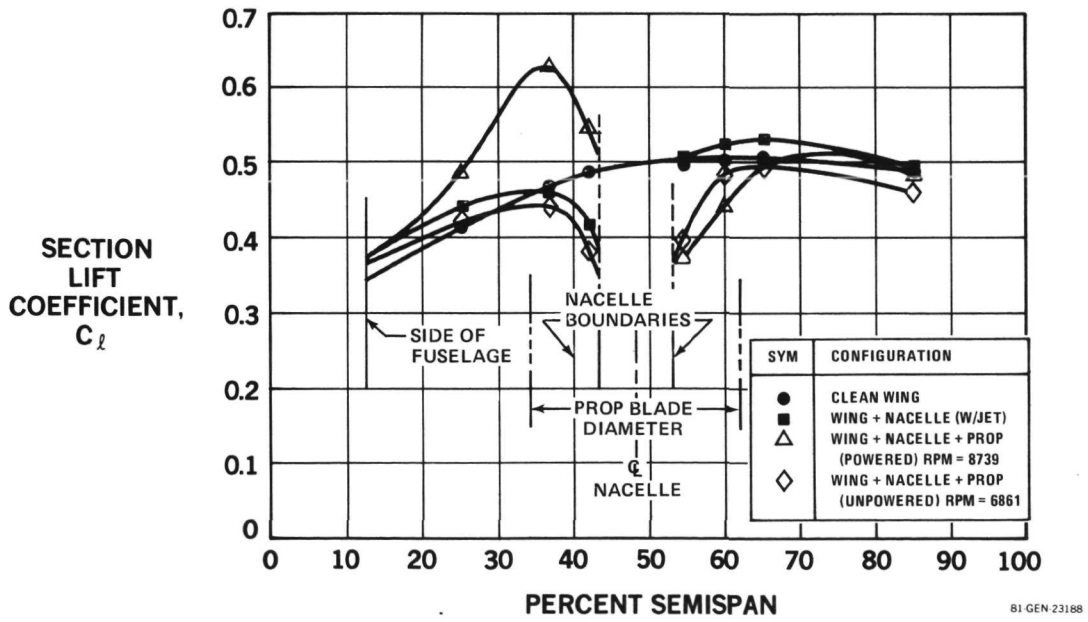

FIGURE 20. LIFT DISTRIBUTION USED FOR INDUCED DRAG CALCULATION

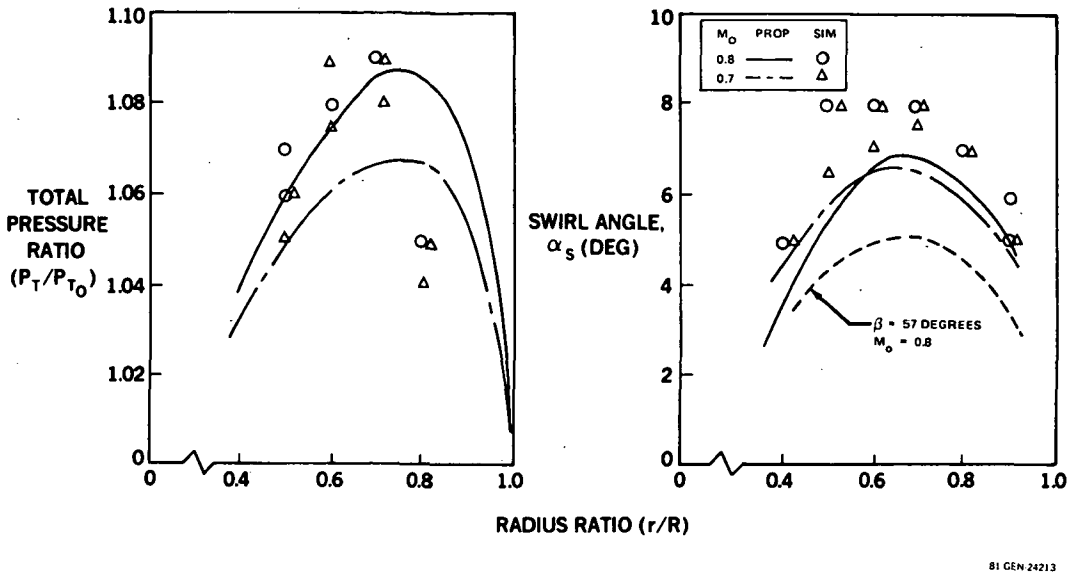

FIGURE 21. COMPARISON OF SIMULATOR EXIT CONDITIONS AND ISOLATED PROPELLER DATA AT β = 59 DEGREES

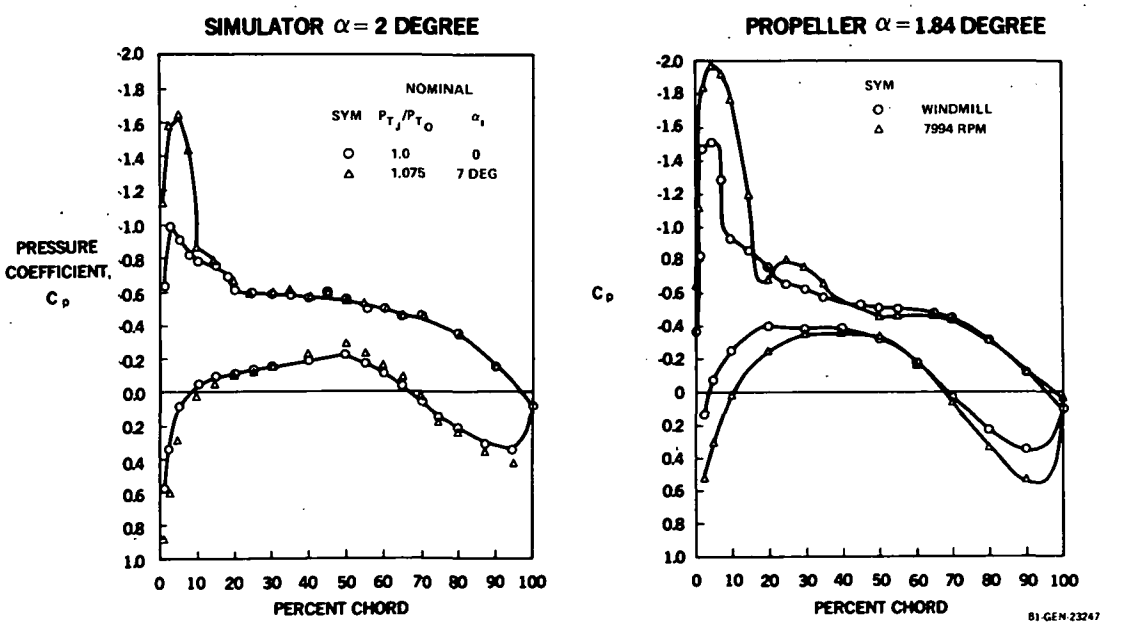

FIGURE 22. COMPARISON OF SIMULATOR AND PROPELLER DATA AT M = 0.7 AND η = 0.36

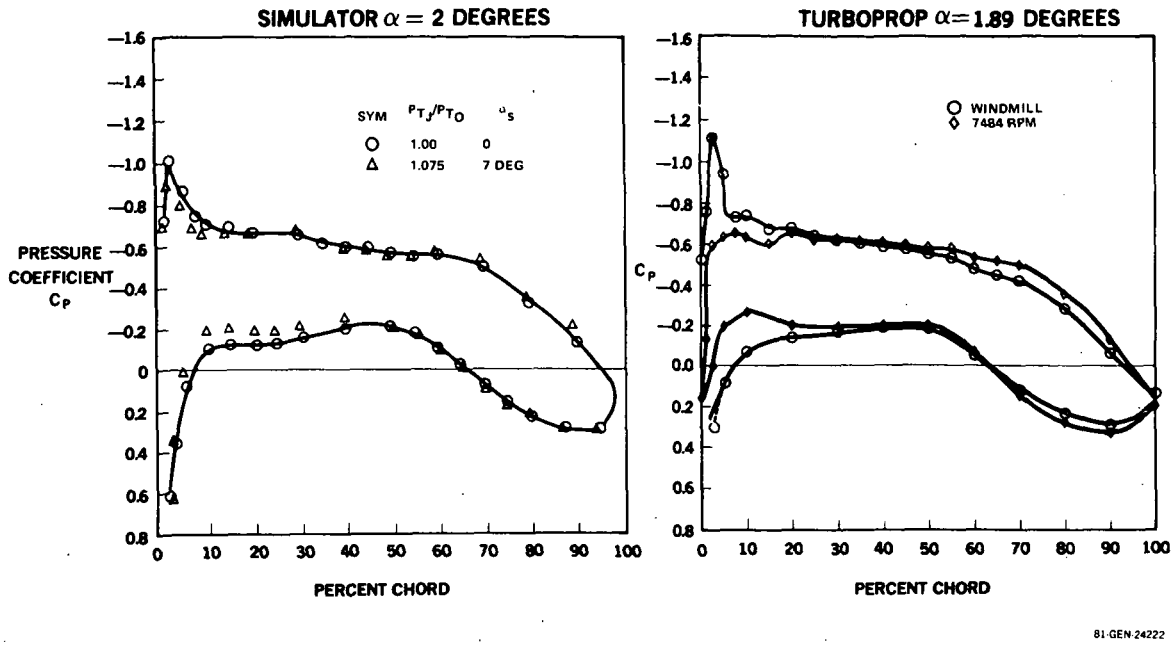

FIGURE 23. COMPARISON OF SIMULATOR AND PROPELLER DATA AT M_o = 0.7 AND η = 0.5

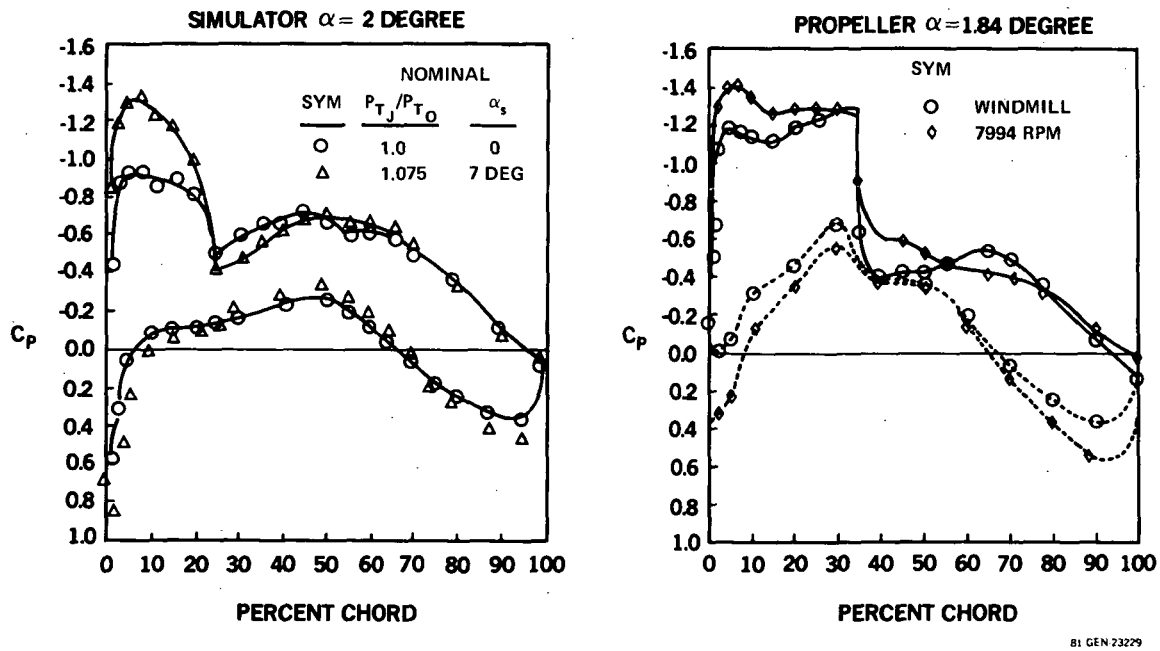

FIGURE 24. COMPARISON OF SIMULATOR AND PROPELLER DATA AT M_o = 0.8 AND η = 0.36

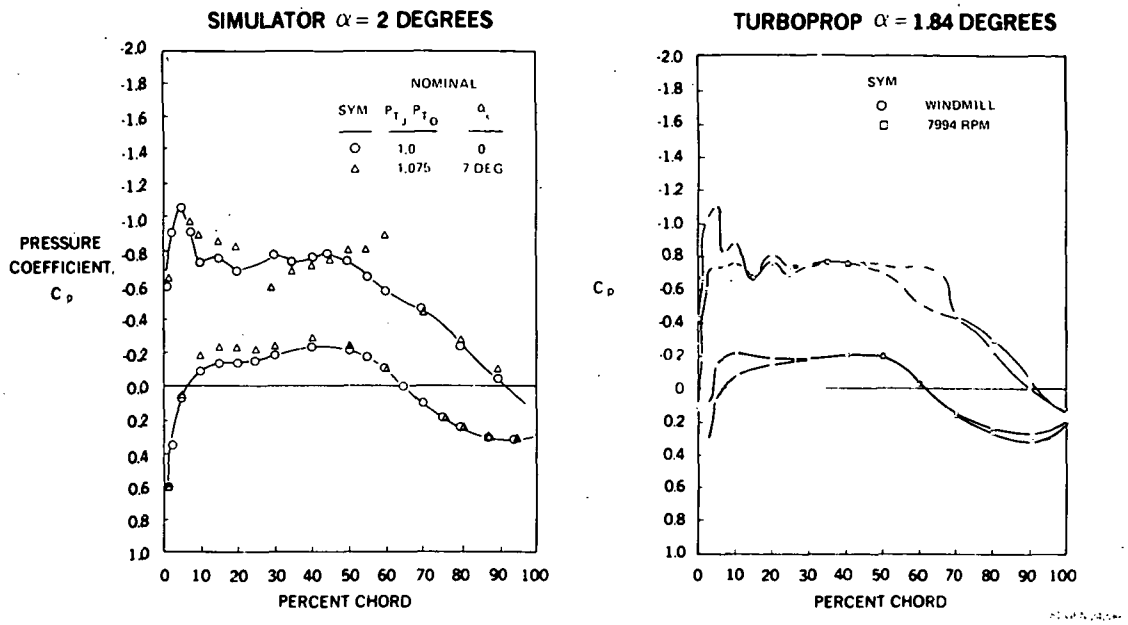

FIGURE 25. COMPARISON OF SIMULATOR AND PROPELLER DATA AT M_o = 0.8 AND η = 0.5

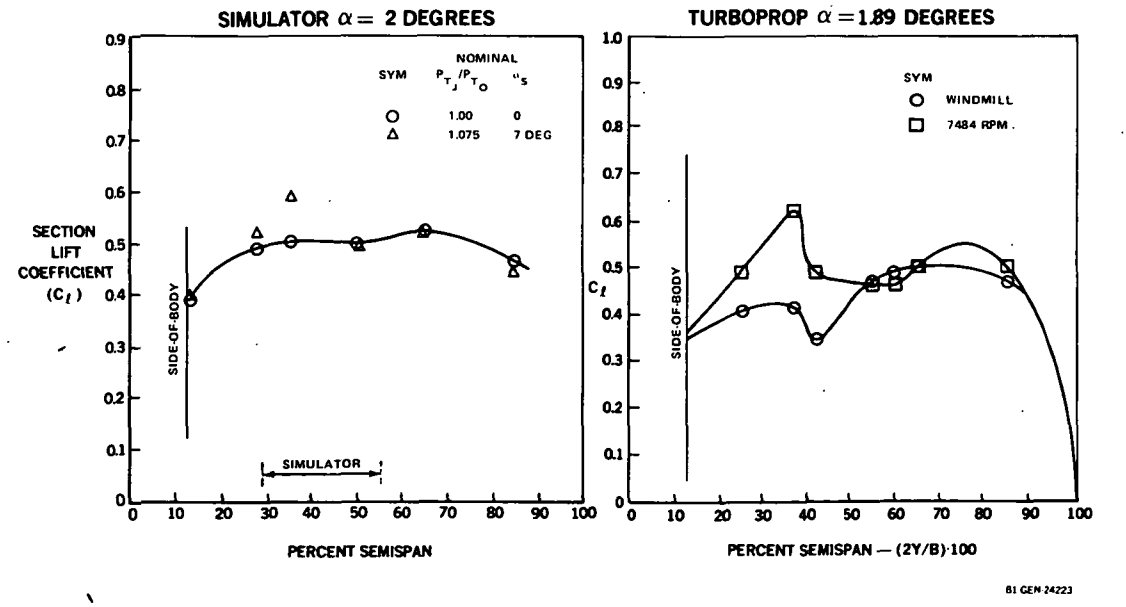

FIGURE 26. COMPARISON OF SIMULATOR AND PROPELLER SECTION LIFT DISTRIBUTION AT M_o = 0.7

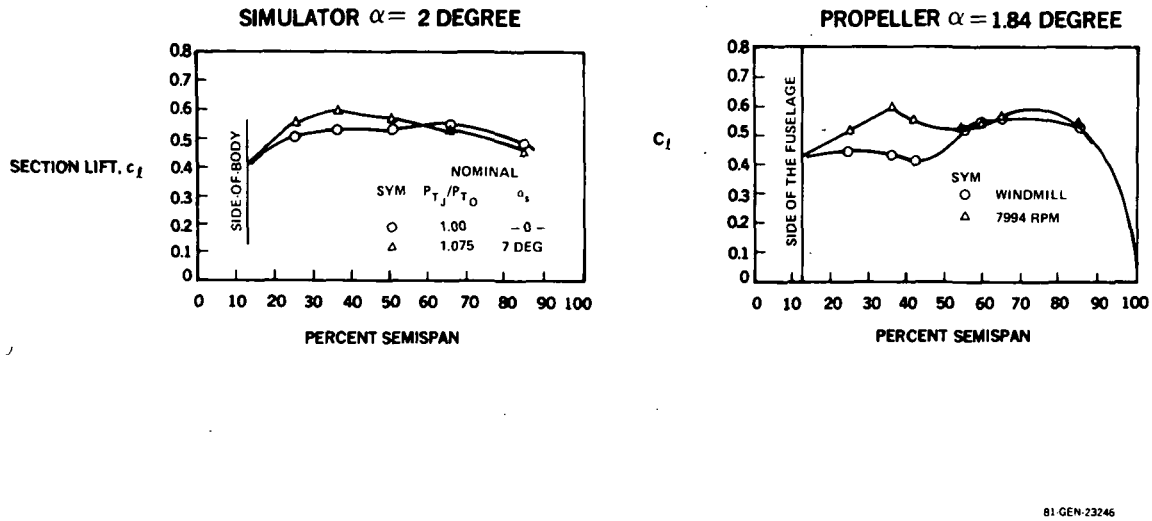

FIGURE 27. COMPARISON OF SIMULATOR AND PROPELLER SECTION LIFT DISTRIBUTION AT M = 0.8

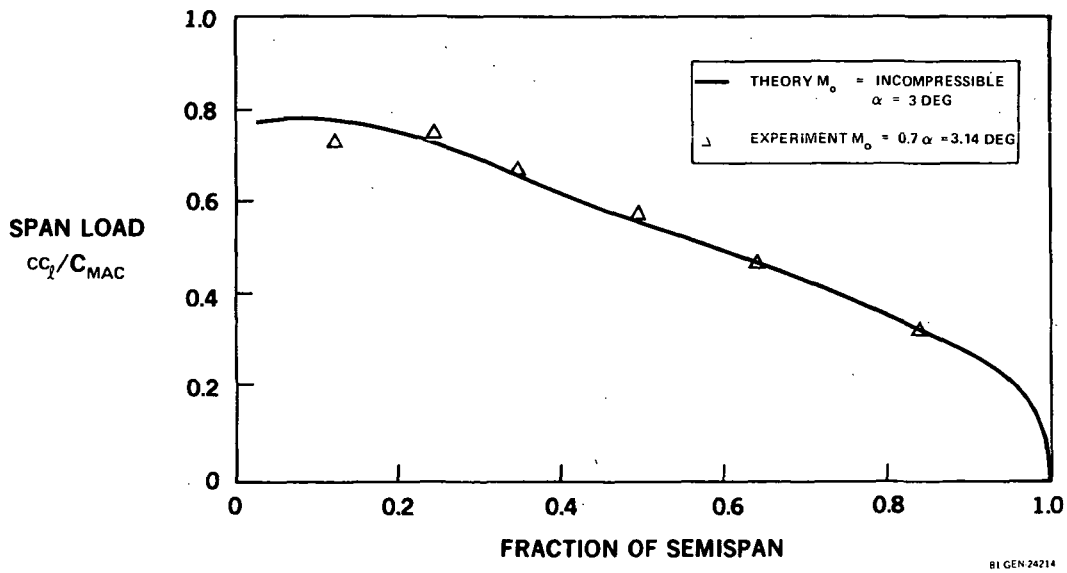

FIGURE 28. COMPARISON OF LIFTING LINE AND EXPERIMENTAL SPAN LOAD FOR CLEAN WING

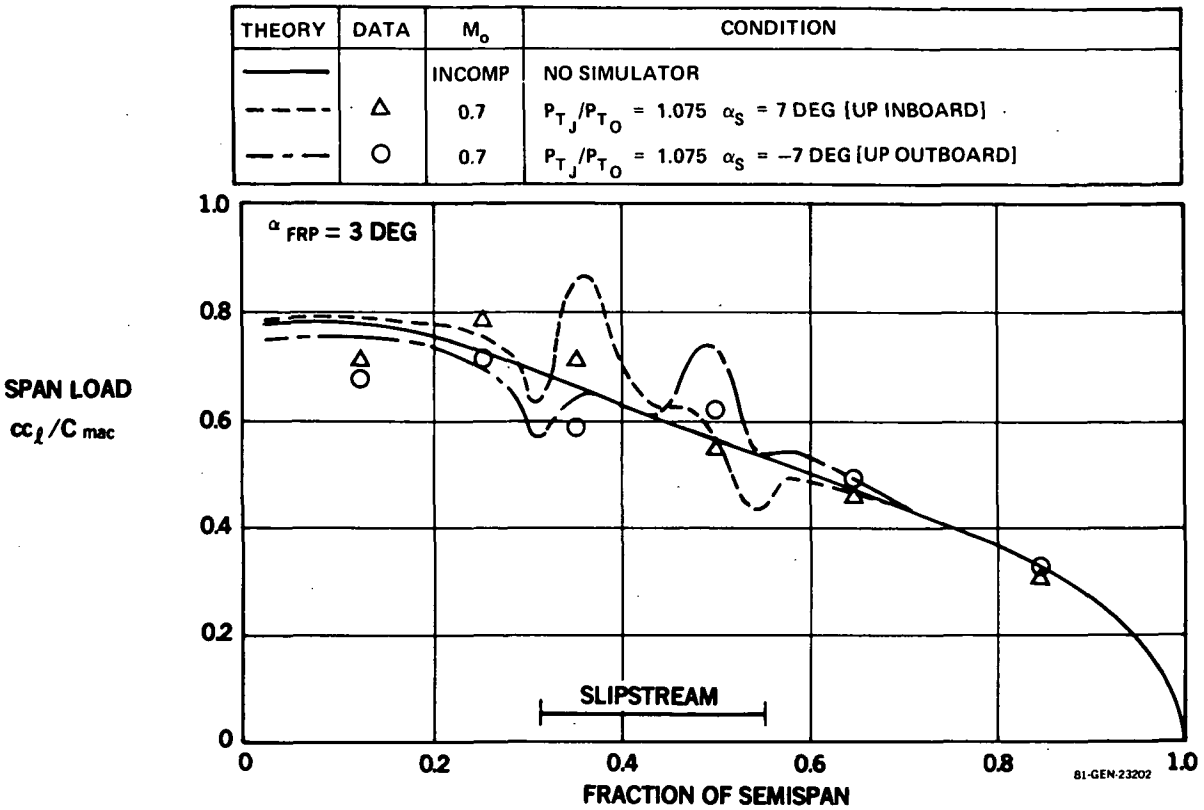

FIGURE 29. COMPARISON OF WING SECTION LIFT DISTRIBUTION WITH LIFTING LINE THEORY – SIMULATOR MODEL

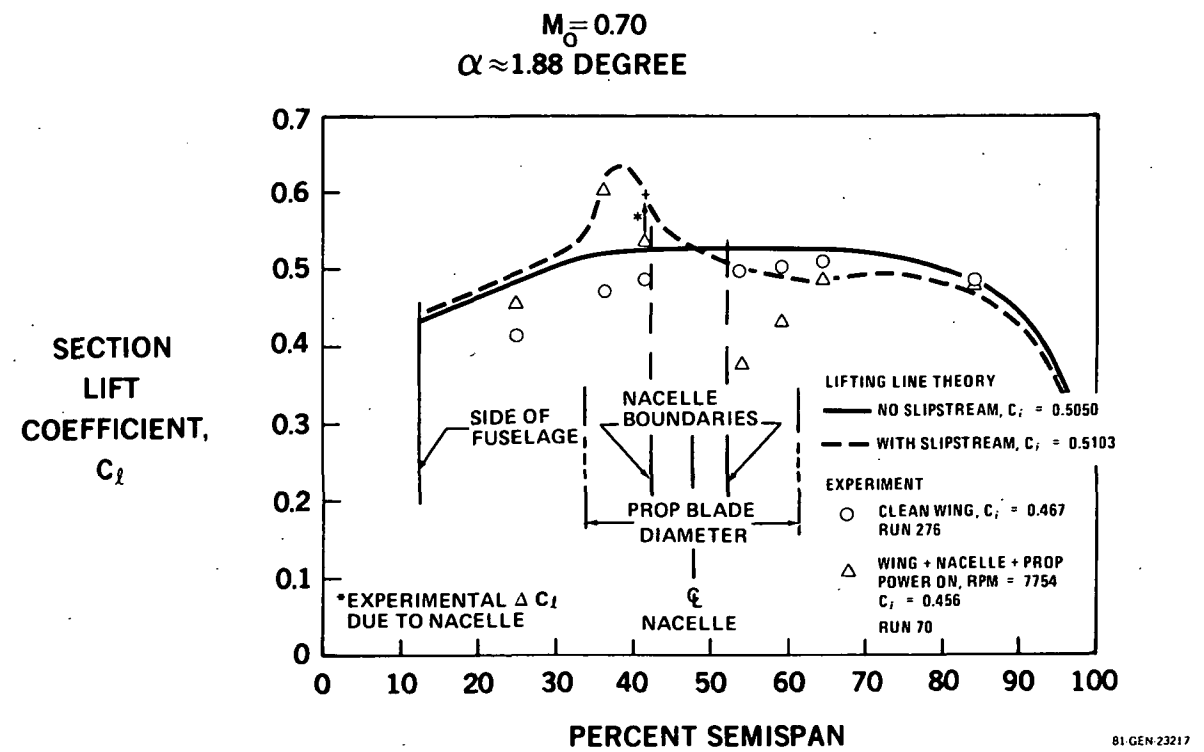

FIGURE 30. COMPARISON OF WING SECTION LIFT DISTRIBUTIONS WITH LIFTING LINE THEORY – PROPELLER MODEL

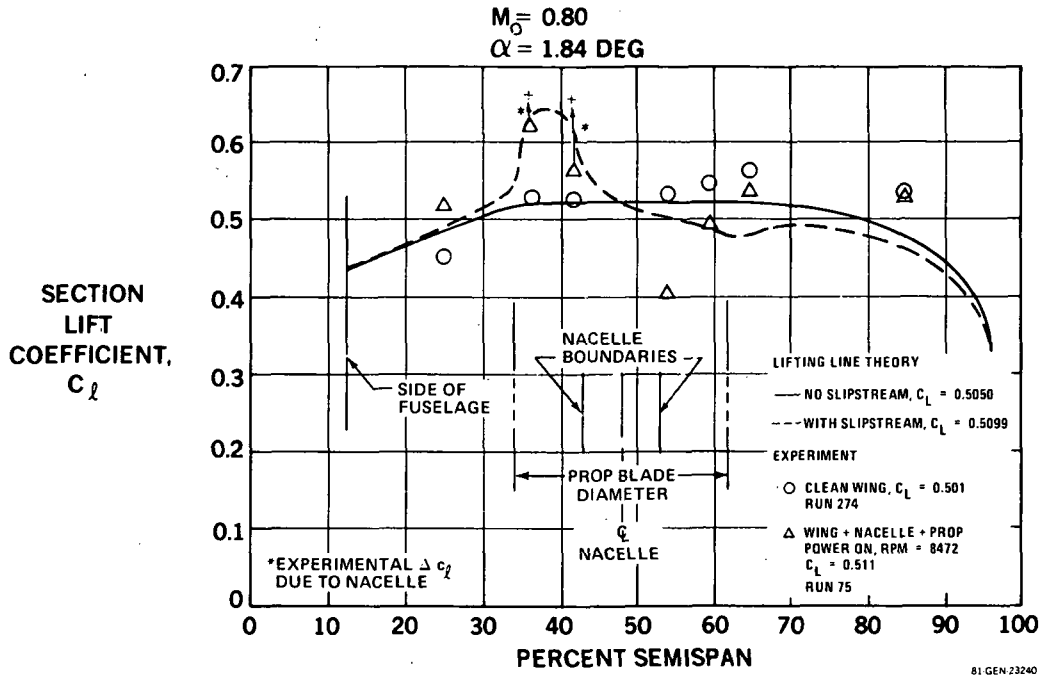

FIGURE 31. COMPARISON OF WING SECTION LIFT DISTRIBUTIONS WITH LIFTING LINE THEORY – PROPELLER MODEL

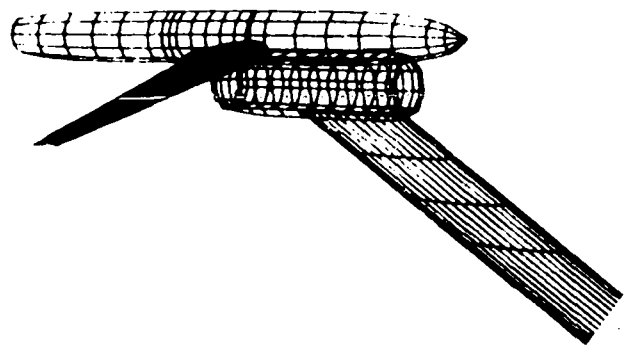

81-GEN-23191

FIGURE 32. NEUMANN PANELING FOR SIMULATOR MODEL

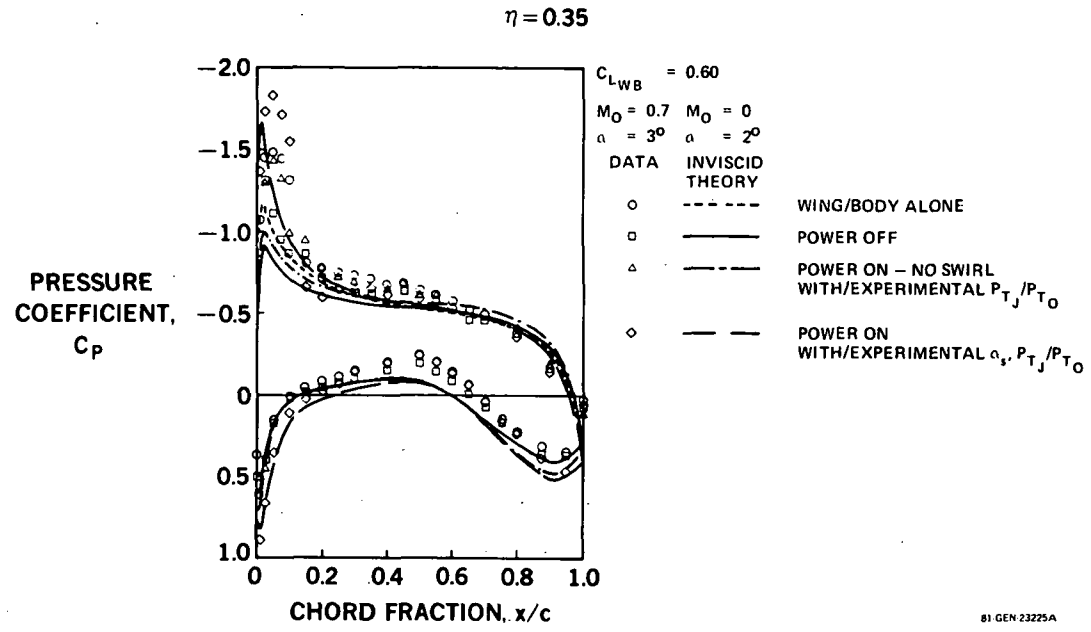

FIGURE 33. SIMULATOR/NEUMANN PRESSURE DISTRIBUTION COMPARISON

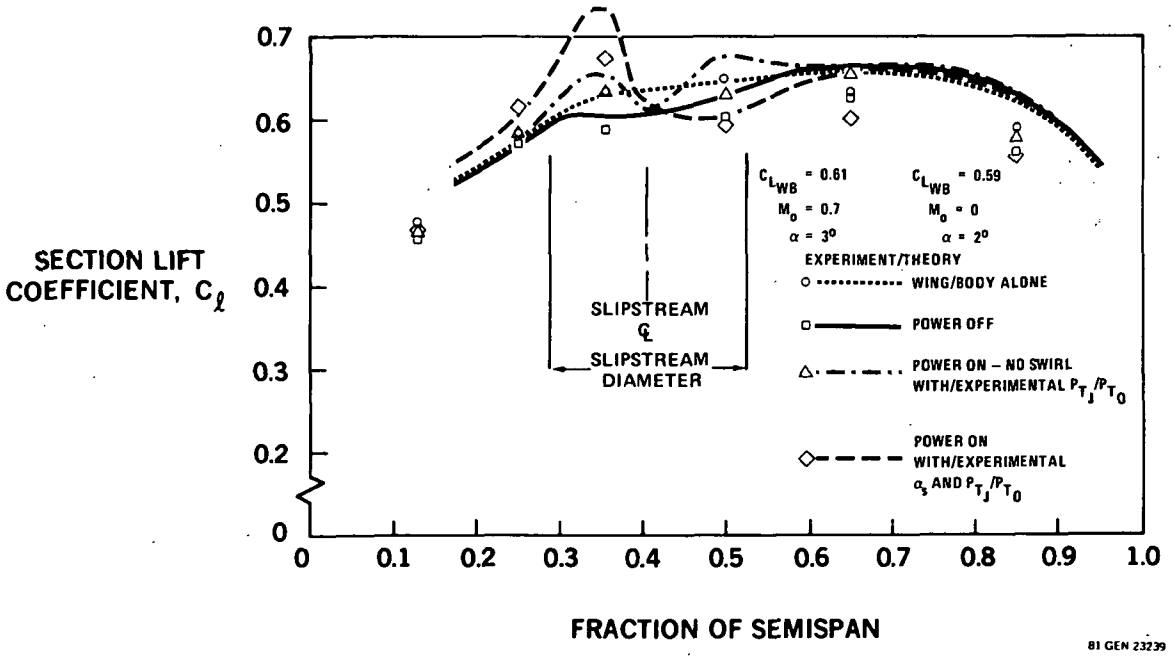

FIGURE 34. SIMULATOR/NEUMANN SECTION LIFT COEFFICIENT COMPARISON

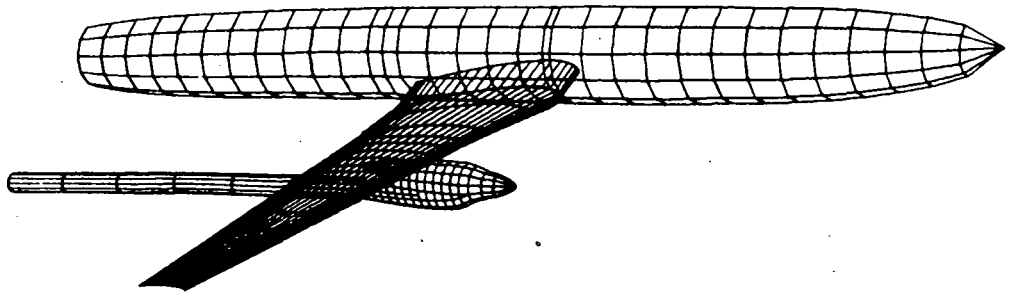

81-GEN-23201

FIGURE 35. NEUMANN PANELING FOR PROPELLER MODEL

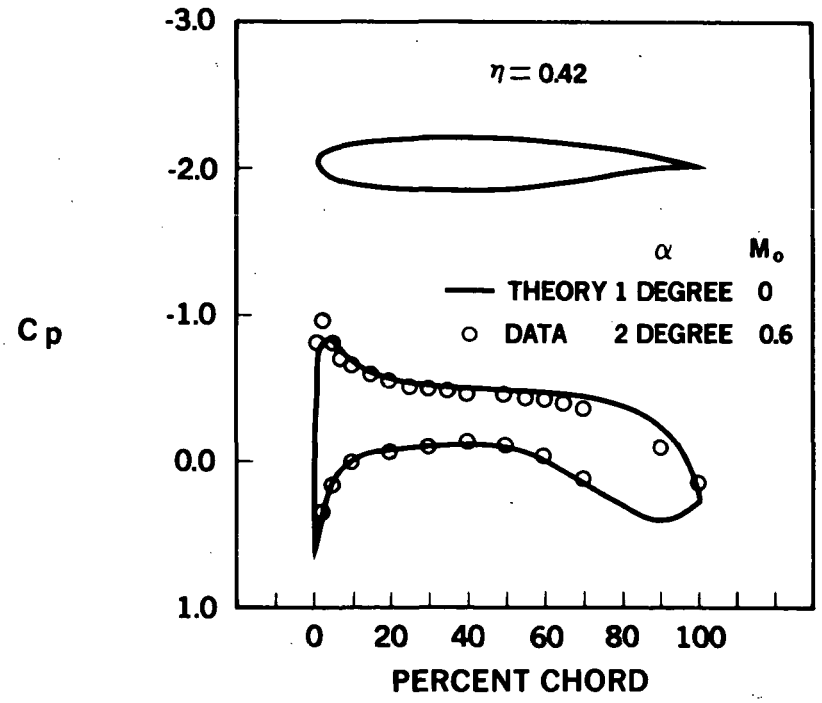

81-GEN-23198

FIGURE 36. COMPARISON OF NEUMANN AND DATA FOR CLEAN WING

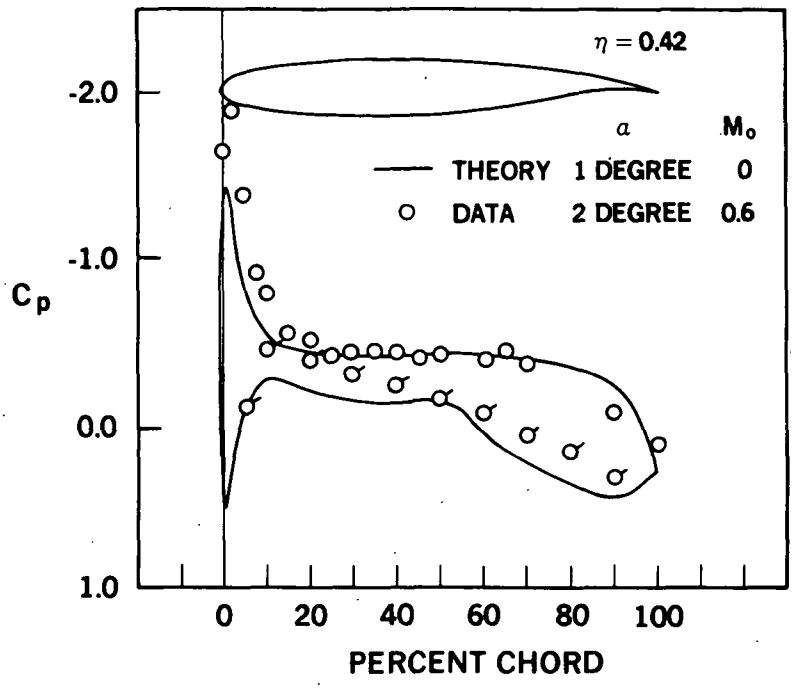

FIGURE 37. COMPARISON OF NEUMANN AND DATA FOR WING AND NACELLE – NO POWER

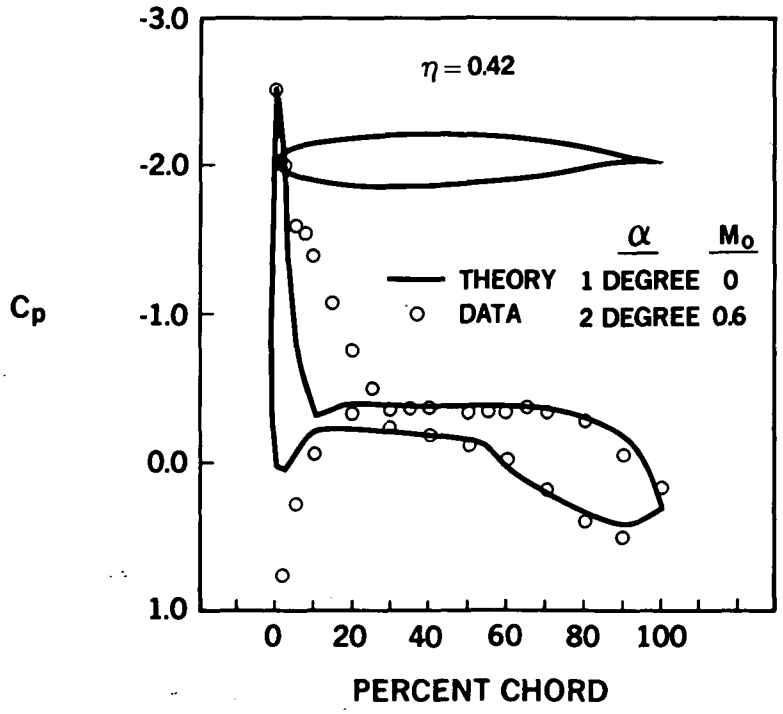

FIGURE 38. COMPARISON OF NEUMANN AND DATA FOR WING AND NACELLE WITH POWER

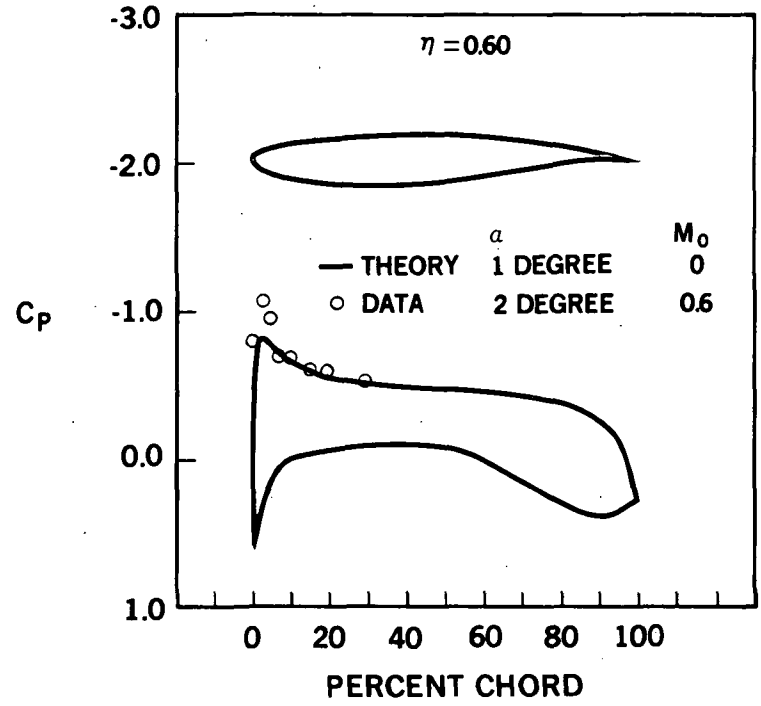

FIGURE 39. COMPARISON OF NEUMANN AND DATA FOR CLEAN WING

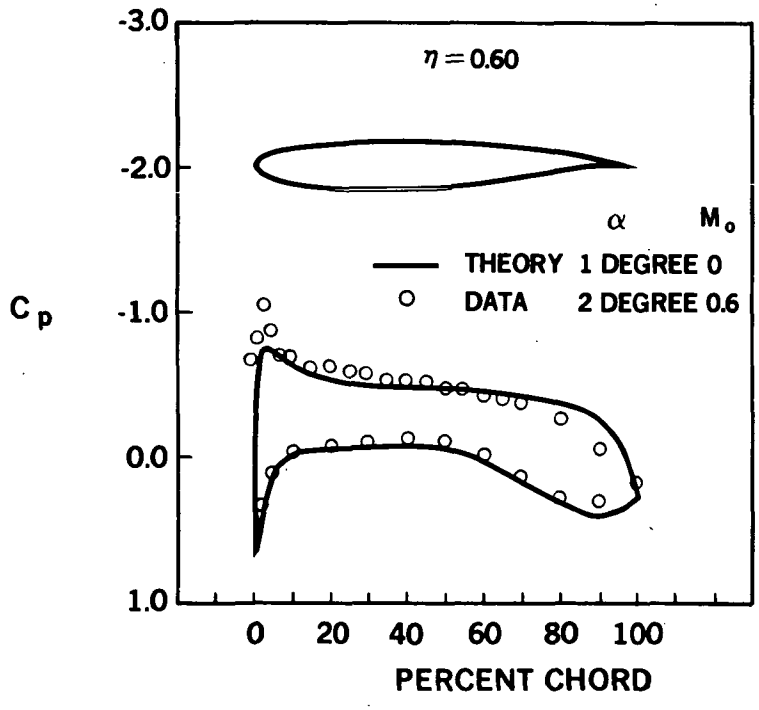

FIGURE 40. COMPARISON OF NEUMANN AND DATA FOR WING AND NACELLE – NO POWER

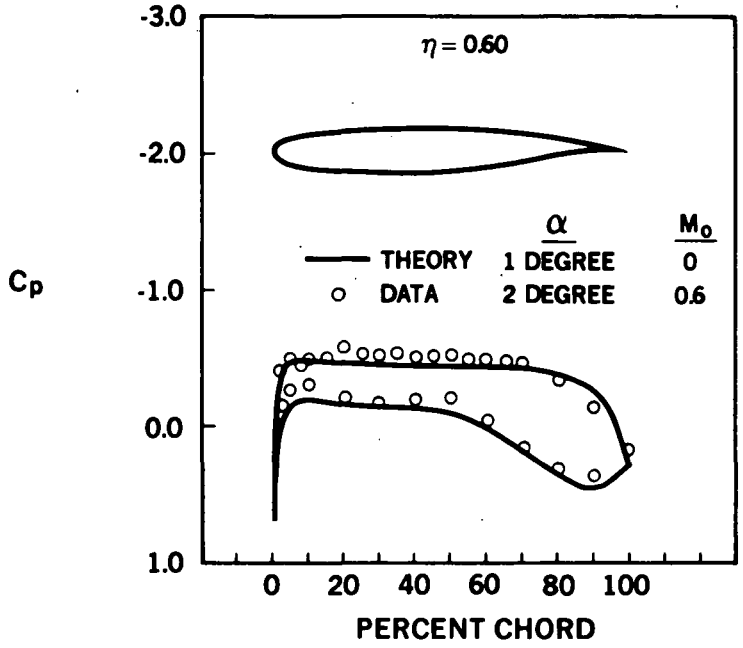

FIGURE 41. COMPARISON OF NEUMANN AND DATA FOR WING AND NACELLE WITH POWER

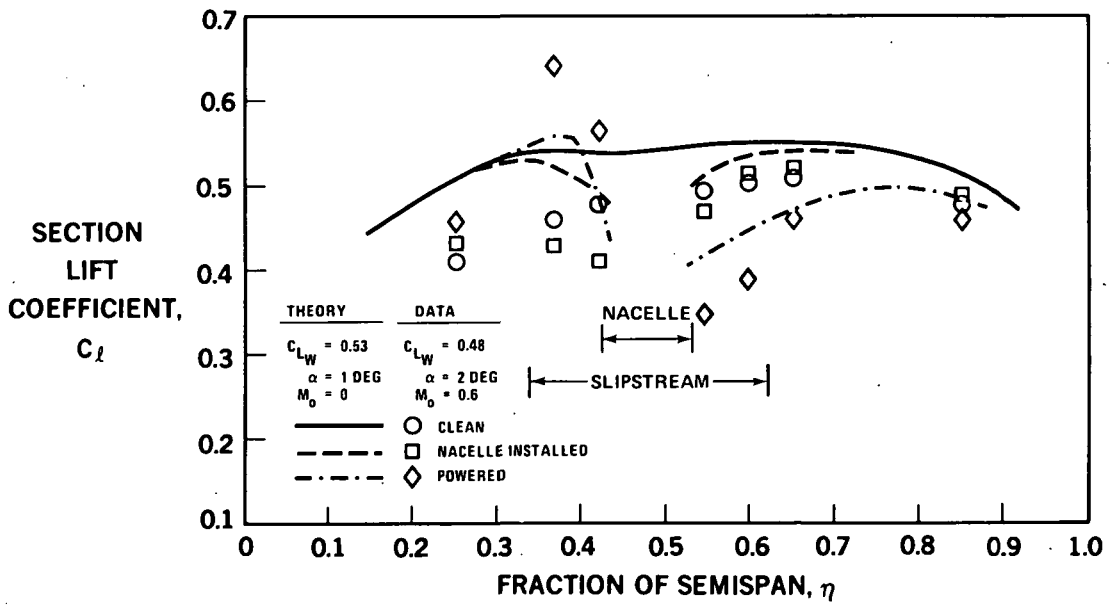

FIGURE 42. DATA COMPARISON OF SECTION LIFT DISTRIBUTION FOR NEUMANN

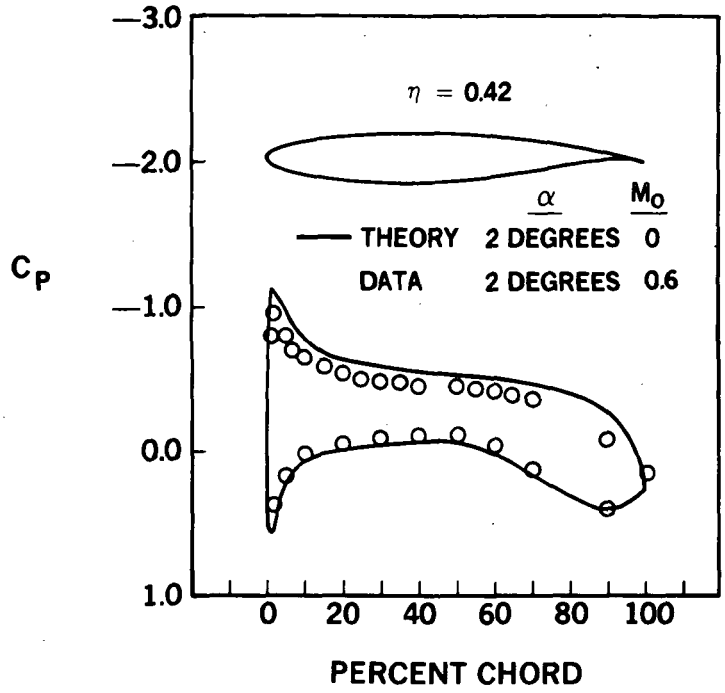

FIGURE 43. COMPARISON OF NEUMANN AND DATA FOR CLEAN WING AT α = 2 DEGREES

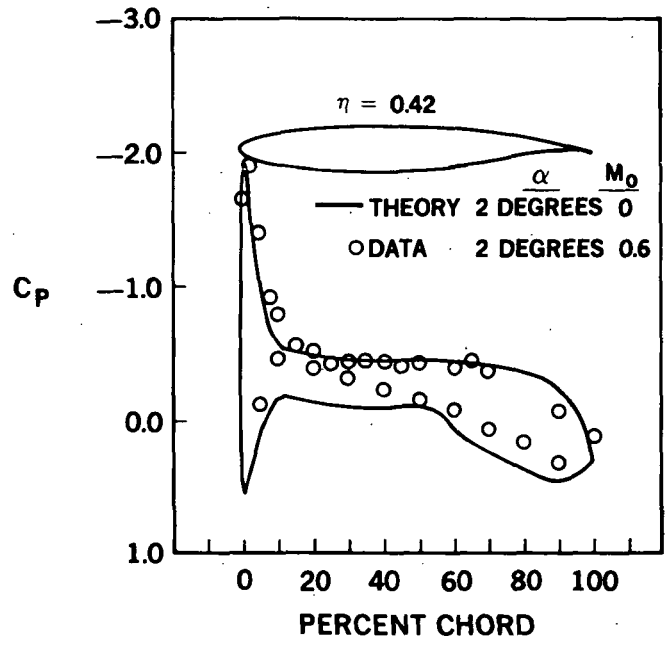

81-GEN-24184

FIGURE 44. COMPARISON OF NEUMANN AND DATA FOR WING/NACELLE NO POWER AT α = 2 DEGREES

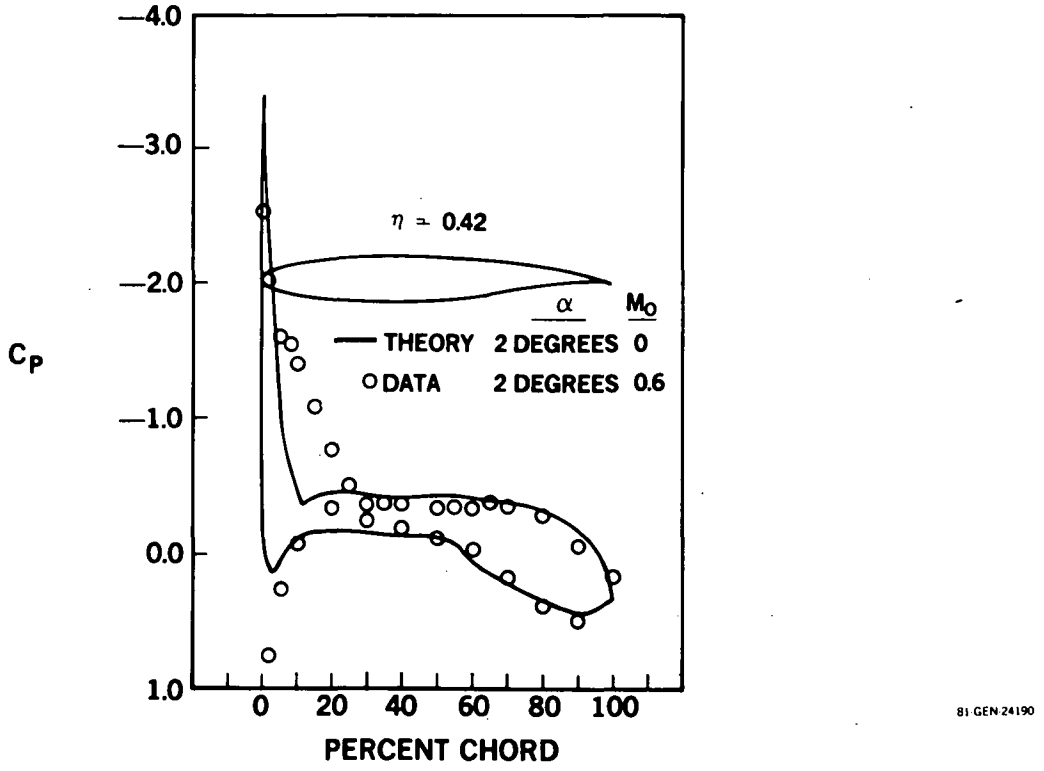

FIGURE 45. COMPARISON OF NEUMANN AND DATA WITH POWER AT α = 2 DEGREES

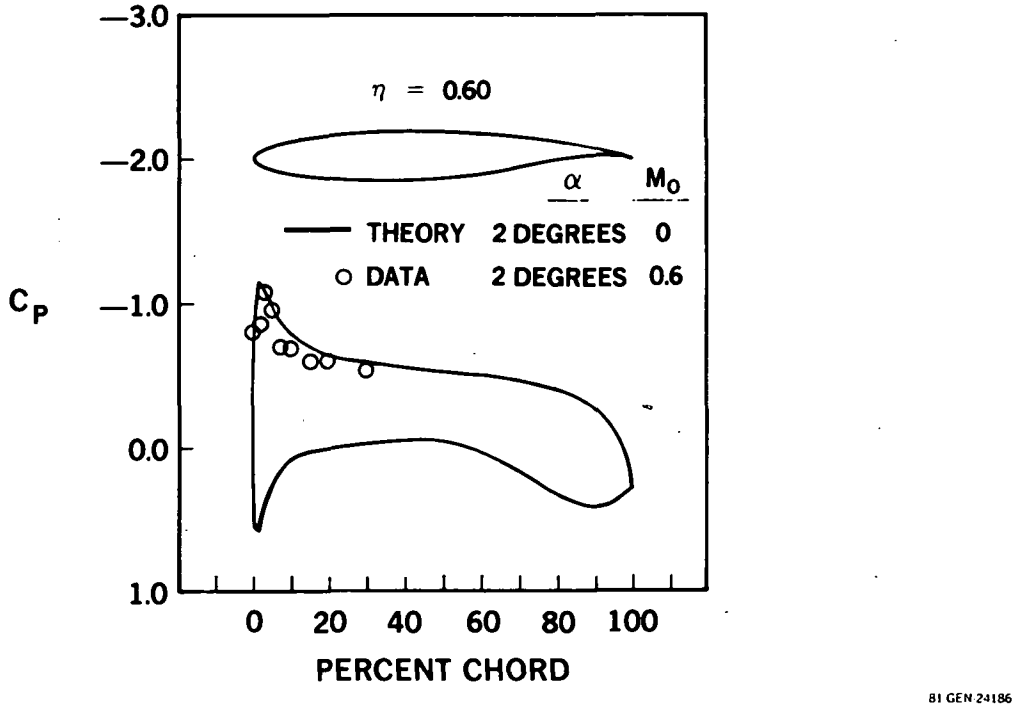

FIGURE 46. COMPARISON OF NEUMANN AND DATA FOR CLEAN WING AT α = 2 DEGREES

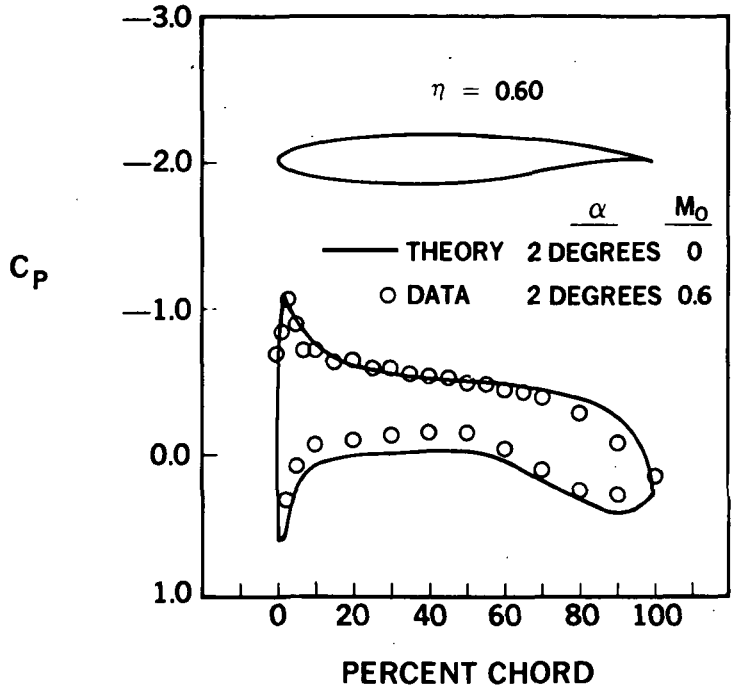

FIGURE 47. COMPARISON OF NEUMANN AND DATA FOR WING NACELLE NO POWER AT α = 2 DEGREES

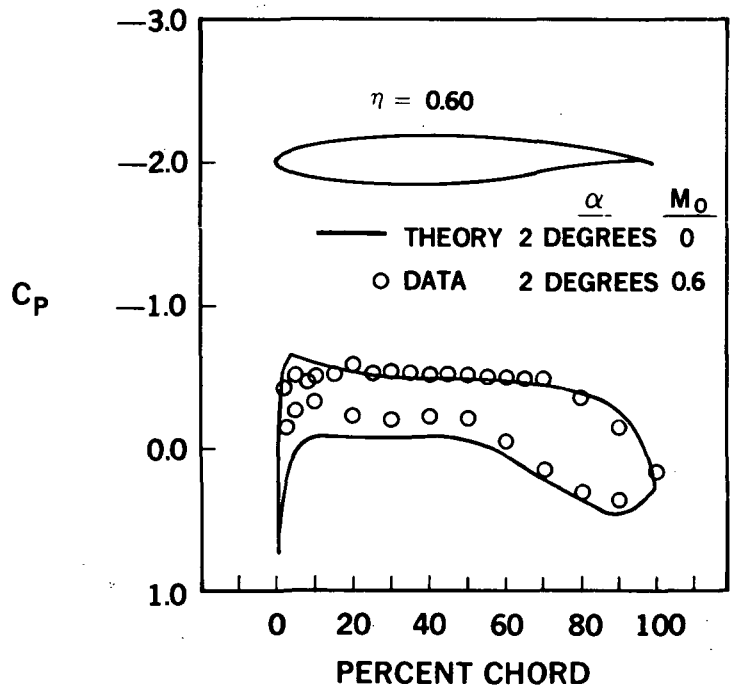

FIGURE 48. COMPARISON OF NEUMANN AND DATA WITH POWER AT α = 2 DEGREES

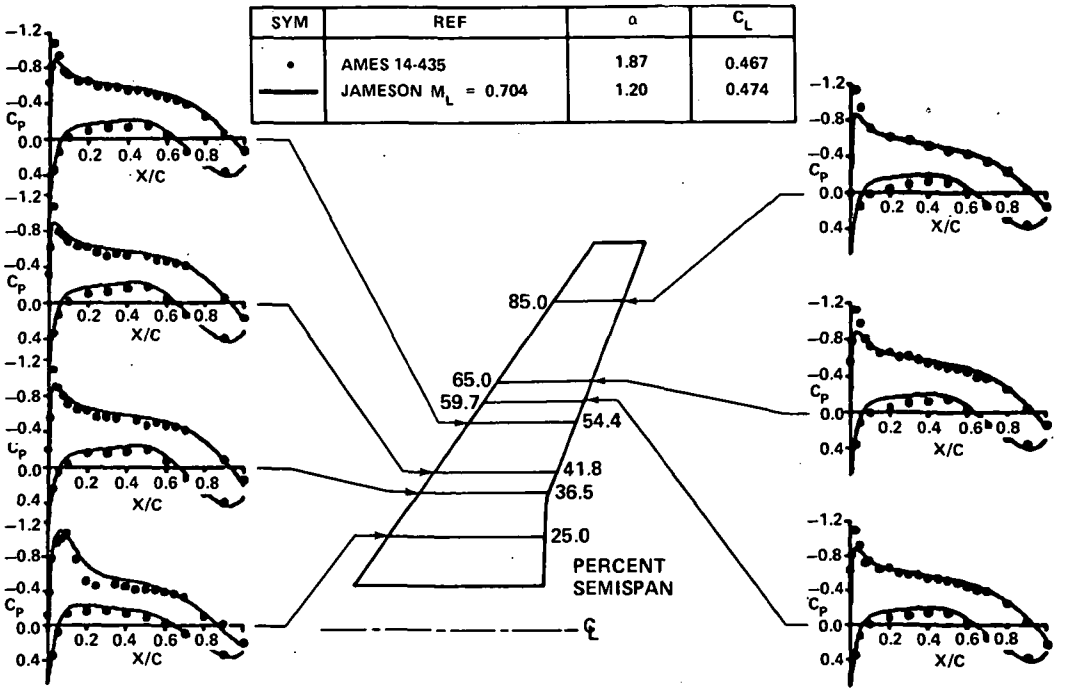

FIGURE 49. COMPARISON OF JAMESON AND EXPERIMENTAL CHORDWISE PRESSURE DISTRIBUTIONS FOR CLEAN WING CONFIGURATION M_o = 0.7

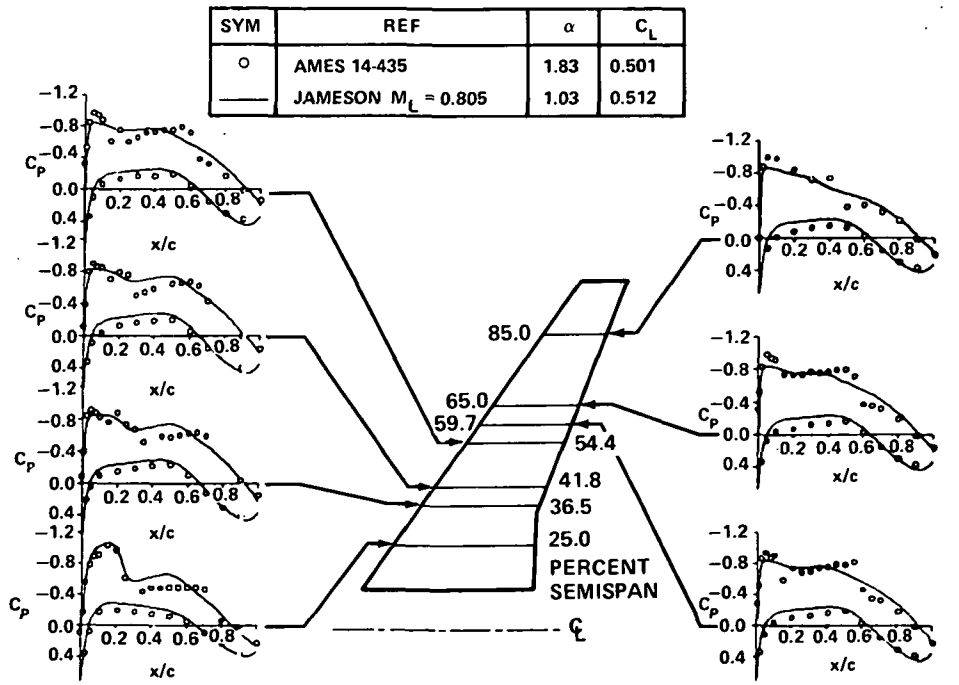

81-GEN-23243-A

FIGURE 50. COMPARISON OF JAMESON AND EXPERIMENTAL CHORDWISE PRESSURE DISTRIBUTIONS FOR CLEAN WING CONFIGURATION M_o = 0.800

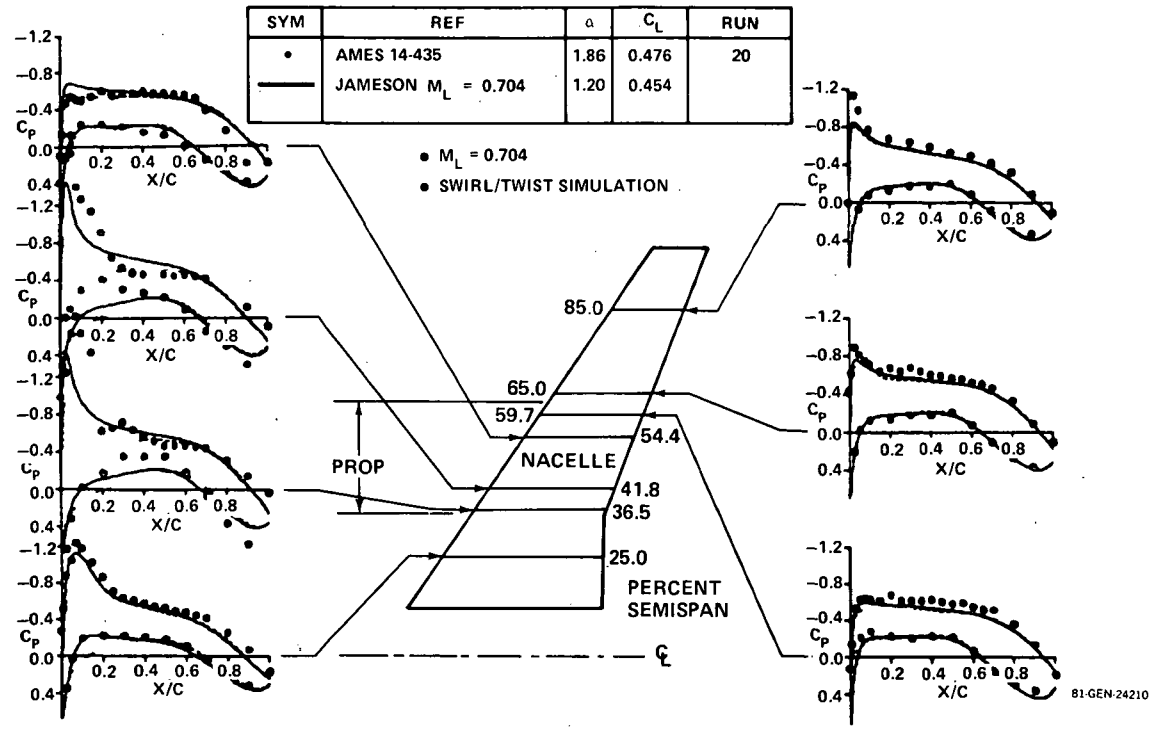

FIGURE 51. COMPARISON OF JAMESON AND EXPERIMENTAL CHORDWISE PRESSURE DISTRIBUTIONS – WITH POWER M_0 = 0.7

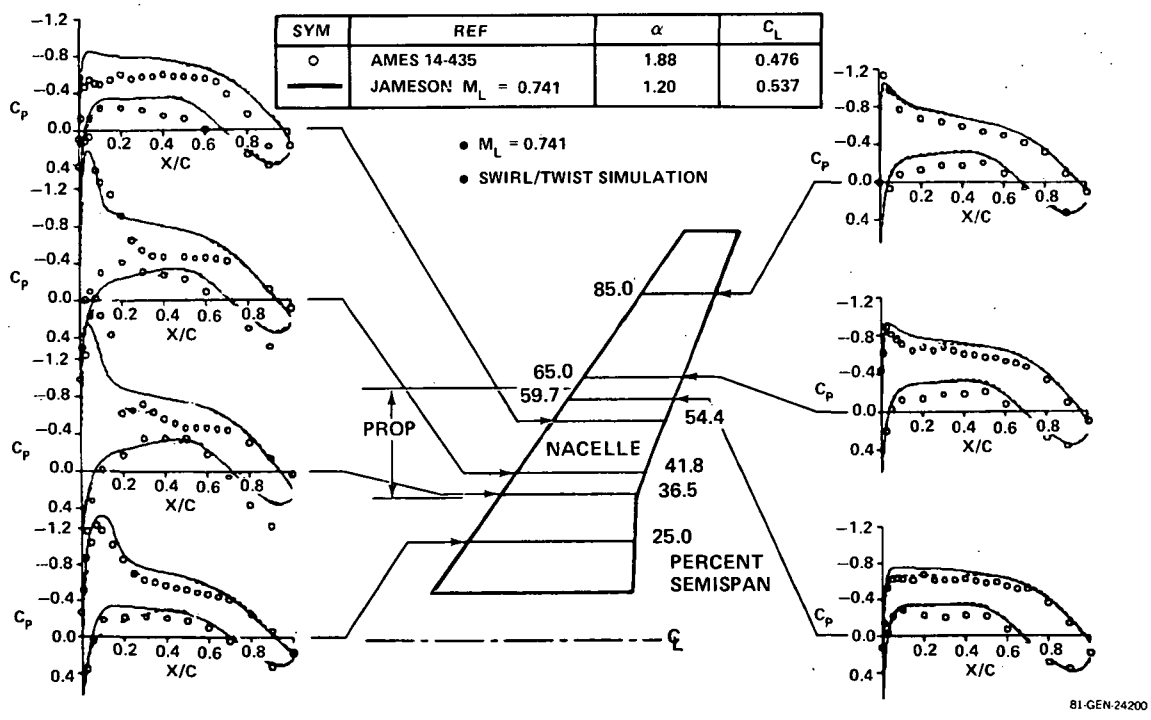

FIGURE 52. COMPARISON OF JAMESON AND EXPERIMENTAL CHORDWISE PRESSURE DISTRIBUTIONS – WITH POWER M_0 = 0.7

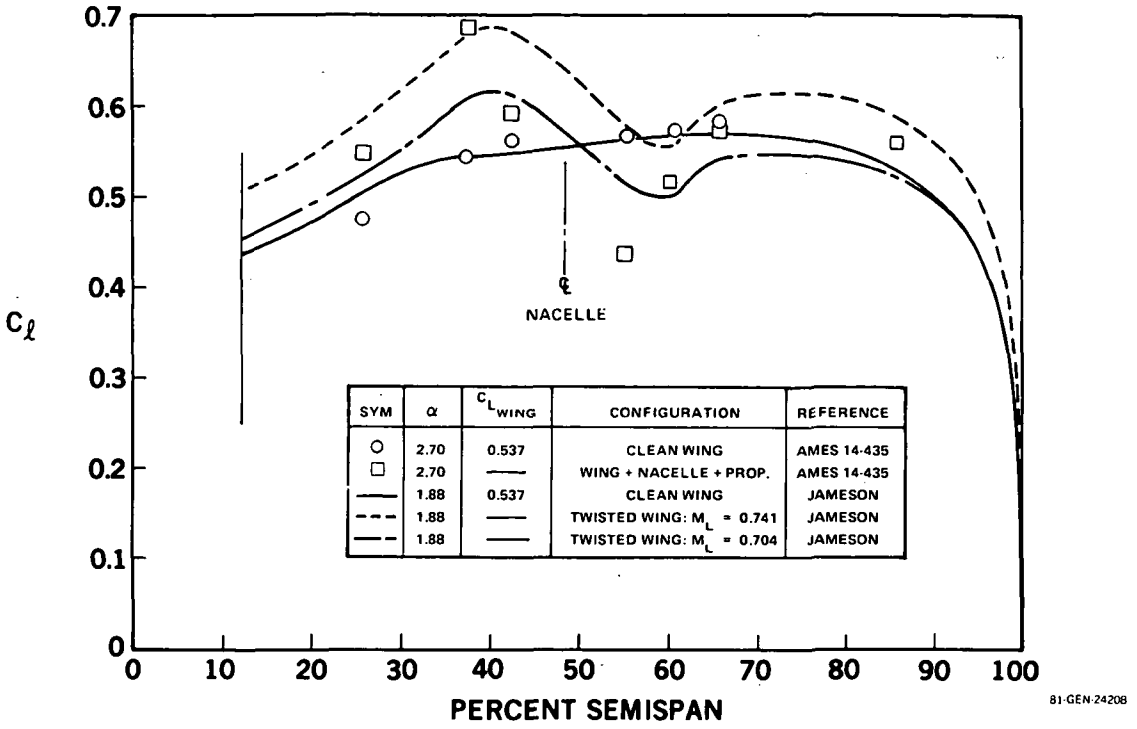

FIGURE 53. EXPERIMENTAL WING SECTION LIFT COMPARISON WITH THEORY AT M_o = 0.7

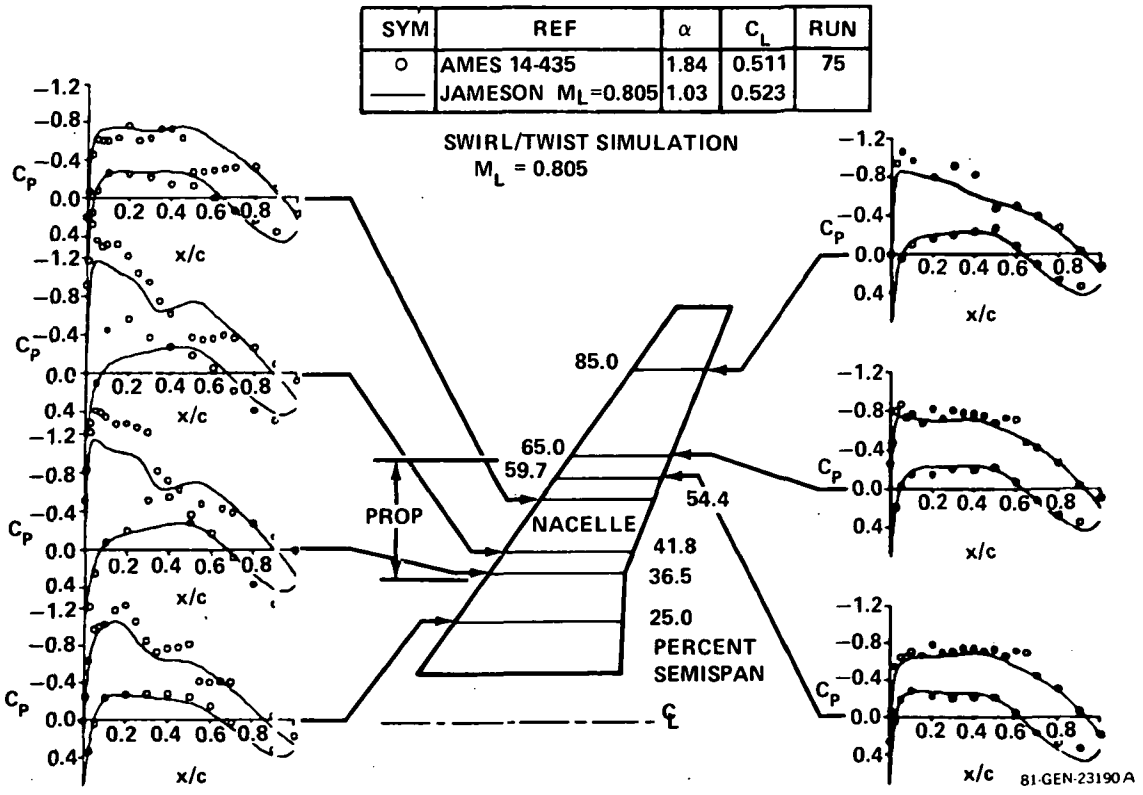

FIGURE 54. COMPARISON OF JAMESON AND EXPERIMENTAL CHORDWISE PRESSURE DISTRIBUTIONS FOR POWERED PROP CONFIGURATION

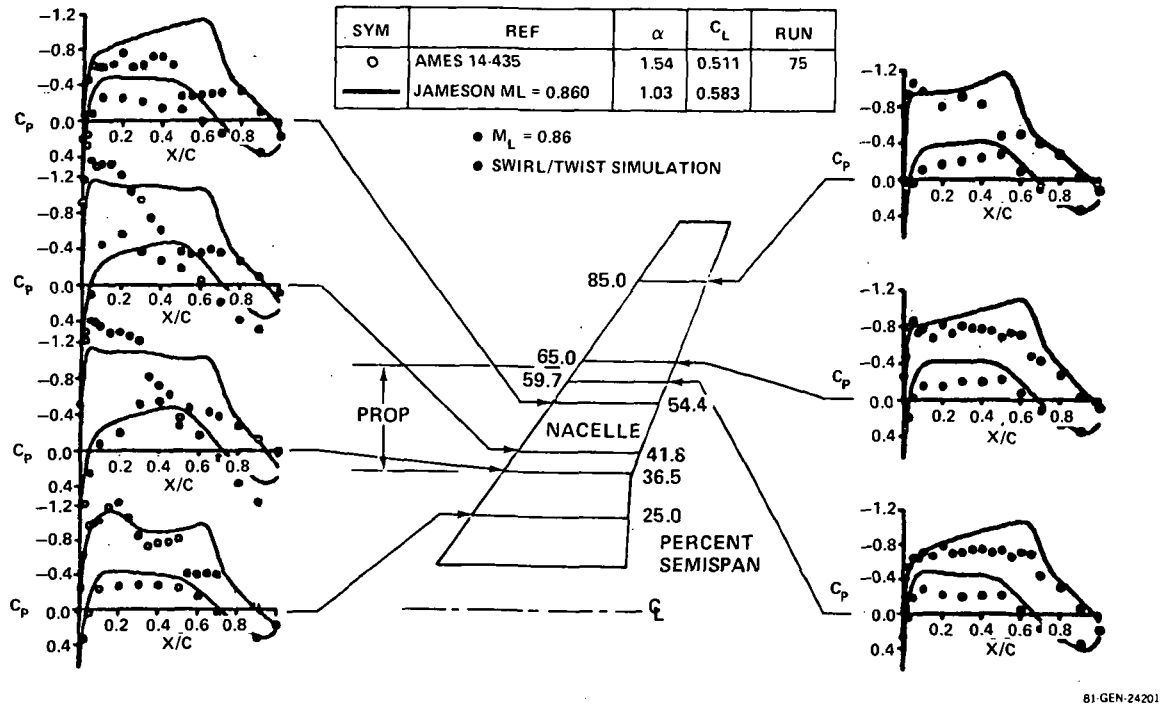

FIGURE 55. COMPARISON OF JAMESON AND EXPERIMENTAL CHORDWISE PRESSURE DISTRIBUTIONS FOR POWERED PROP CONFIGURATION AT M_o = 0.8

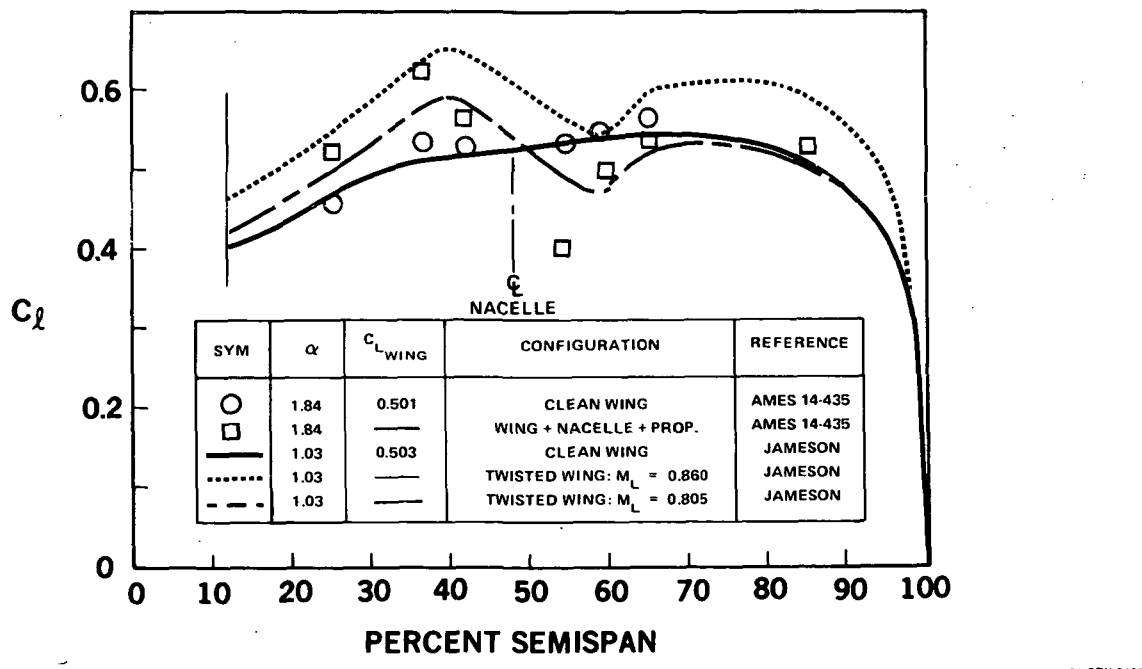

FIGURE 56. WING SECTION LIFT COMPARISON WITH THEORY AT M_o = 0.8

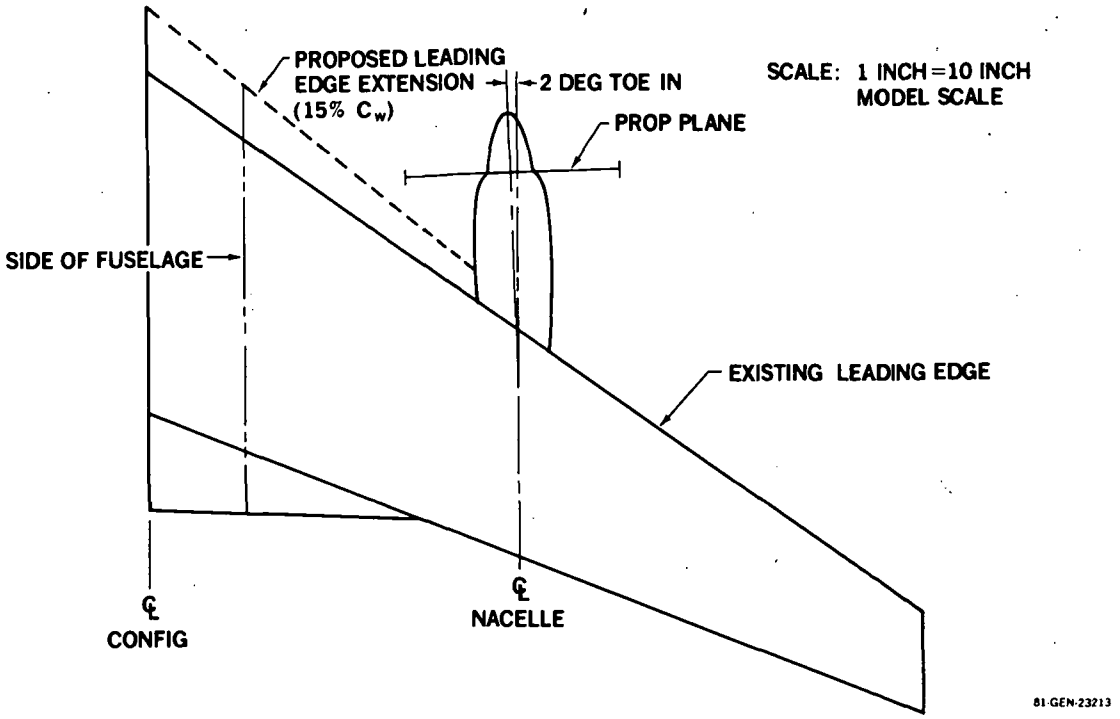

FIGURE 57. PLANFORM MODIFICATION

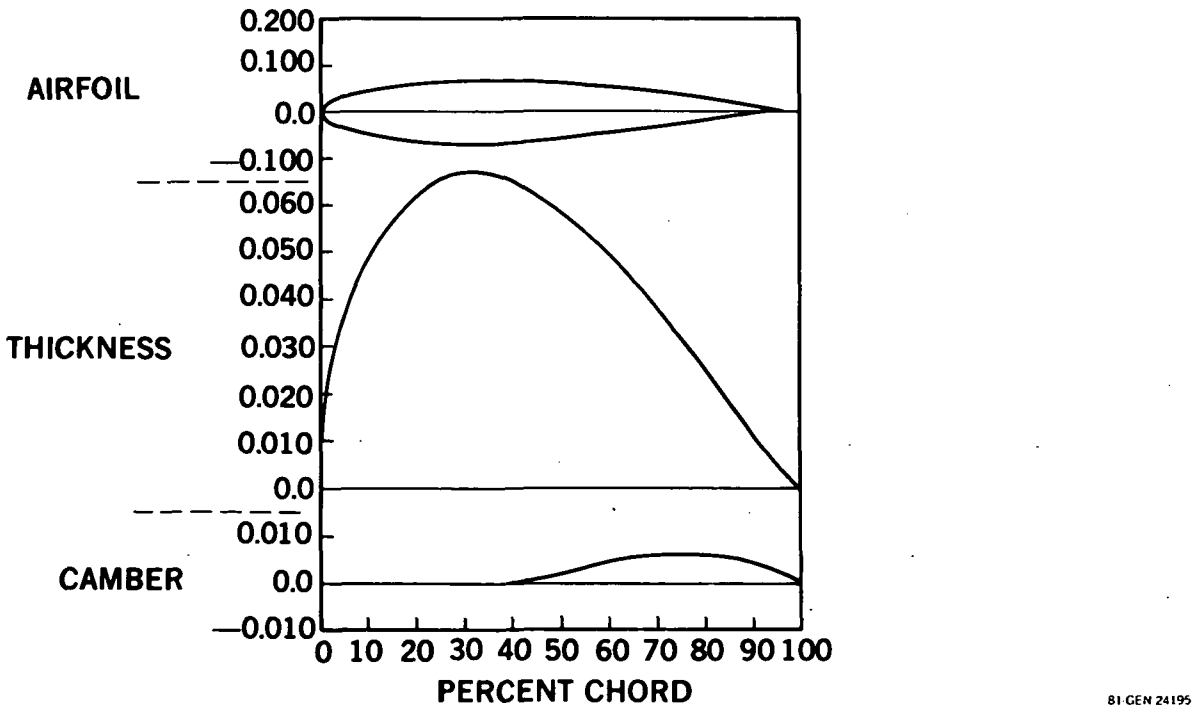

FIGURE 58. MOD 2 AND MOD 3 AIRFOILS AT η = 0.120

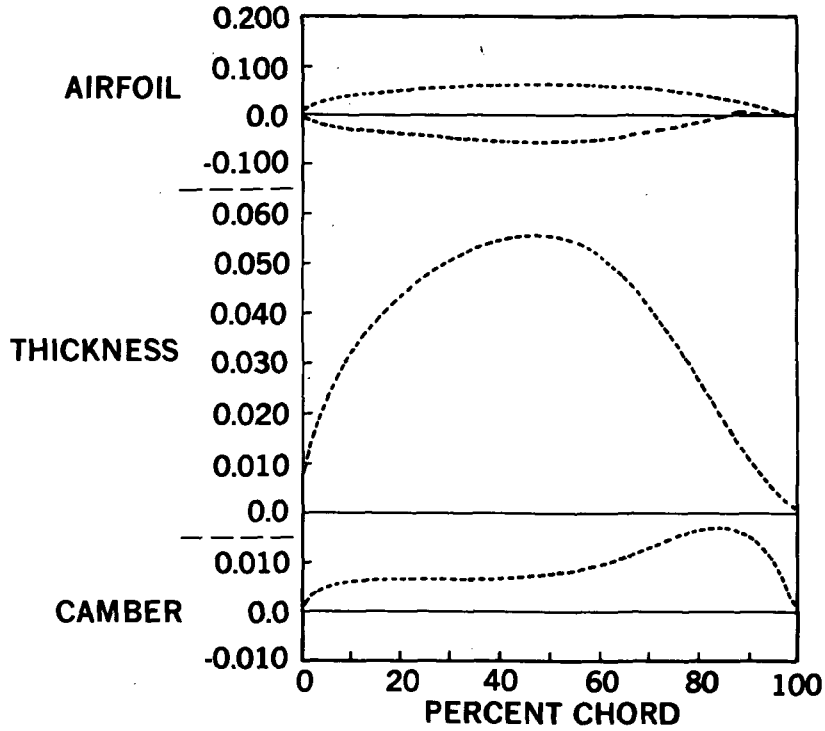

81-GEN-23212

FIGURE 59. MOD 2 AIRFOIL AT η = 0.350

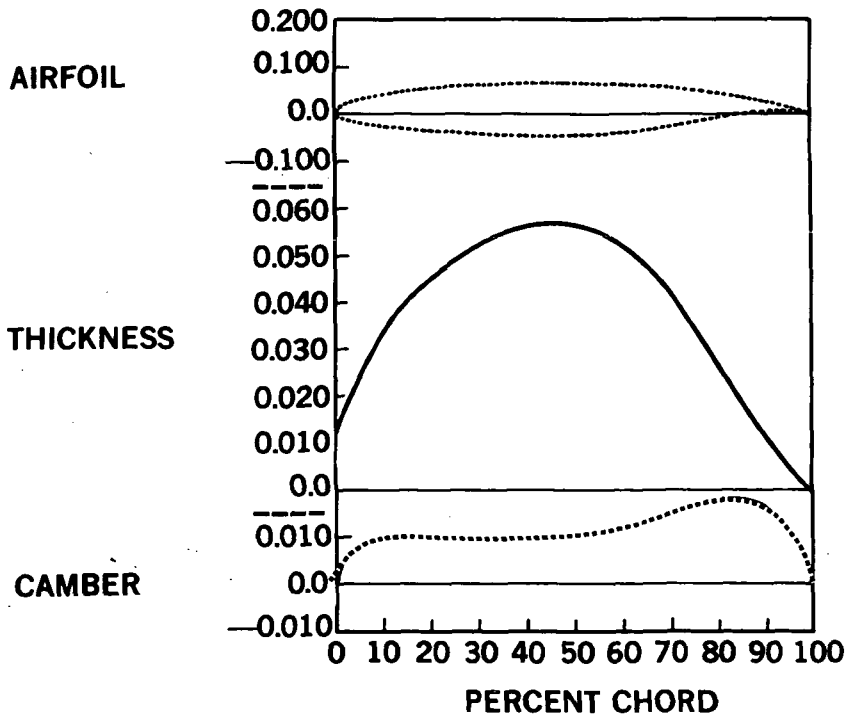

81-GEN-24193

FIGURE 60. MOD 2 AIRFOIL AT η = 0.43

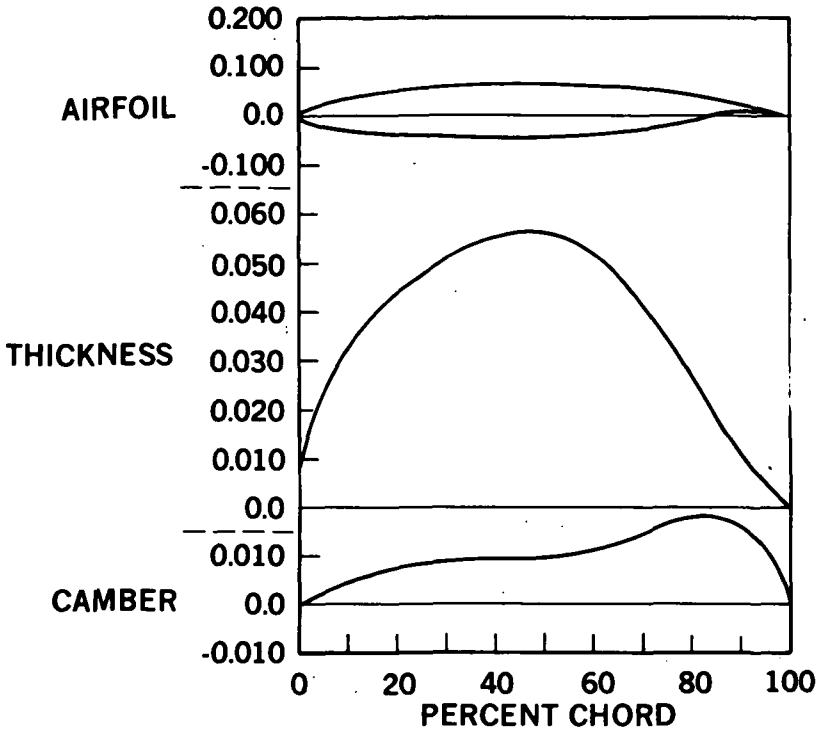

81-GEN-23226

FIGURE 61. MOD 3 AIRFOIL AT η = 0.350

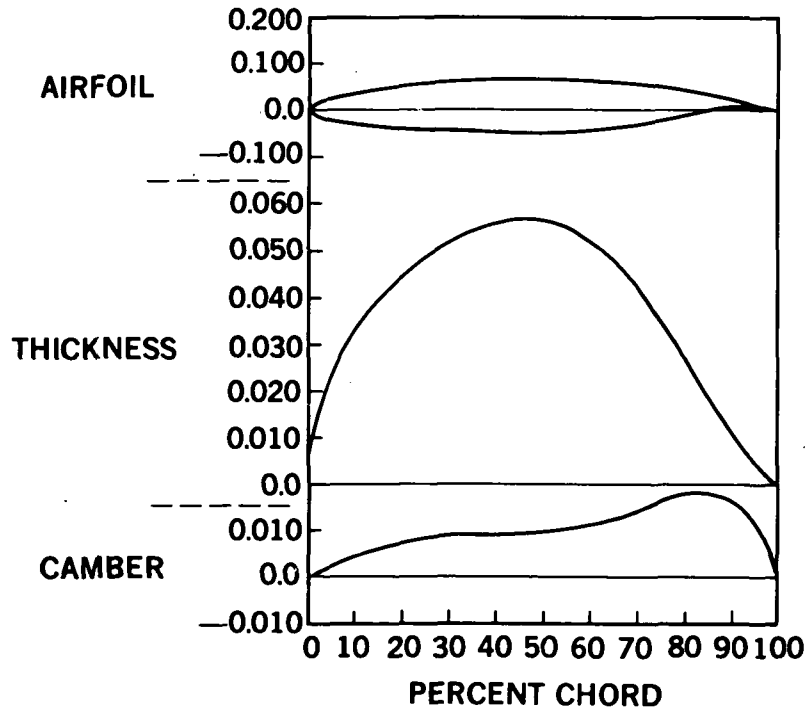

81-GEN-24194

FIGURE 62. MOD 3 AIRFOIL AT η = 0.43

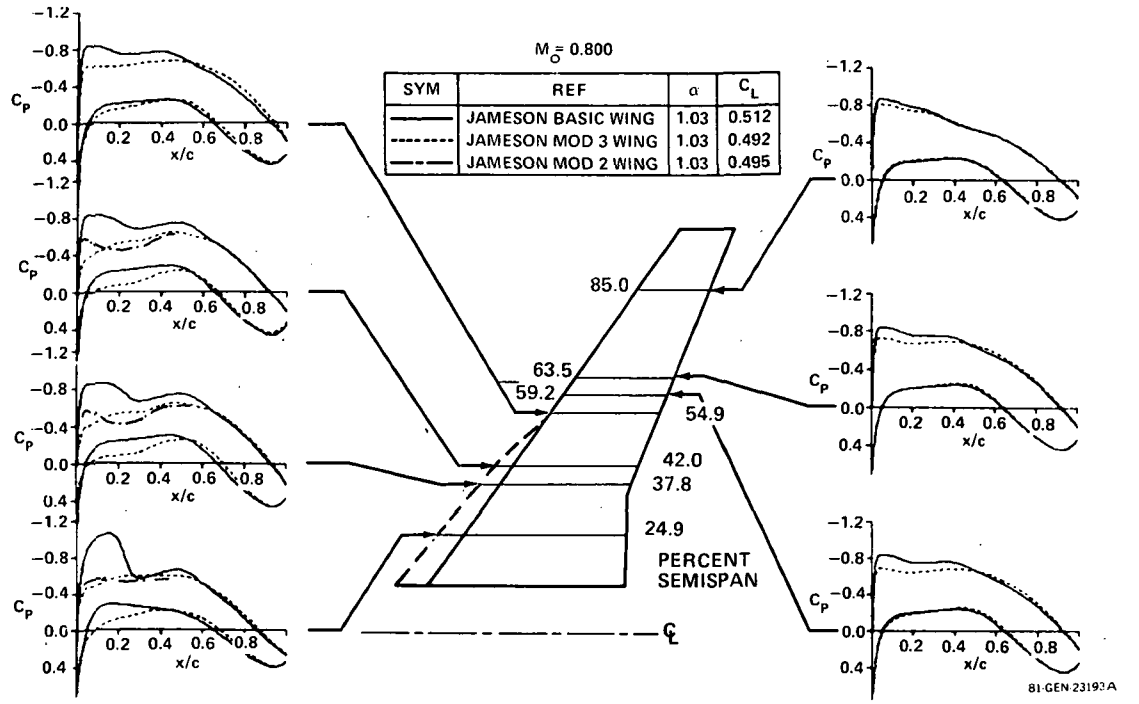

FIGURE 63. COMPARISON OF CALCULATED CHORDWISE PRESSURE DISTRIBUTIONS USING JAMESON – CLEAN WING M_o = 0.800

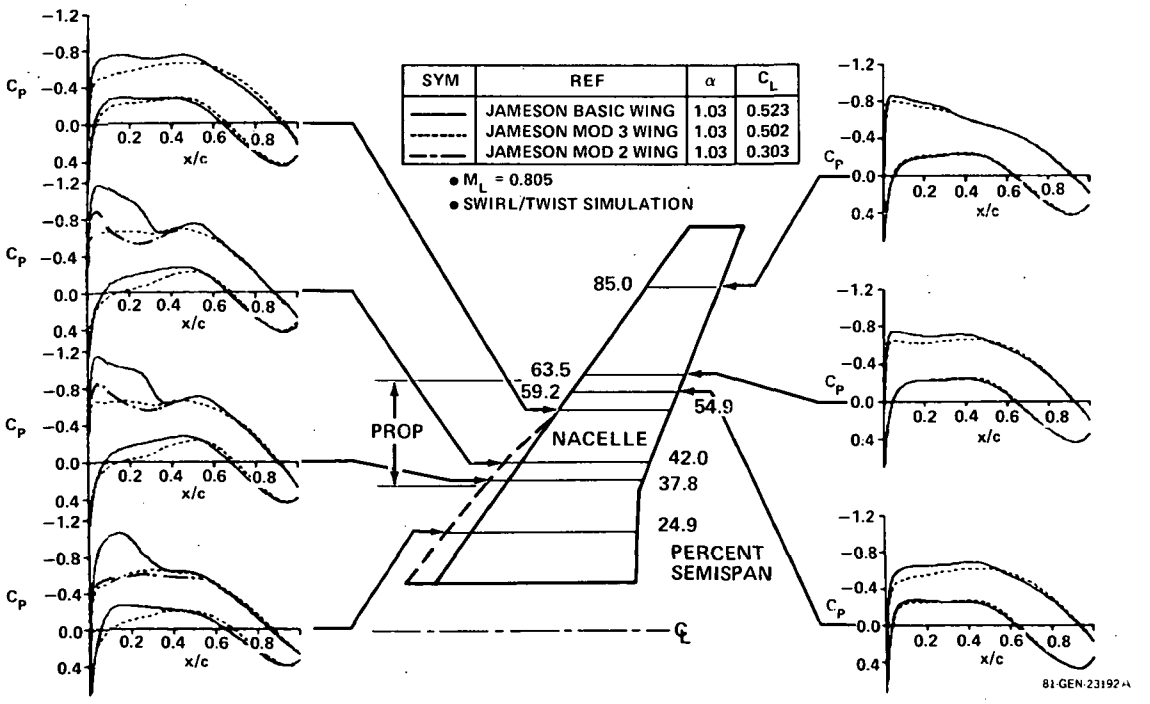

FIGURE 64. COMPARISON OF JAMESON CALCULATED CHORDWISE PRESSURE DISTRIBUTIONS FOR POWERED CONFIGURATIONS M_o = 0.800

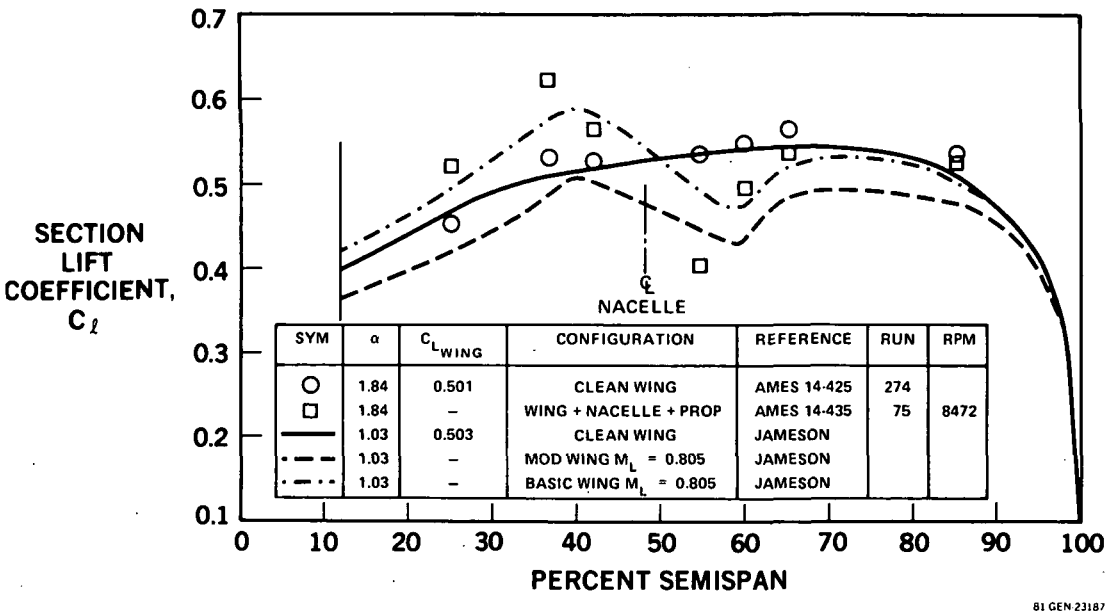

SYM	α	$C_{L_{WING}}$	CONFIGURATION	REFERENCE	RUN	RPM
○	1.84	0.501	CLEAN WING	AMES 14-425	274	
□	1.84	–	WING + NACELLE + PROP	AMES 14-435	75	8472
———	1.03	0.503	CLEAN WING	JAMESON		
– – –	1.03	–	MOD WING M_L = 0.805	JAMESON		
– · – ·	1.03	–	BASIC WING M_L = 0.805	JAMESON		

FIGURE 65. SECTION LIFT CHANGE DUE TO WING MOD 2 AND MOD 3

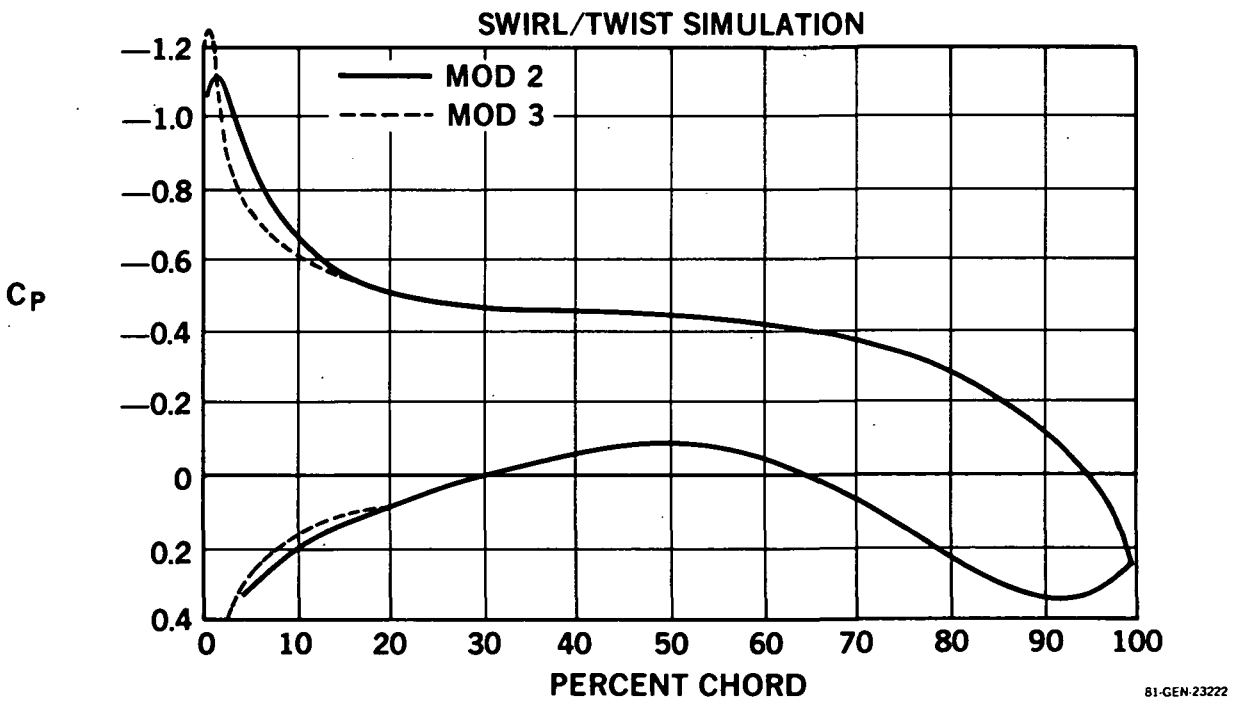

FIGURE 66. INCOMPRESSIBLE JAMESON AT η = 0.38

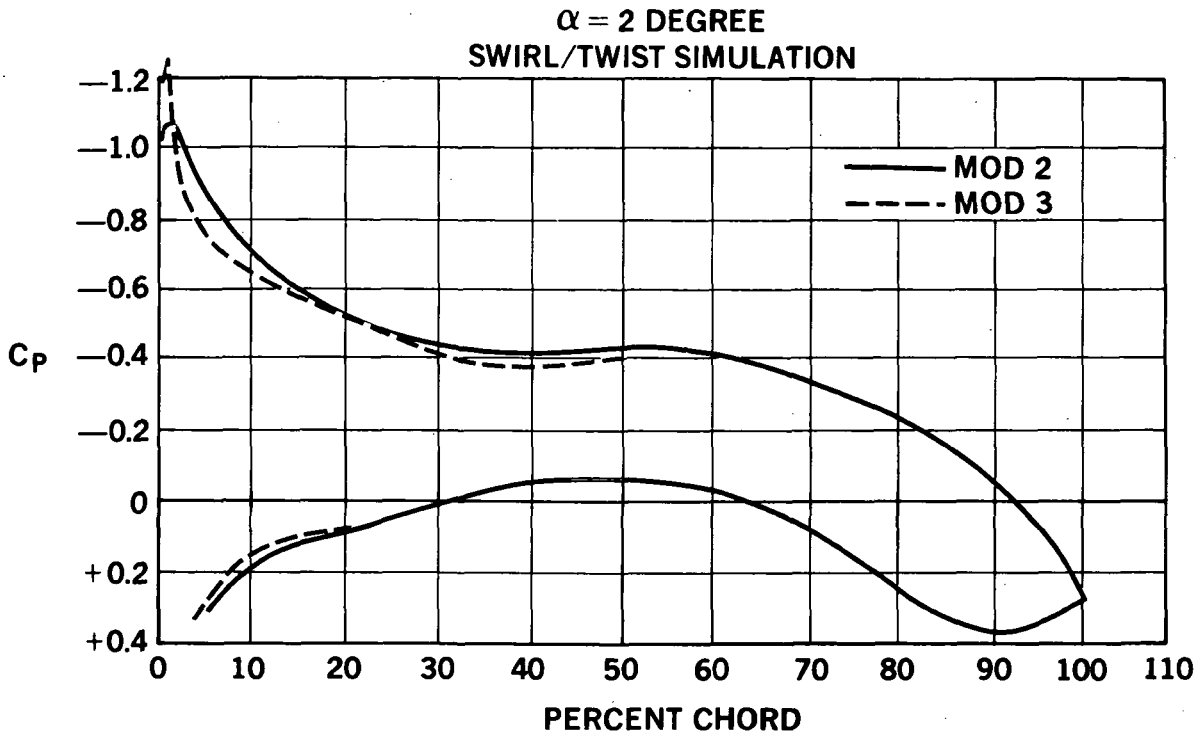

FIGURE 67. INCOMPRESSIBLE JAMESON AT η = 0.42

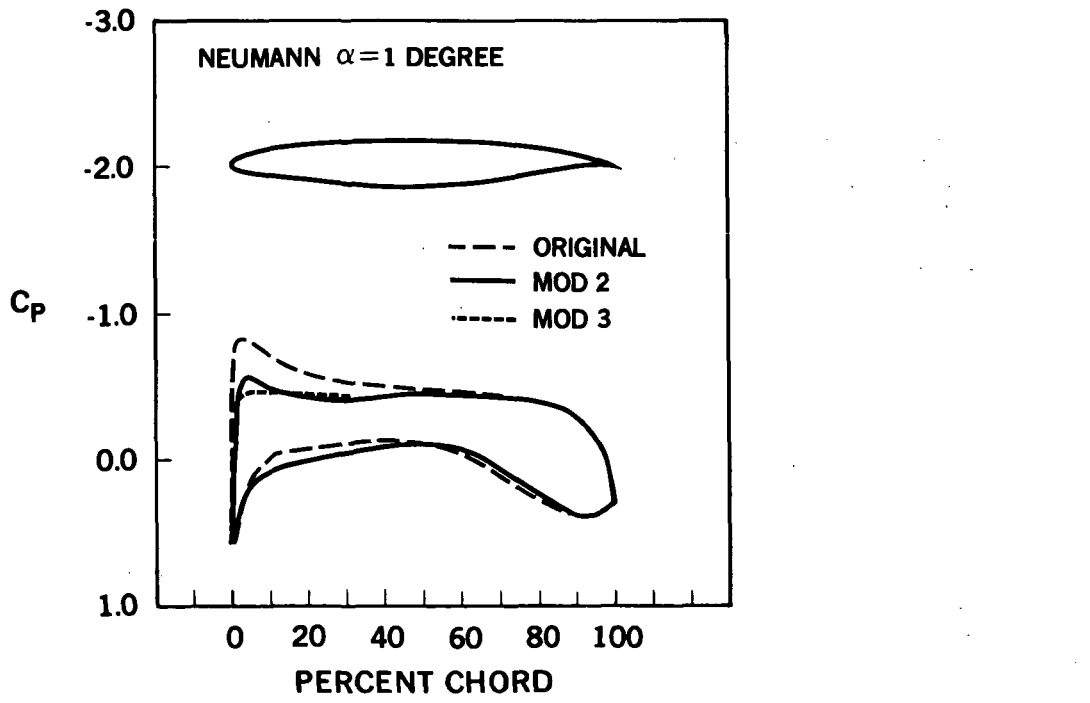

FIGURE 68. PRESSURE DISTRIBUTION FOR CLEAN WINGS AT η = 0.37

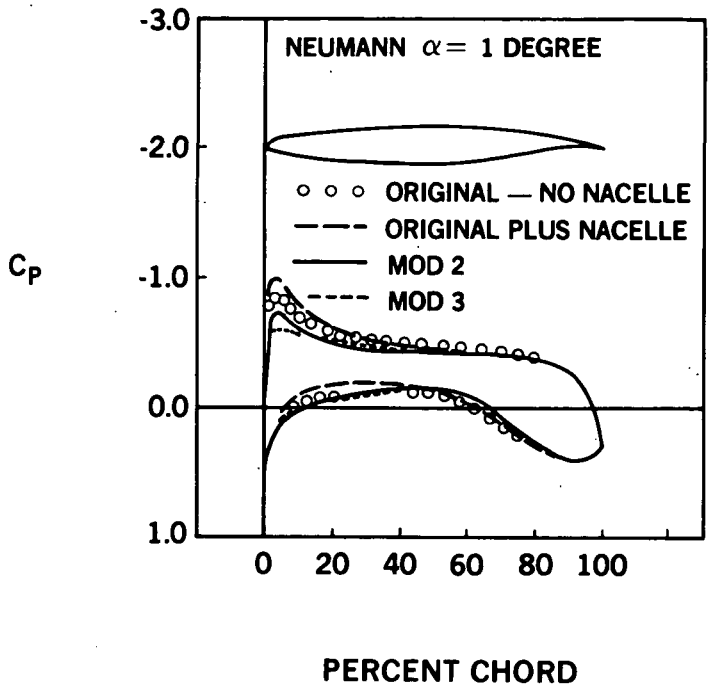

FIGURE 69. PRESSURE DISTRIBUTION FOR WINGS PLUS NACELLE WITHOUT POWER AT η = 0.37

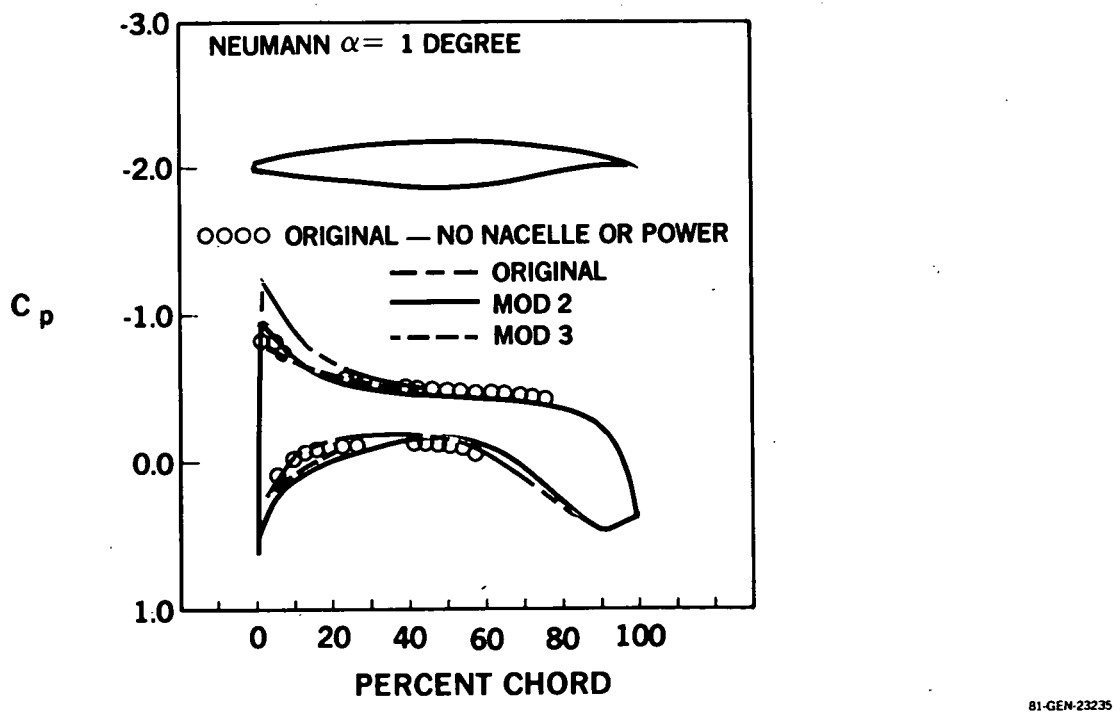

FIGURE 70. PRESSURE DISTRIBUTION FOR WINGS WITH NACELLES AND POWER AT η = 0.37

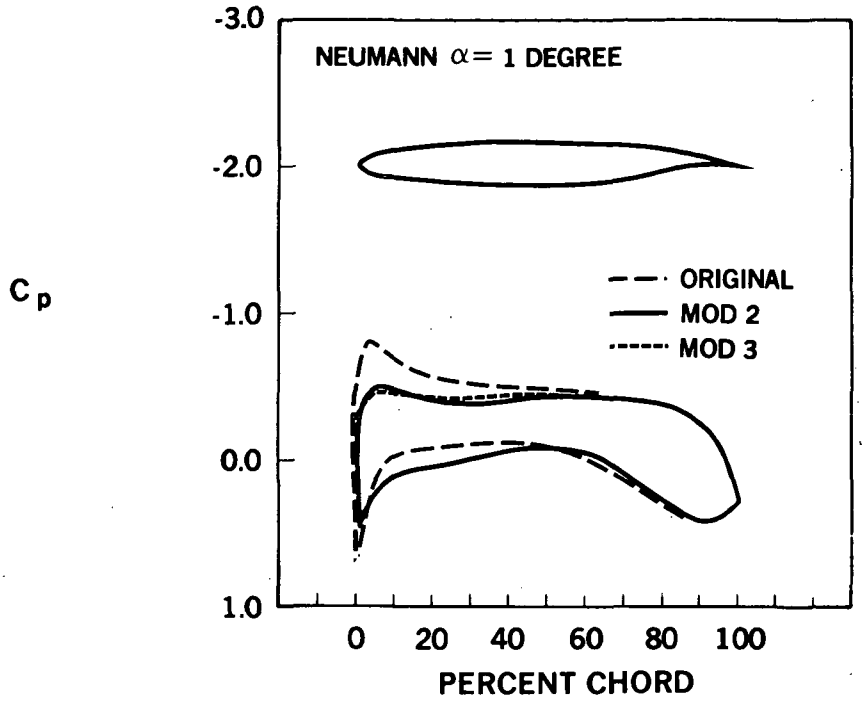

FIGURE 71. PRESSURE DISTRIBUTION FOR CLEAN WINGS AT η = 0.41

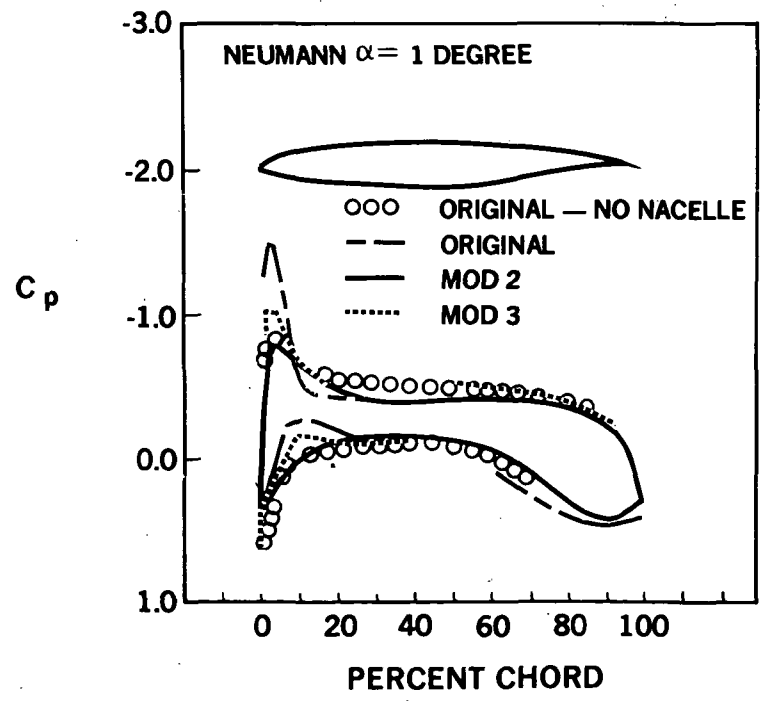

FIGURE 72. PRESSURE DISTRIBUTION FOR WINGS PLUS NACELLE WITHOUT POWER AT η = 0.41

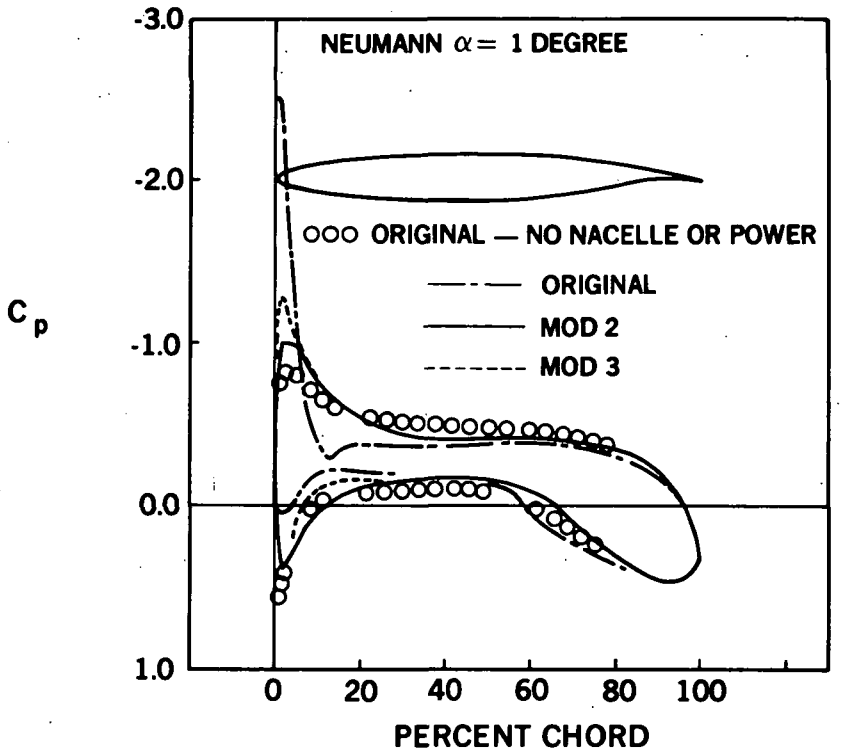

FIGURE 73. PRESSURE DISTRIBUTIONS FOR WINGS WITH NACELLES AND POWER AT η = 0.41

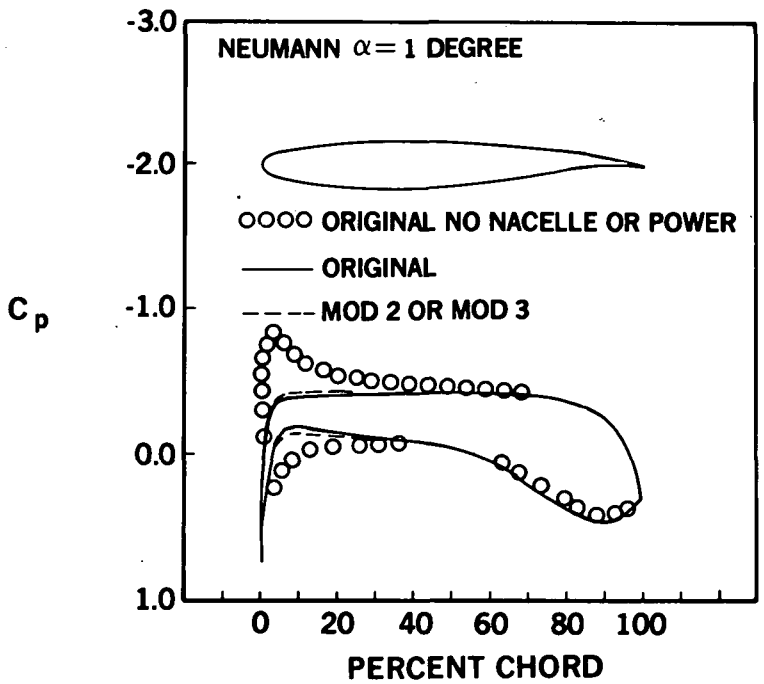

FIGURE 74. PRESSURE DISTRIBUTION OUTBOARD OF NACELLE, WITH NACELLE AND POWER η = 0.56

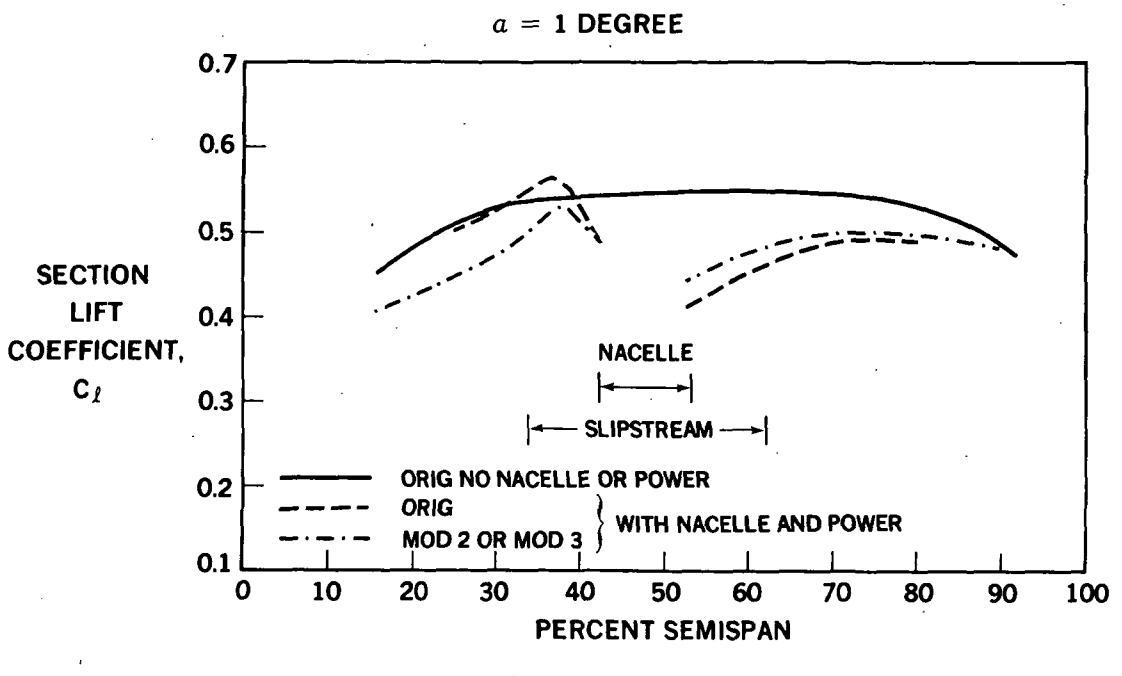

FIGURE 75. COMPARISON OF SECTION LIFT DISTRIBUTION CALCULATED USING NEUMANN

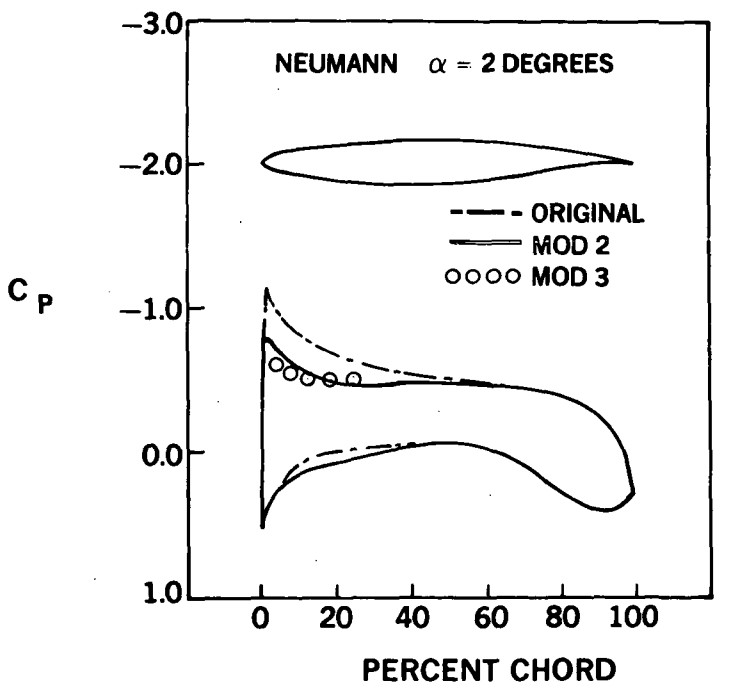

FIGURE 76. PRESSURE DISTRIBUTION FOR CLEAN WING AT η = 0.37 AND α = 2 DEGREES

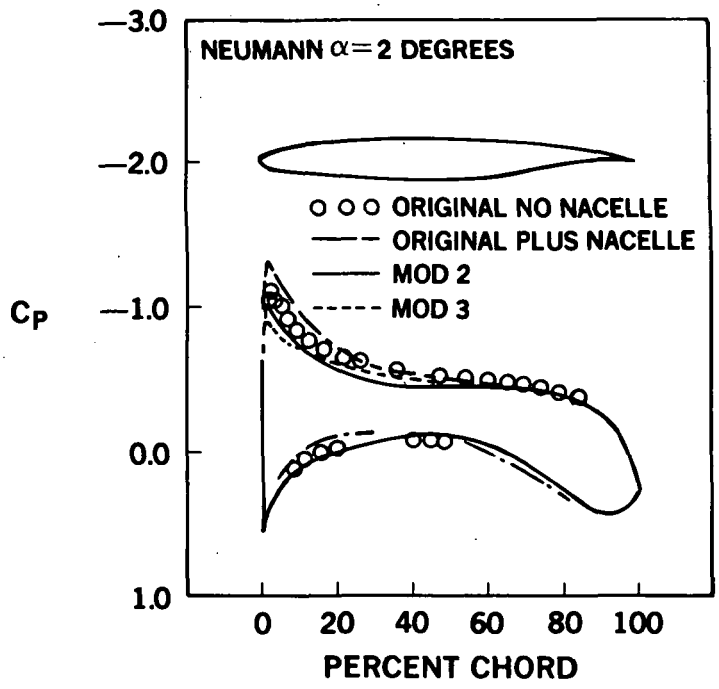

FIGURE 77. PRESSURE DISTRIBUTION FOR WINGS PLUS NACELLE WITHOUT POWER η = 0.37 AND α = 2 DEGREES

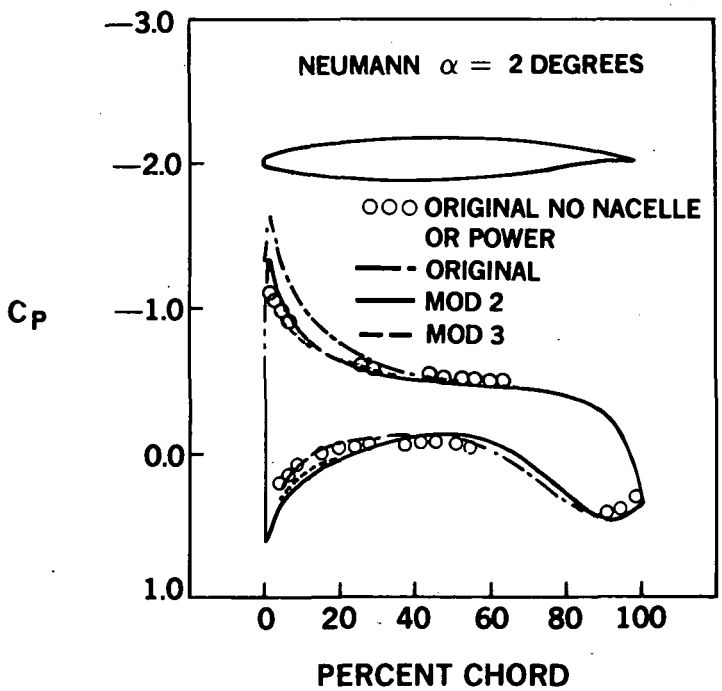

FIGURE 78. PRESSURE DISTRIBUTION FOR WINGS WITH NACELLE AND POWER AT η = 0.37 AND α = 2 DEGREES

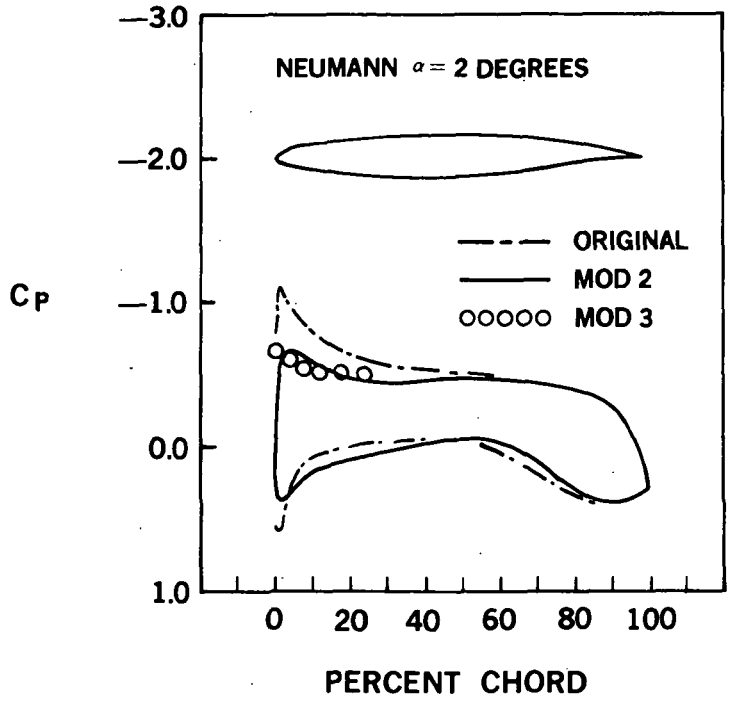

FIGURE 79. PRESSURE DISTRIBUTION FOR CLEAN WINGS AT η = 0.41 AND α = 2 DEGREES

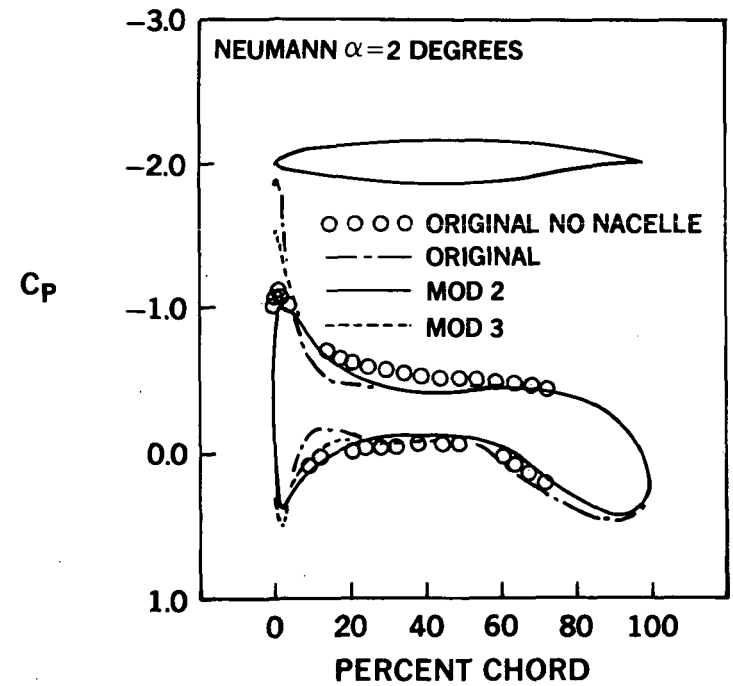

FIGURE 80. PRESSURE DISTRIBUTION FOR WINGS PLUS NACELLE WITHOUT POWER AT η = 0.41 AND α = 2 DEGREES

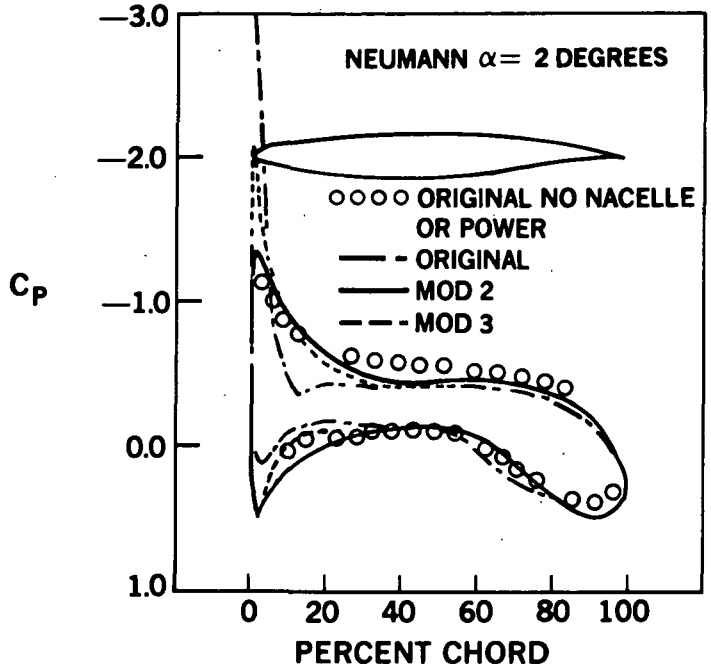

81-GEN-24191

FIGURE 81. PRESSURE DISTRIBUTIONS FOR WINGS WITH NACELLES AND POWER AT η = 0.41 AND α = 2 DEGREES

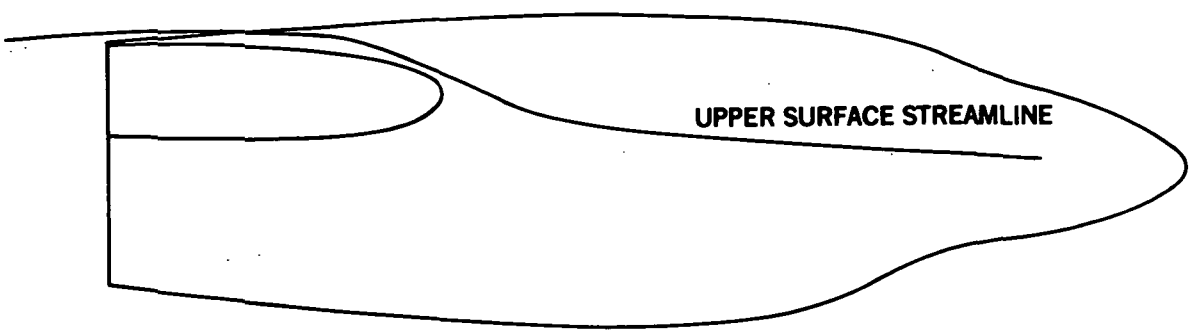

81-GEN-23203

FIGURE 82. CLEAN WING STREAMLINE – PROFILE VIEW

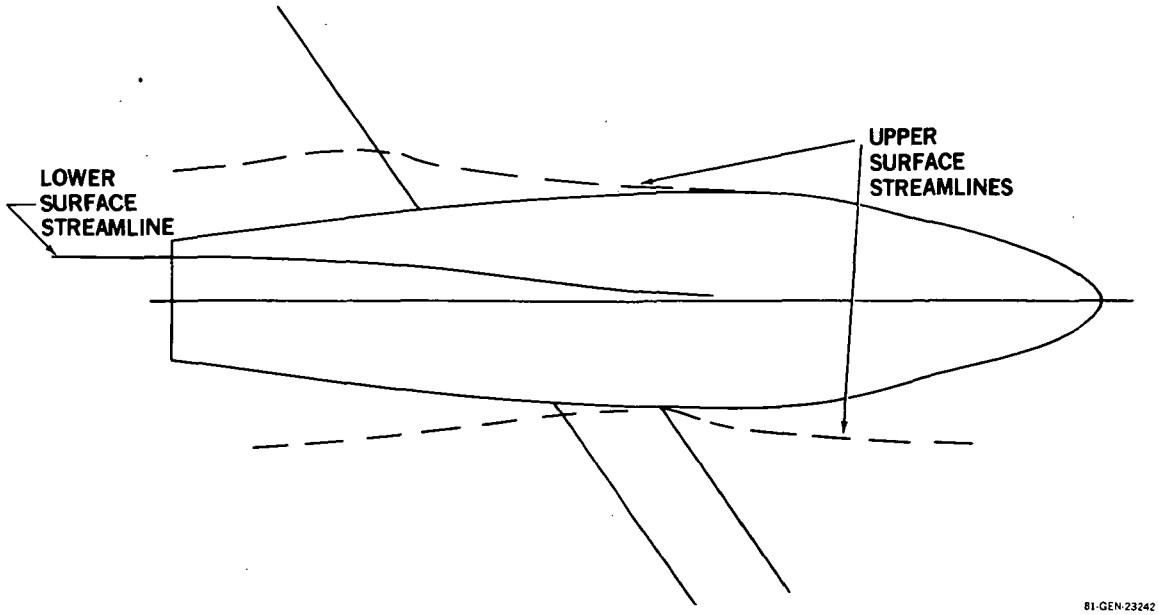

FIGURE 83. CLEAN WING STREAMLINES – PLAN VIEW

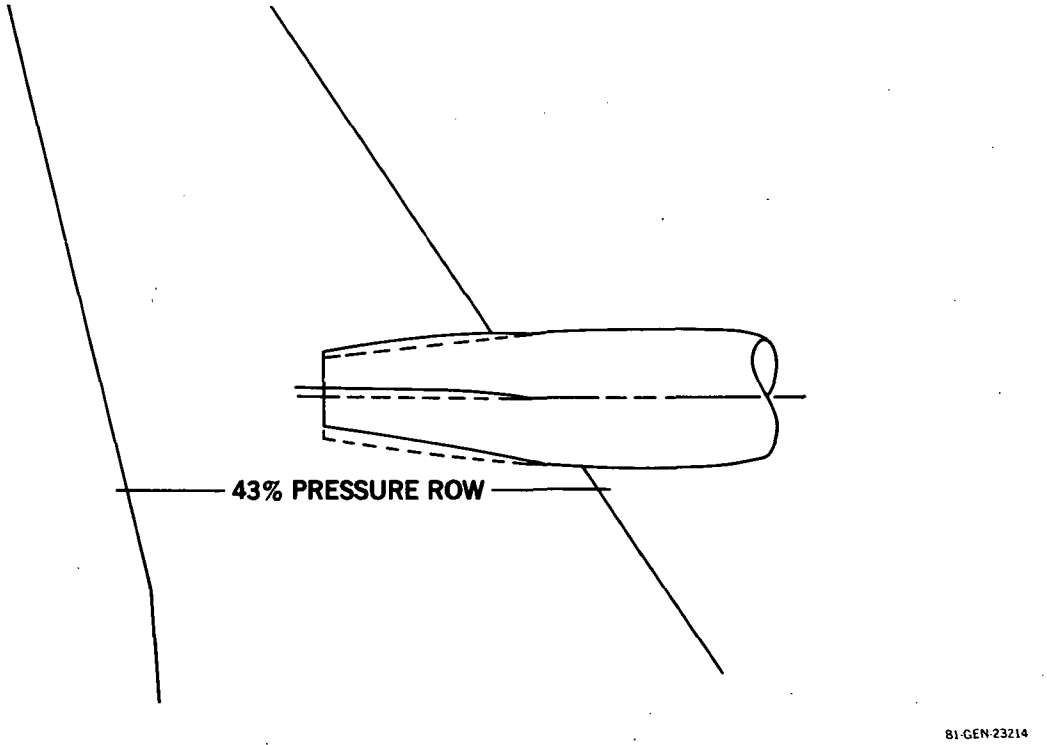

FIGURE 84. STREAMLINE CONTOURED LOWER SURFACE AFT NACELLE

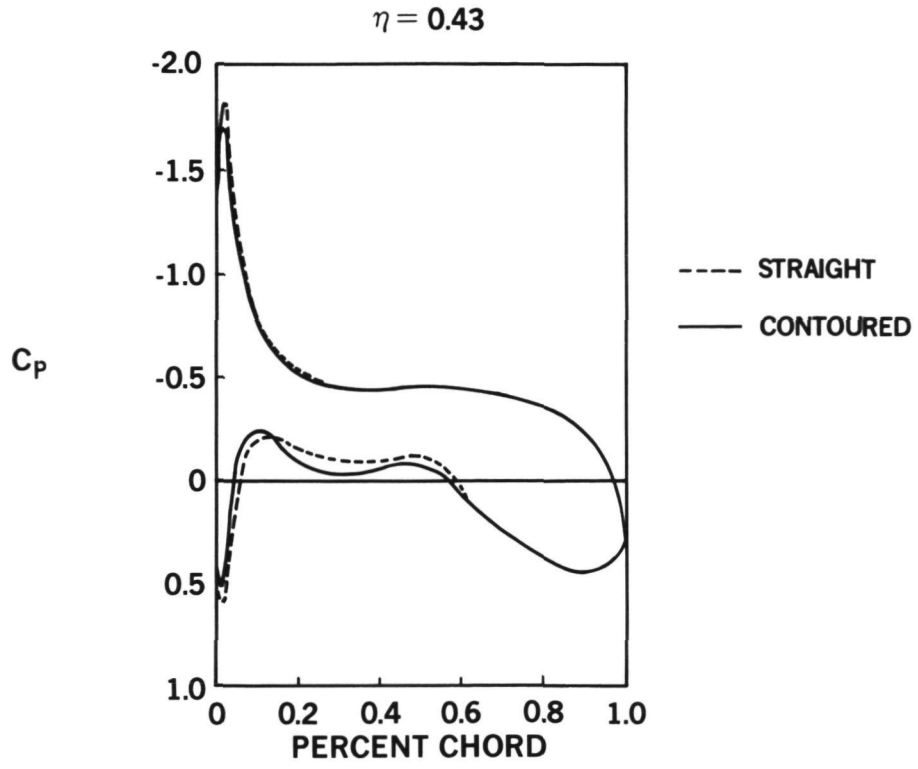

FIGURE 85. EFFECT OF CONTOURING AFT PORTION OF UNDERWING NACELLE

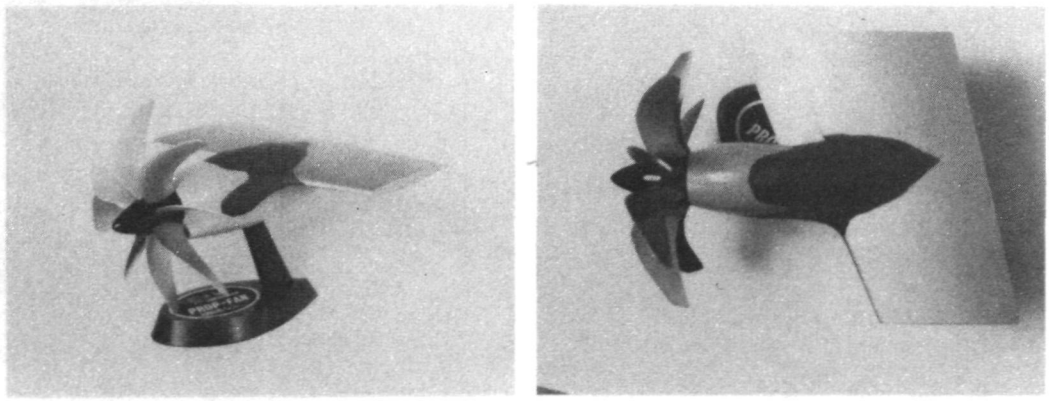

FIGURE 86. SUBSCALE MOCKUP OF POTENTIAL UNDERWING NACELLE CONTOURING

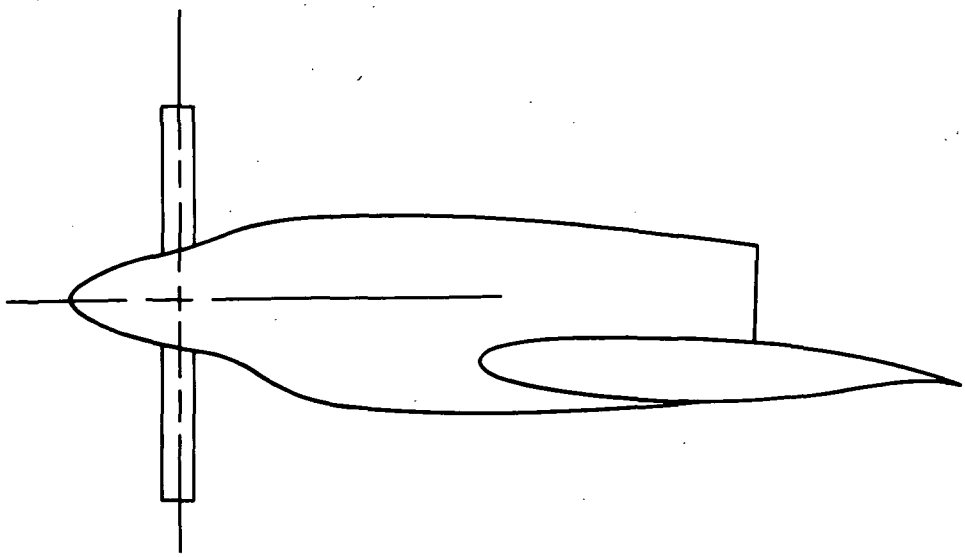

81-GEN-24203

FIGURE 87. SIDE VIEW NONCONTOURED OVERWING NACELLE

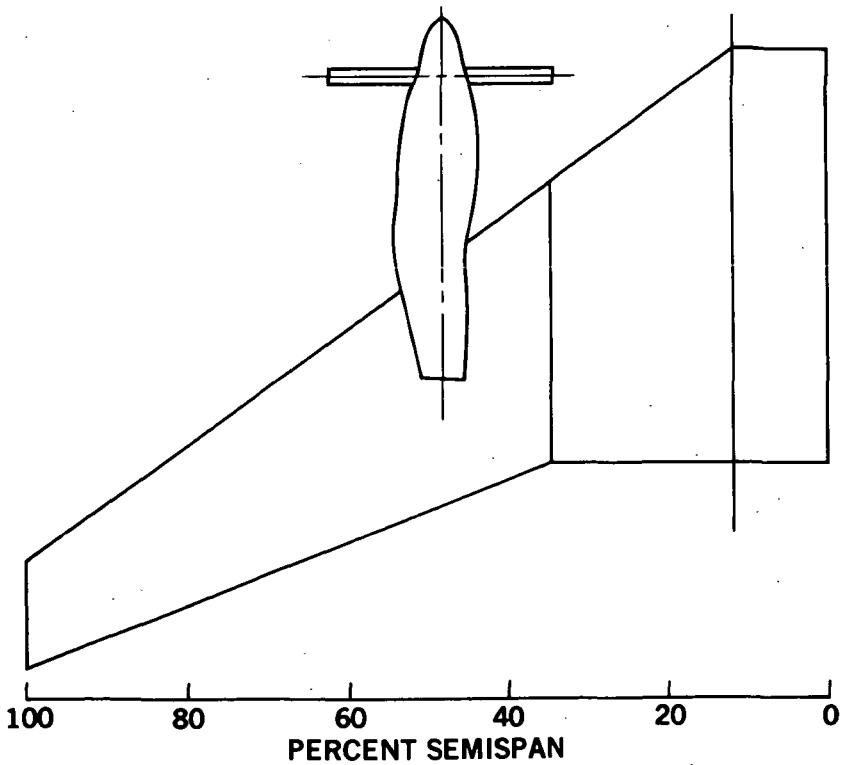

81-GEN-23218

FIGURE 88. PLAN VIEW OF OVERWING CONTOURED NACELLE

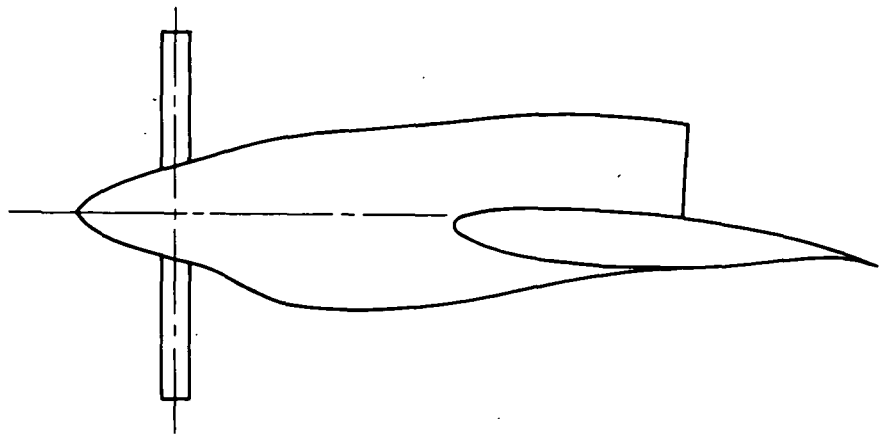

81-GEN-23220

FIGURE 89. SIDE VIEW OF OVERWING CONTOURED NACELLE

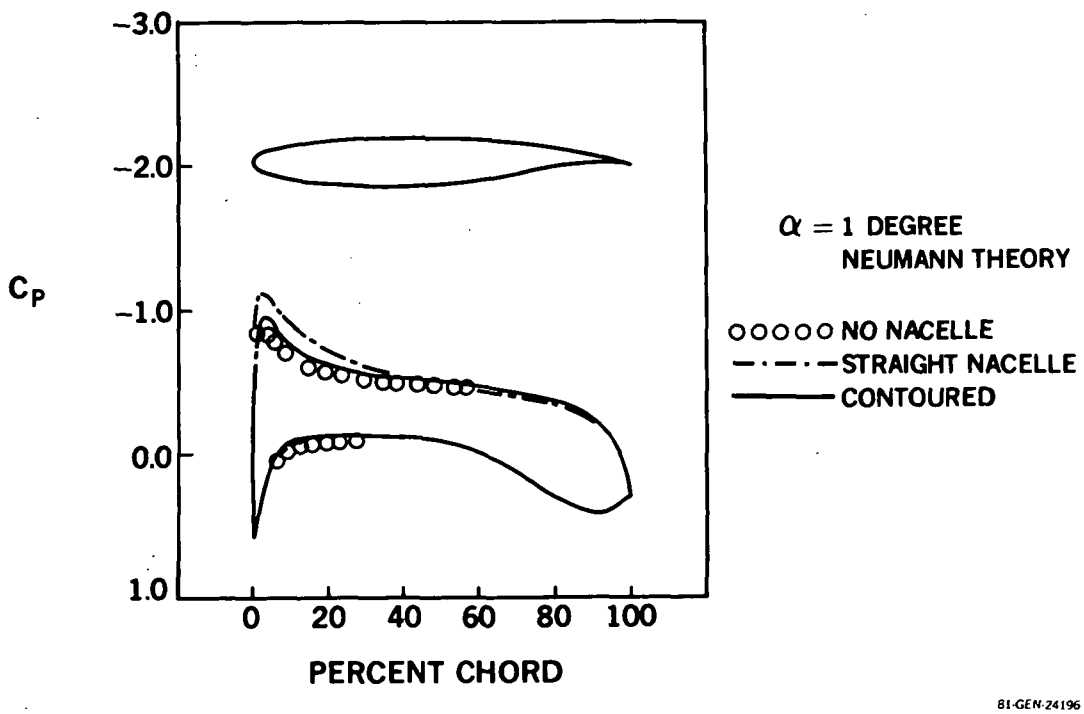

81-GEN-24196

FIGURE 90. PRESSURE DISTRIBUTION COMPARISON FOR CONTOURED NACELLE AT η = 0.37 PERCENT

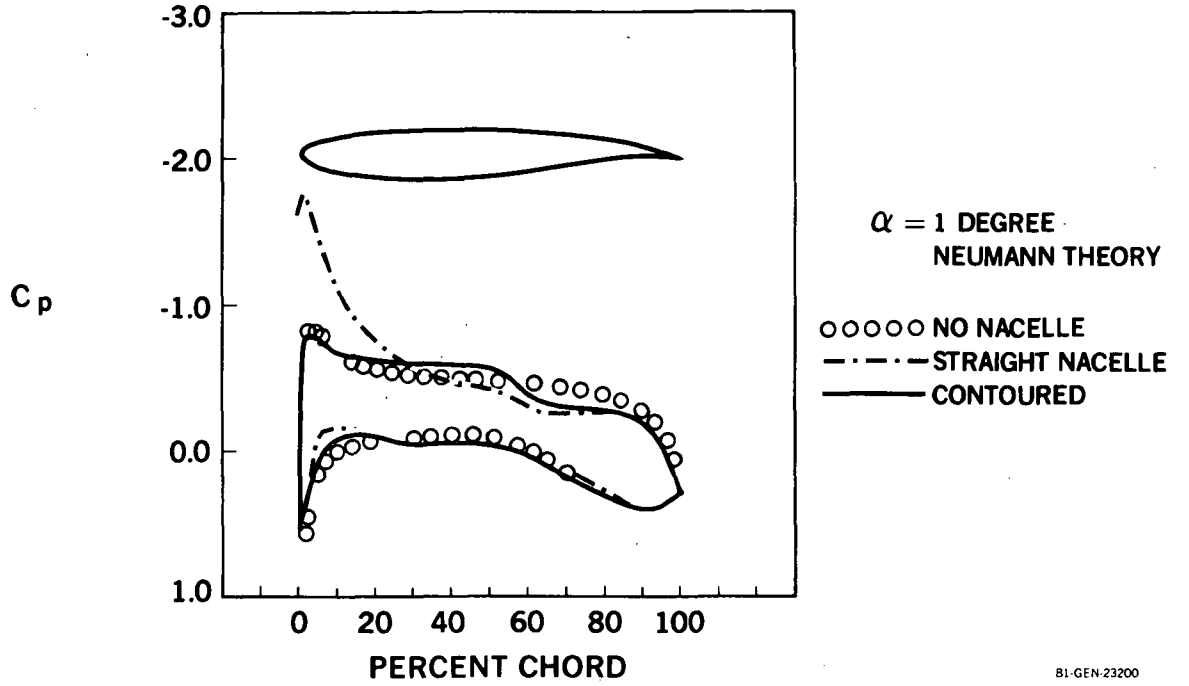

FIGURE 91. PRESSURE DISTRIBUTION COMPARISON FOR CONTOURED NACELLE AT η = 43 PERCENT

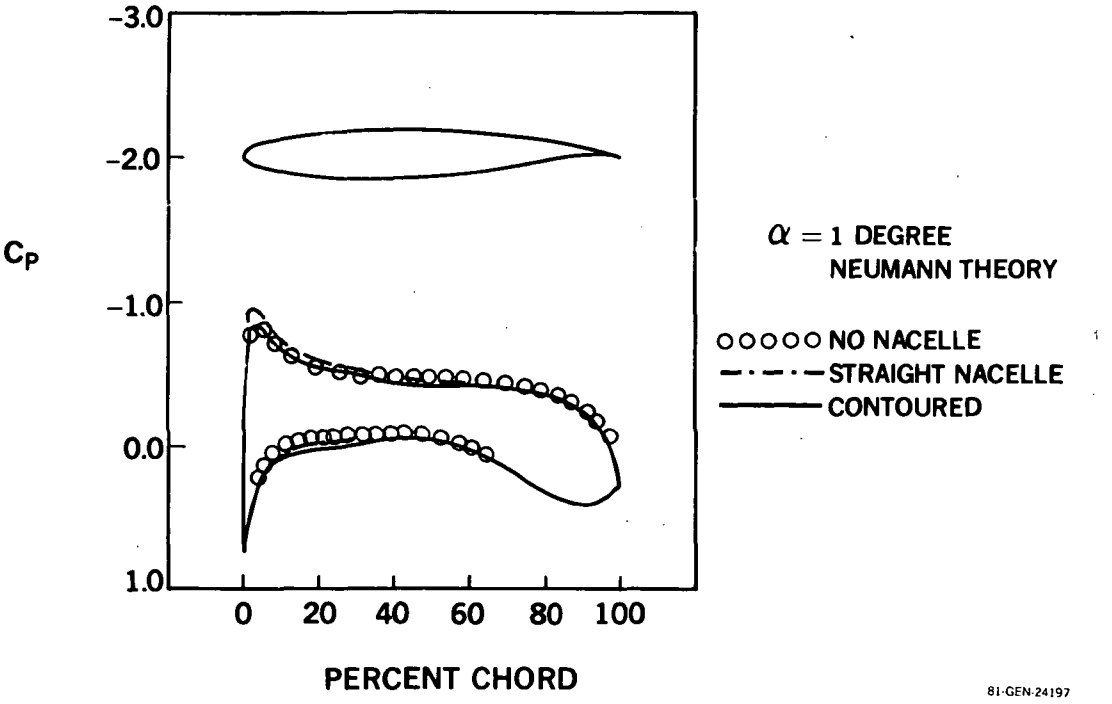

FIGURE 92. PRESSURE DISTRIBUTION FOR CONTOURED NACELLE AT η = 0.56 PERCENT

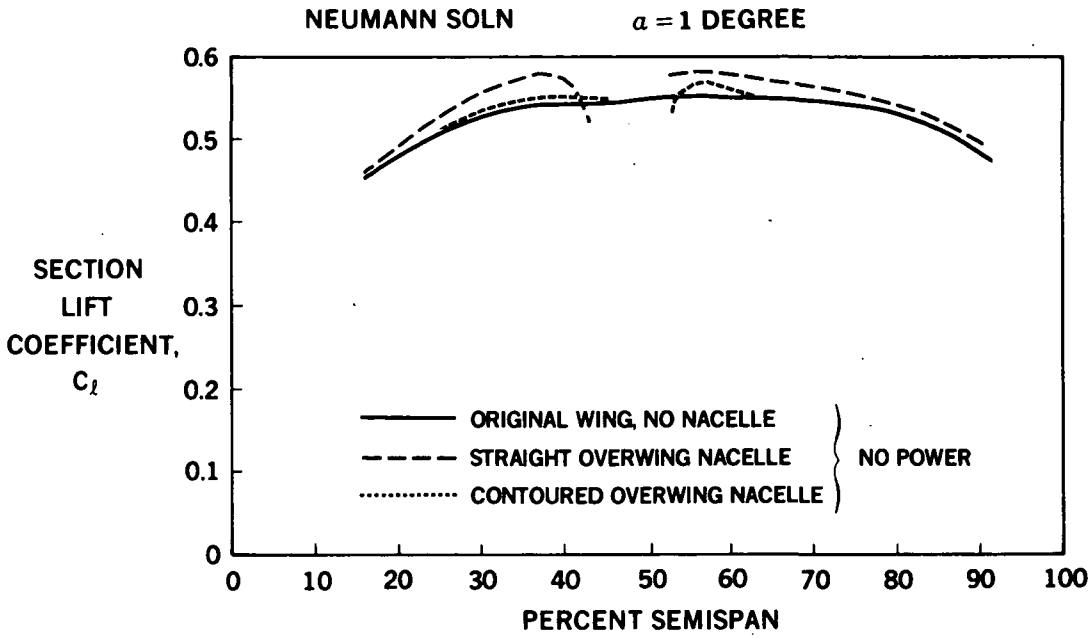

FIGURE 93. EFFECT OF NACELLE CONTOURING ON SECTION LIFT DISTRIBUTION

1. Report No.	2. Government Accession No.	3. Recipient's Catalog No.
NASA CR 166214		

4. Title and Subtitle	5. Report Date
Analysis of Mach Number 0.8 Turboprop Slipstream Wing/Nacelle Interactions	August 6, 1981
	6. Performing Organization Code

7. Author(s)	8. Performing Organization Report No.
H. Robert Welge, Dan H. Neuhart, John A. Dahlin	ACEE-25-FR-1564
	10. Work Unit No.

9. Performing Organization Name and Address	11. Contract or Grant No.
Douglas Aircraft Company 3855 Lakewood Blvd. Long Beach, Ca 90846	NAS2-10881
	13. Type of Report and Period Covered

12. Sponsoring Agency Name and Address	13. Type of Report and Period Covered
National Aeronautics and Space Administration Ames Research Center Moffett Field, CA 94035	Contract Final Report
	14. Sponsoring Agency Code

15. Supplementary Notes

Technical Monitor: Al Levin (227-2)
NASA Research Center
Moffett Field, CA 94035

16. Abstract

An experimental test program of a powered propeller and nacelle mounted on a supercritical wing was conducted by the NASA Ames Research Center in the 14-foot tunnel. Analysis of this data by the Douglas Aircraft Company, under contract to NASA with Al Lavin as the program manager, is contained in this report. The design condition for this study was $M_O = 0.8$.

Analysis of the data indicated that the installation of the nacelle significantly affected the wing flow and that the flow on the upper surface of the wing is separated near the leading edge under powered conditions. Comparisons of various theories with the data indicated that the Neumann surface panel solution and the Jameson transonic solution gave results adequate for design purposes. A modified wing design was developed (Mod 3) which reduces the wing upper surface pressure coefficients and section lift coefficients at powered conditions to levels below those of the original wing without nacelle or power. A contoured over-the-wing nacelle is described that can be installed on the original wing without any appreciable interference to the wing upper surface pressures.

17. Key Words (Suggested by Author(s))	18. Distribution Statement
Turboprop Propfan Wing Design Propulsion Integration	Unrestricted

19. Security Classif. (of this report)	20. Security Classif. (of this page)	21. No. of Pages	22. Price*
Unclassified	Unclassified		

* For sale by the National Technical Information Service, Springfield, Virginia 22151

DOUGLAS AIRCRAFT COMPANY

3855 Lakewood Boulevard, Long Beach, California 90846 (213) 593-5511

MCDONNELL DOUGLAS CORPORATION

Printed in U.S.A. 8/81 S81-2445